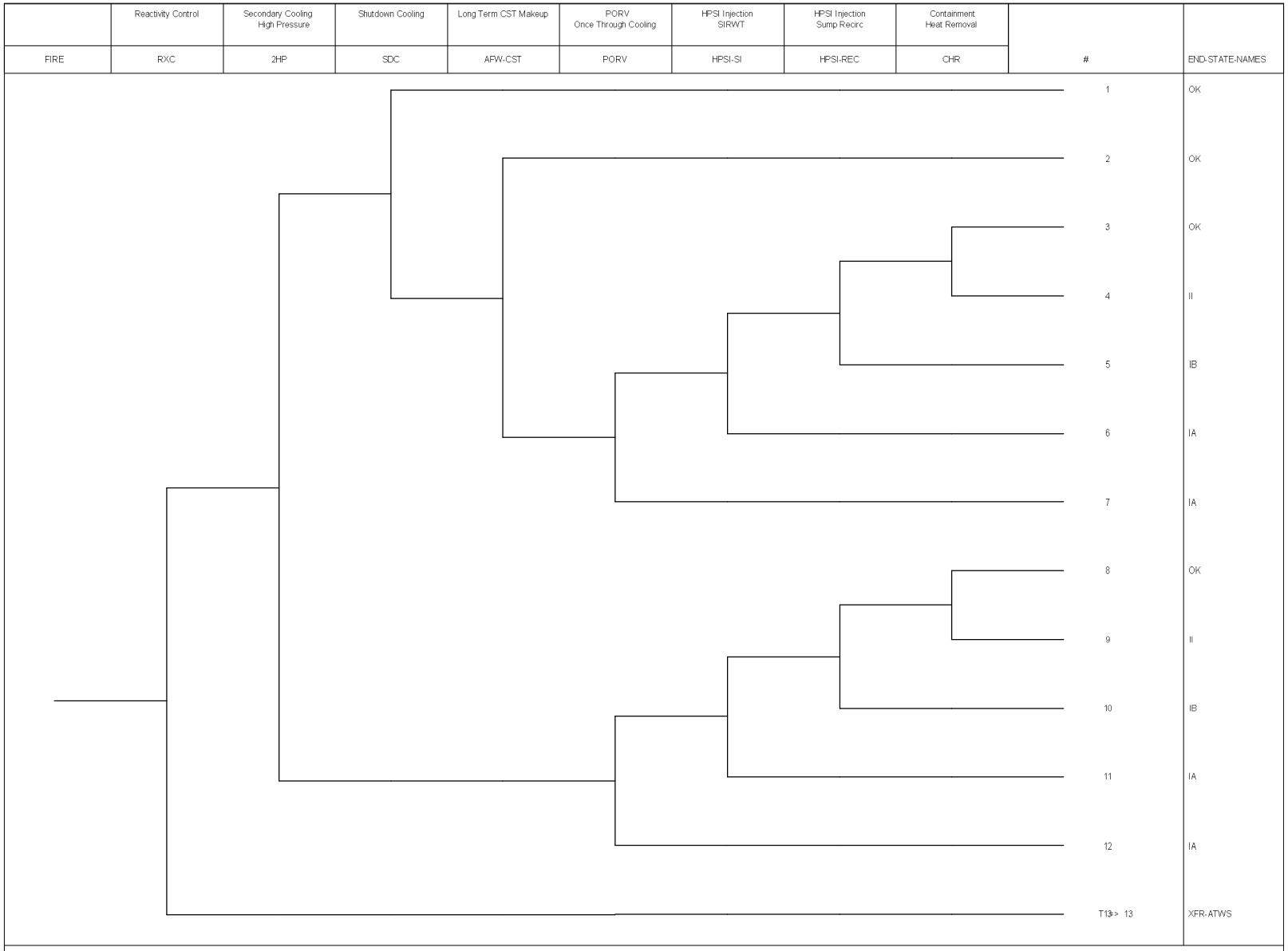

Figure A7.10 - Aux Building Corridor and Turbine Building Fire Accident Sequences

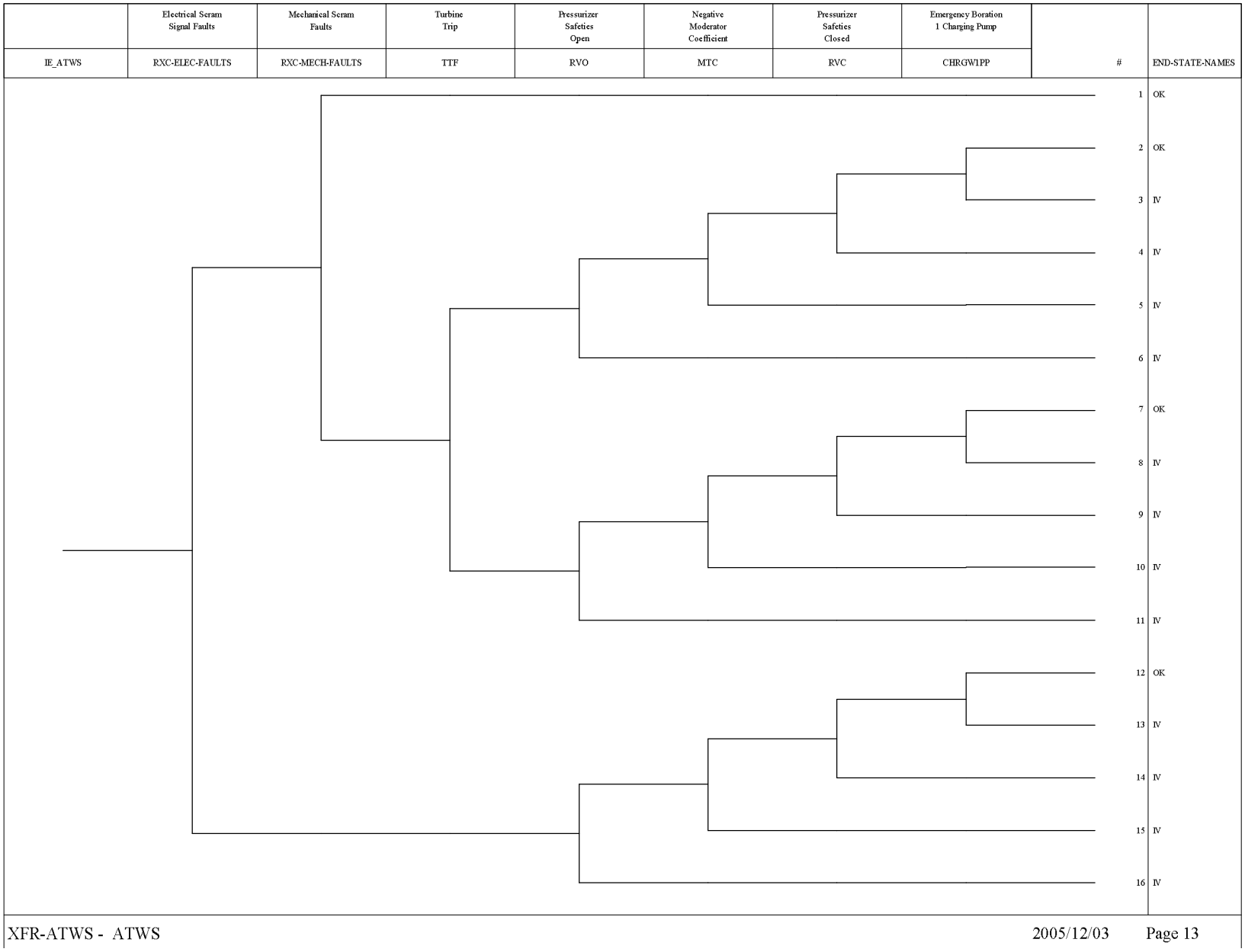

Figure A7.11 - Anticipated Transient Without Scram Accident Sequences

Table A7.1

Rules for Fire Area 1

```
if init(FIRE-CR)then
      eventree(FIRE-CR)=FALSE(HSE-NOTFA1);
endif

if FA-1 then eventree( FA-1 )=TRUE(IE-FA-1); endif
if FA-1-EC-01L then eventree( FA-1 )=TRUE(IE-FA-1-EC-01L ); endif
if FA-1-EC-01R then eventree( FA-1 )=TRUE(IE-FA-1-EC-01R ); endif
if FA-1-EC-02L then eventree( FA-1 )=TRUE(IE-FA-1-EC-02L ); endif
if FA-1-EC-02R then eventree( FA-1 )=TRUE(IE-FA-1-EC-02R ); endif
if FA-1-EC-03L then eventree( FA-1 )=TRUE(IE-FA-1-EC-03L ); endif
if FA-1-EC-03R then eventree( FA-1 )=TRUE(IE-FA-1-EC-03R ); endif
if FA-1-EC-04L then eventree( FA-1 )=TRUE(IE-FA-1-EC-04L ); endif
if FA-1-EC-04R then eventree( FA-1 )=TRUE(IE-FA-1-EC-04R ); endif
if FA-1-EC-08L then eventree( FA-1 )=TRUE(IE-FA-1-EC-08L ); endif
if FA-1-EC-08R then eventree( FA-1 )=TRUE(IE-FA-1-EC-08R ); endif
if FA-1-EC-11L then eventree( FA-1 )=TRUE(IE-FA-1-EC-11L ); endif
if FA-1-EC-11R then eventree( FA-1 )=TRUE(IE-FA-1-EC-11R ); endif
if FA-1-EC-12L then eventree( FA-1 )=TRUE(IE-FA-1-EC-12L ); endif
if FA-1-EC-12R then eventree( FA-1 )=TRUE(IE-FA-1-EC-12R ); endif
if FA-1-EC-13L then eventree( FA-1 )=TRUE(IE-FA-1-EC-13L ); endif
if FA-1-EC-13R then eventree( FA-1 )=TRUE(IE-FA-1-EC-13R ); endif
if FA-1-EC-106 then eventree( FA-1 )=TRUE(IE-FA-1-EC-106 ); endif
if FA-1-EC-126 then eventree( FA-1 )=TRUE(IE-FA-1-EC-126 ); endif
```

Table A7.2

Rules for Fire Area 2

```
if init(FIRE-CS)then
      eventree(FIRE-CS)=FALSE(HSE-NOTFA2);
endif

if FA-2 then eventree(FA-2) = TRUE(IE-FA-2); endif
if FA-2-EB-01 then eventree( FA-2 )=TRUE(IE-FA-2-EB-01 ); endif
if FA-2-EB-02 then eventree( FA-2 )=TRUE(IE-FA-2-EB-02 ); endif
if FA-2-EB-11 then eventree( FA-2 )=TRUE(IE-FA-2-EB-11 ); endif
if FA-2-EB-12 then eventree( FA-2 )=TRUE(IE-FA-2-EB-12 ); endif
if FA-2-EB-21 then eventree( FA-2 )=TRUE(IE-FA-2-EB-21 ); endif
if FA-2-EB-23 then eventree( FA-2 )=TRUE(IE-FA-2-EB-23 ); endif
if FA-2-EB-24 then eventree( FA-2 )=TRUE(IE-FA-2-EB-24 ); endif
if FA-2-ED-06 then eventree( FA-2 )=TRUE(IE-FA-2-ED-06 ); endif
if FA-2-ED-07 then eventree( FA-2 )=TRUE(IE-FA-2-ED-07 ); endif
if FA-2-ED-08 then eventree( FA-2 )=TRUE(IE-FA-2-ED-08 ); endif
if FA-2-ED-09 then eventree( FA-2 )=TRUE(IE-FA-2-ED-09 ); endif
if FA-2-ED-10 then
      eventree( FA-2 )=TRUE(IE-FA-2-ED-10 );
      eventree(FA-2)=FALSE(HSE-NOTFA2-ED-10);
      endif
if FA-2-ED-11 then eventree( FA-2 )=TRUE(IE-FA-2-ED-11 ); endif
if FA-2-ED-15 then eventree( FA-2 )=TRUE(IE-FA-2-ED-15 ); endif
if FA-2-ED-16 then eventree( FA-2 )=TRUE(IE-FA-2-ED-16 ); endif
if FA-2-ED-17 then eventree( FA-2 )=TRUE(IE-FA-2-ED-17 ); endif
if FA-2-ED-18 then eventree( FA-2 )=TRUE(IE-FA-2-ED-18 ); endif
if FA-2-ED-20 then
      eventree( FA-2 )=TRUE(IE-FA-2-ED-20 );
      eventree (FA-2) = FALSE(HSE-NOTFA2-ED-20);
endif
if FA-2-ED-21 then eventree( FA-2 )=TRUE(IE-FA-2-ED-21 ); endif
if FA-2-EJ-14A then eventree( FA-2 )=TRUE(IE-FA-2-EJ-14A ); endif
if FA-2-EJ-542 then eventree( FA-2 )=TRUE(IE-FA-2-EJ-542 ); endif
if FA-2-EJ-543 then eventree( FA-2 )=TRUE(IE-FA-2-EJ-543 ); endif
if FA-2-EJ-575 then eventree( FA-2 )=TRUE(IE-FA-2-EJ-575 ); endif
if FA-2-EJ-576 then eventree( FA-2 )=TRUE(IE-FA-2-EJ-576 ); endif
if FA-2-EY-01 then eventree( FA-2 )=TRUE(IE-FA-2-EY-01 ); endif
if FA-2-EY-10 then eventree( FA-2 )=TRUE(IE-FA-2-EY-10 ); endif
if FA-2-EY-20 then eventree( FA-2 )=TRUE(IE-FA-2-EY-20 ); endif
if FA-2-EY-30 then eventree( FA-2 )=TRUE(IE-FA-2-EY-30 ); endif
if FA-2-EY-40 then eventree( FA-2 )=TRUE(IE-FA-2-EY-40 ); endif
if FA-2-EY-50 then eventree( FA-2 )=TRUE(IE-FA-2-EY-50 ); endif
```

Table A7.3

Rules for Fire Area 3

```
if FA-3 then
      eventree(FIRE-CS)=FALSE(HSE-NOTFA3);
endif
if /FA-3 then
      eventree(FIRE)=FALSE(HSE-NOTFA3);
endif

if FA-3-EA-12 then eventree( FA-3 )=TRUE(IE-FA-3-EA-12 ); endif
if FA-3-EB-22 then eventree( FA-3 )=TRUE(IE-FA-3-EB-22 ); endif
if FA-3-EC-181 then eventree( FA-3 )=TRUE(IE-FA-3-EC-181 ); endif
if FA-3-EC-187 then eventree( FA-3 )=TRUE(IE-FA-3-EC-187 ); endif
if FA-3-EJ-1005 then eventree( FA-3 )=TRUE(IE-FA-3-EJ-1005 ); endif
if FA-3-EJ-1006 then eventree( FA-3 )=TRUE(IE-FA-3-EJ-1006 ); endif
if FA-3-EJ-1051 then eventree( FA-3 )=TRUE(IE-FA-3-EJ-1051 ); endif
if FA-3-EJ-1052 then eventree( FA-3 )=TRUE(IE-FA-3-EJ-1052 ); endif
if FA-3-EJ-9401 then eventree( FA-3 )=TRUE(IE-FA-3-EJ-9401 ); endif
```

Table A7.4

Rules for Fire Area 4

```
if FA-4 then eventree(FA-4) = TRUE(IE-FA-4);endif
if FA-4 then
      eventree(FIRE-CS)=FALSE(HSE-NOTFA4);
endif
if /FA-4 then
      eventree(FIRE)=FALSE(HSE-NOTFA4);
endif
if FA-4-EA-11 then eventree( FA-4 )=TRUE(IE-FA-4-EA-11 ); endif
if FA-4-ED-11A then eventree( FA-4 )=TRUE(IE-FA-4-ED-11A ); endif
if FA-4-EJ-9400 then eventree( FA-4 )=TRUE(IE-FA-4-EJ-9400 ); endif
```

Table A7.5

Rules for Fire Area 13

```
if FA-13-13A1 then
      eventree( FA-13 )=TRUE(IE-FA-13-13A1 );
      eventree(FA-13) = FALSE (HSE-NOTFA13A);
endif
if FA-13-13A2 then
      eventree( FA-13 )=TRUE(IE-FA-13-13A2 );
      eventree(FA-13) = FALSE (HSE-NOTFA13A);
endif
if FA-13-13B then eventree( FA-13 )=TRUE(IE-FA-13-13B ); endif
if FA-13-13C then eventree( FA-13 )=TRUE(IE-FA-13-13C ); endif
```

Table A7.6

Rules for Fire Area 23

```
if FA-23-23E then
      eventree( FA-23 ) =TRUE(IE-FA-23-23E );
      eventree (FA-23) = FALSE(HSE-NOTFA23);
      eventree (FA-23) = FALSE(HSE-NOTFA23ES);
endif
if FA-23-23S then
      eventree( FA-23 )=TRUE(IE-FA-23-23S );
      eventree (FA-23) = FALSE(HSE-NOTFA23);
      eventree (FA-23) = FALSE(HSE-NOTFA23ES);
endif
if FA-23-23W then
      eventree( FA-23 )=TRUE(IE-FA-23-23W );
      eventree (FA-23) = FALSE(HSE-NOTFA23);
endif
```

Table A7.7

Rules for Transfers to Control Room Fire Event Tree

```
| Set motor driven AFW pumps and auto start of P8B to failure
if 2HP then
|2HP = AFW-CST;
eventree(FIRE-CR)=TRUE(A-PMMG-P-8A);
eventree(FIRE-CR)=TRUE(A-PMME-P-8A);
eventree(FIRE-CR)=TRUE(A-PMMG-P-8C);
eventree(FIRE-CR)=TRUE(A-PMME-P-8C);
eventree(FIRE-CR)=TRUE(A-REMB-62-2P8B);
endif

if /2HP then
eventree(FIRE-CR)=TRUE(A-PMMG-P-8A);
eventree(FIRE-CR)=TRUE(A-PMME-P-8A);
eventree(FIRE-CR)=TRUE(A-PMMG-P-8C);
eventree(FIRE-CR)=TRUE(A-PMME-P-8C);
eventree(FIRE-CR)=TRUE(A-REMB-62-2P8B);
endif
```

Table A7.8

Rules for Transfers to Cable Spreading Room, Bus 1C and Bus 1D Fire Event Tree

```
| Set motor driven AFW pumps and P8B auto start to failure
if 2HP then
eventree(FIRE-CS)=TRUE(A-PMMG-P-8A);
eventree(FIRE-CS)=TRUE(A-PMMG-P-8C);
eventree(FIRE-CS)=TRUE(A-REMB-62-2P8B);
endif

if /2HP then
eventree(FIRE-CS)=TRUE(A-PMMG-P-8A);
eventree(FIRE-CS)=TRUE(A-PMMG-P-8C);
eventree(FIRE-CS)=TRUE(A-REMB-62-2P8B);
endif
```

Table A7.9

Rules for Aux Building and Turbine Building Fires

None

Table A7.10

Rules for Transfers to ATWS Event Tree

```
|Define Success Boundary Conditions
|
if /TTF then
/MTC = MTC-TTRIP;
MTC = MTC-TTRIP;
endif
|
|Define Failure Boundary Conditions
|
if TTF then
/MTC = MTC-NOTTRIP;
MTC = MTC-NOTTRIP;
endif
if RXC-ELEC-FAULTS then
/MTC = MTC-NOTTRIP;
MTC = MTC-NOTTRIP;
endif
```

Lucius Pitkin, Inc. *Consulting Engineers*

Advanced Analysis
Fitness-For-Service
Failure & Materials Evaluation
Nondestructive Engineering

METALLURGICAL AND FAILURE ANALYSIS OF SWS PUMP P-7C COUPLING #6

Report No. F11358-R-001
Revision 1

December, 2011

Prepared For

ENTERGY NUCLEAR OPERATIONS, INC.
PALISADES NUCLEAR PLANT

Boston Area Office, 36 Main Street, Amesbury, MA 01913
Tel: 978-517-3100 Fax: 978-517-3110 www.luciuspitkin.com

New York,NY Boston,MA Richland,WA

DOCUMENT RECORD

Document Type:	☐ **Calculation** ☒ **Report** ☐ **Procedure**	
Document No:	F11358-R-001	
Document Title:	Metallurgical and Failure Analysis of SWS Pump P-7C Coupling #6	
Client:	Entergy Nuclear Operations, Inc.	
Client Facility:	Palisades Nuclear Plant	
Client PO No:	10325528	
Quality Assurance:	**Nuclear Safety Related?** ☐ **No** ☒ **Yes**	
Computer Software Used:	☐ **No**[1] ☒ **Yes**[2]	1. Check NO when EXCEL, MathCAD and/or similar programs are used since algorithms are explicitly displayed. 2. Include Software Record for each computer program utilized
Instrument Used	☐ **No** ☒ **Yes**[3]	3. Include Document Instrument Record

Revision	Approval Date	Preparer	Checker	Design Verification	Approver[4]
0	10/17/11	S. Yim Ryan Chen (Section 4.3)	John Mills, Ph.D B. Elaidi (Section 4.3)	P. Bruck	P. Bruck
1	12/5/11	S. Yim	John Mills, Ph.D	P. Streeter	P. Bruck

[4] The Approver of this document attests that all project examinations, inspections, tests and analysis (as applicable) have been conducted using approved LPI Procedures and are in conformance to the contract/purchase order. Individual tests and inspections as documented in the attachments were performed and reviewed by various LPI personnel, not reflected in the document record.

Page	**2**	**of**	**230**	**Total Pages**	Include any Title Sheet and Attachments in page count

DESIGN VERIFICATION CHECKLIST

Document No(s)[1]:	F11358-R-001	Rev.:	1

Review Method:	X	Design Review		Alternate Calculation		Test

	Criteria	DV[2]
1	Were the inputs correctly selected and incorporated into design?	
2	Are assumptions necessary to perform the design activity adequately described and reasonable? Where necessary, are the assumptions identified for subsequent re-verifications when the detailed design activities are completed? If applicable, has an as built verification been performed and reconciled?	
3	Are the appropriate quality and quality assurance requirements specified?	
4	Are the applicable codes, standards and regulatory requirements including issue and addenda properly identified and are their requirements for design met?	N/A
5	Have applicable construction and operating experience been considered, including operation procedures?	N/A
6	Have the design interface requirements been satisfied?	
7	Was an appropriate design method used?	
8	Is the output reasonable compared to inputs?	
9	Are the specified parts, equipment, and processes suitable for the required application?	N/A
10	Are the specified materials compatible with each other and the design environmental conditions to which the material will be exposed?	N/A
11	Have adequate maintenance features and requirements been specified?	N/A
12	Are accessibility and other design provisions adequate for performance of needed maintenance and repair?	N/A
13	Has adequate accessibility been provided to perform the in-service inspection expected to be required during the plant life?	N/A
14	Has the design properly considered radiation exposure to the public and plant personnel?	N/A
15	Are the acceptance criteria incorporated in the design documents sufficient to allow verification that design requirements have been satisfactorily accomplished?	
16	Have adequate pre-operational and subsequent periodic test requirements been appropriately specified?	N/A
17	Are adequate handling, storage, cleaning and shipping requirements specified?	N/A
18	Are adequate identification requirements specified?	N/A
19	Are requirements for record preparation review, approval, retention, etc., adequately specified?	N/A
20	Has an internal design review been performed for applicable design projects? Have comments from the Internal Design Review been appropriately considered/addressed?	N/A

(1) Include any drawings developed from reviewed documents, or include separate checklist sheet for drawings
(2) Design Verifier shall initial indicating review and mark N/A where not applicable

DV Completed By:	Printed Name	Signature	Date
	P. Streeter		12/5/11

Page 1 of 1 Total Pages

Include DV Checklist and Comment Resolution sheets in page count

RECORD OF REVISION

Revision No.	Date	Description of Change	Reason
0	*	Original Issue	
1	*	Changes are denoted by a revision bar.	Incorporated comments provided in Attachment X

* See Document Record

DOCUMENT SOFTWARE RECORD (Include Separate Sheet for Each Software Package Utilized)			
1	**Computer Software Used** (Code/Version)	ANSYS Version 11.0	
2	**Software Supplier**	ANSYS, Inc.	
3	**Software Update Review**	☒ Error notices; describe: Reviewed error reports for elements used ☐ Other; describe:	
4	**Nuclear Safety Related Software**	☐ NO ☒ YES[1]	1. If YES: Hardware identification # used for execution: *Desktop Serial #: J2WTBM1* Basis for V & V: [17]
5	**Input Listing(s)**	☐ Input listing(s) attached: ☒ Not attached; identify File/Disc ID*: Coupling Pump Bearing & Bending.txt Coupling Pump Bearing.txt Coupling Pump No Bearing.txt *A CD with input listings and output data to be provided on project completion.	
6		☐ Output results attached: ☒ Not attached; identify File/Disc ID*: *A CD with input listings and output data to be provided on project completion.	
7	**Output Identifier(s)***	(see 6 above)	
	*e.g., run date/time; use for reference, as appropriate, within body of calculation		
8	**Comments**		
9	**Keywords****	SOLID45, Static	
	**For use in describing software features used in this calculation; use common terms based on software user manual.		
10	**Project Manager Name:**	S. Yim	
If computer software was used on project, complete form with required information. Update the LPI Computer Software Use List per LPI Procedure 13.1 requirements.			

DOCUMENT INSTRUMENT RECORD				
Instrument Used		**Instrument Description**	**Serial No.**	**Calibration Due Date**
1	☒	Tensile Testing Machine (120 kips)	Baldwin 37205	4/7/12
2	☒	Extensometer (1 in)	2620-824/1033	4/7/12
3	☒	Charpy Impact Tester	Satec Model SI-1K/1306	6/17/12
4	☒	Hardness Tester	Wilson 5YR/58	4/7/12
5	☒	Thermocouple	Omega 650 J/8320	7/12/12
6	☒	Caliper	Fowler 6”/7082002	6/21/12
7	☒	Magnetic Yoke	Magnaflux Y-6/43530	*Per use calibration*
8	☒	Caliper	Starrett 6”/09324754	6/24/12
9	☒	Caliper	Mitutoyo 12”/06535451	6/21/12
10	☒	Caliper	VME 6”/2-12005	6/21/12
11	☒	SEM/Oxford EDS	17218-118-01	*Per use calibration*
12	☐			
13	☐			
14	☐			
	Project Manager Name:	S. Yim		

For instrument(s) used on the project, identify instrument and include the instrument calibration due date.
Update the LPI *Instrument Use List* per LPI Procedure 13.1 requirements.

TABLE OF CONTENTS

LIST OF ATTACHMENTS

LIST OF FIGURES

LIST OF TABLES

1.0 INTRODUCTION/BACKGROUND

Two failed Type 416 stainless steel (SS) couplings along with other intact couplings and shafts extracted from service of the Service Water System (SWS) pumps at Palisades Nuclear Plant (PLP) were submitted to **LPI** (Lucius Pitkin, Inc.) for material and failure assessment, as documented in the receipt inspections provided in Attachment B. One of the two failed couplings was from a failure event in September 2009 as documented in CR-PLP-2009-04519 [1][1] and the other was from a failure event in August 2011 as documented in CR-PLP-2011-03902 [2]. The failed couplings from the 2009 and 2011 failure events are herein referred to as "09-P7C-7F" and "11-P7C-6F", respectively (refer to coupling identification convention in Section 2.1). Photographs of couplings 09-P7C-7F[2] and 11-P7C-6F are presented in Figure 1-1 and Figure 1-2, respectively. The majority of intact couplings (22 in total) and two (2) shafts were from all three SWS pumps following the 2011 failure event and remaining couplings (3 in total) were extracted from pump P-7C following the 2009 event.

The SWS is comprised of three motor driven vertical multistage pumps, tagged P-7A, P-7B and P-7C, supplying water from Lake Michigan to three service water headers. All three SWS pumps are similar in design in that they are comprised of two stage stainless steel impellers coupled to the motor by six line shafts, a packing shaft and a motor shaft for a total height of over forty (40) feet from suction to discharge. Figure 1-3 shows the shaft and coupling arrangement for the SWS pumps and identifies the location of couplings 09-P7C-7F and 11-P7C-6F. As can be seen in Figure 1-3, 09-P7C-7F is coupling #7 and 11-P7C-6F is coupling #6 in the assembly. A rendering that identifies the pump components (excluding the motor) is provided in Figure 1-4.

P-7A and P-7C are Layne and Bowler Model 25RKHC pumps while P-7B is a Johnston Model 25NMC pump. Each pump is driven by a 350 horsepower (HP) motor providing a rated 8000 GPM at 140 ft total developed head (TDH), which is 50% of the service system capacity [1].

The specified material of all shaft couplings on the three SWS pumps, including 09-P7C-7F and 11-P7C-6F, was ASTM A582 Type 416 stainless steel (SS) [4]. The material specification for the shaft couplings on all three pumps was changed from carbon steel to 416 SS and specified with a Rockwell C hardness (HRC) value of 28 to 32 under engineering change EC-50000121762 [4] in December

[1] Numbers in brackets (e.g. [5]), indicate references listed in Section 6.0.
[2] Only the bottom half or impeller end of 09-P7C-7F was available for examination. The other half had been utilized in support of failure analysis in 2009.

2007. The couplings were also redesigned to incorporate an alignment hole that allows verification of proper shaft installation. The shaft couplings for P-7A were replaced on April 4, 2009 per Work Order (WO) 51637416 (see [2]). The shaft couplings for P-7C were replaced on June 12, 2009. The shaft couplings on P-7B were replaced during a rebuild of the pump and installed in June of 2010 [2]. A detailed drawing of the line shaft coupling is provided in Figure 1-5.

1.1 Scope and Purpose

The scope and purpose of this report is to provide results of the metallurgical examination and tests performed in accordance with LPI Procedure F11358-P-001 [5], and provide a probable root cause of the 2011 coupling failure. The scope of tests and examinations performed are provided in the Table 1-1 Test Matrix.

Table 1-1: Test Matrix

Test/Exam	Couplings			
	2011			2009
	P-7C	P-7B	P-7A	P-7C
Visual & Photographic	1 thru 8	4 thru 7	4 thru 7	
Surface Hardness	1 thru 8	4 thru 7	5 thru 7	7
Dimensional Exam	1 thru 8	4 thru 7	4 thru 7	
Comp Analysis of Surface Deposits	6 and 7			
MT Exam	4 thru 7	4 thru 7	4 thru 7	
Tensile Test	5 thru 7	5 thru 7	5 thru 7	
CVN Test	5 thru 7	5 thru 7	5 thru 7	7
Thru Thick Hardness	5 thru 7	5 thru 7	5 thru 7	7
Comp Analysis	5 thru 7	5 thru 7	5 thru 7	
Metallography	6 and 7	5 thru 7	6	
SEM	6			7

1.2 Evaluation Timeline

This section discusses the evaluation and testing timeline of the above scope. Coupling 11-P7C-6F failed on August 9th, 2011. Following the failure, LPI was contracted by Entergy's PLP to provide metallurgical and failure assessment of failed coupling 11-P7C-6F and provide on-site metallurgical support to the root cause evaluation (RCE) team. LPI received couplings 11-P7C-6F, -5, -7K, and shaft 5 and 6 from P-7C as documented in LPI receipt inspection dated 8/17/11. On 8/17/11 following visual examination of 11-P7C-7F, LPI provided a preliminary verbal assessment of the failure mechanism as being typical of stress corrosion cracking (SCC). Based on this preliminary observation, LPI recommended that in the short term PLP should consider replacing (at a minimum) couplings subjected to wet/dry cycles (i.e. couplings 5, 6, and 7) on pumps P-7A and P-7B with available spare couplings. For the long term, LPI advised that a permanent replacement material should be investigated for the service environment but suggested Nitronic 50 or AL-6XN as possible replacement material for the subject SWS pump couplings. The verbal assessment and recommendation were directed to the RCE team and the NRC's special inspection team (SIT).

On 8/18/11, LPI received coupling 09-P7C-6F and remaining couplings 11-P7C-1 through -4 and 11-P7C-8 for testing and evaluation. On 8/19/11, LPI issued two (2) preliminary interim reports, F11358-IR-002 which summarized the finite element analysis model of a typical coupling and F11358-IR-003, which summarized the VT and MT findings of couplings 11-P7C-5, -6F and -7K and hardness testing of 11-P7C-6F. On 8/23/11, Revision 0 of F11358-IR-003 was transmitted to PLP via LPI letter F11358-L-003. F11358-IR-003 summarized the VT, MT, and hardness values of couplings 11-P7C-5, -6F and -7K and Charpy results of couplings 11-P7C-5 and -6F. Based on these results, PLP implemented plans to replace the existing 416 SS couplings on P-7A and P-7B with 17-4PH recommended in [19].

On 8/24/11, the 416SS couplings on P-7A were replaced with 17-4PH couplings. LPI received extracted couplings 11-P7A-1 through -8 on 8/30/11, as documented in the receipt inspection in Attachment B. Preliminary LPI F11358-IR-004 was issued on 9/1/11 which summarized the VT, MT, hardness, tensile and CVN impact test results.

On 8/31/11, the 416SS couplings on P-7B were replaced with 17-4PH couplings. LPI received extracted couplings 11-P7B-4 through -7 on 9/2/11. Preliminary LPI F11358-IR-005 was issued on 9/12/11 which summarized the VT, MT, hardness, and tensile test results.

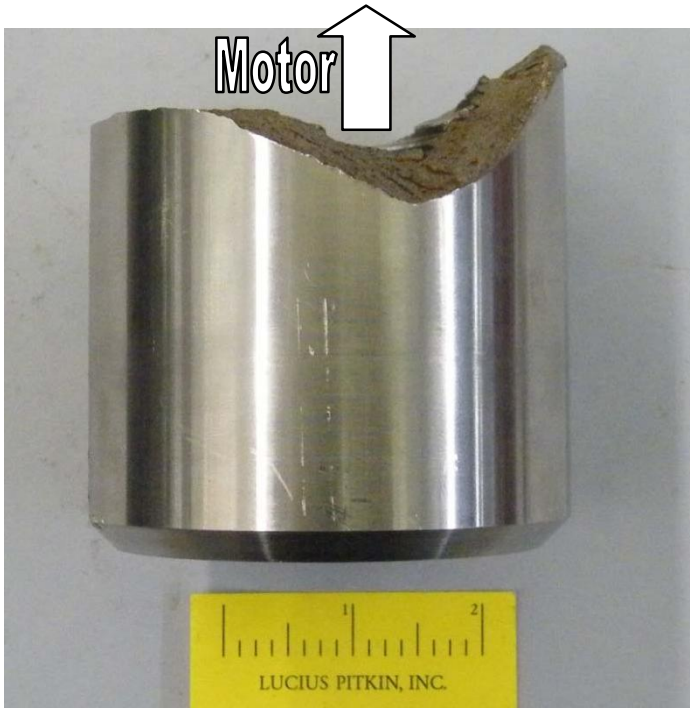

Elevation View

Top View

Figure 1-1: As-Received 09-P7C-7F

(Only the bottom half or impeller end of 09-P7C-7F was available. Scale in units of inches; typical throughout)

Figure 1-2: As-Received 11-P7C-6F

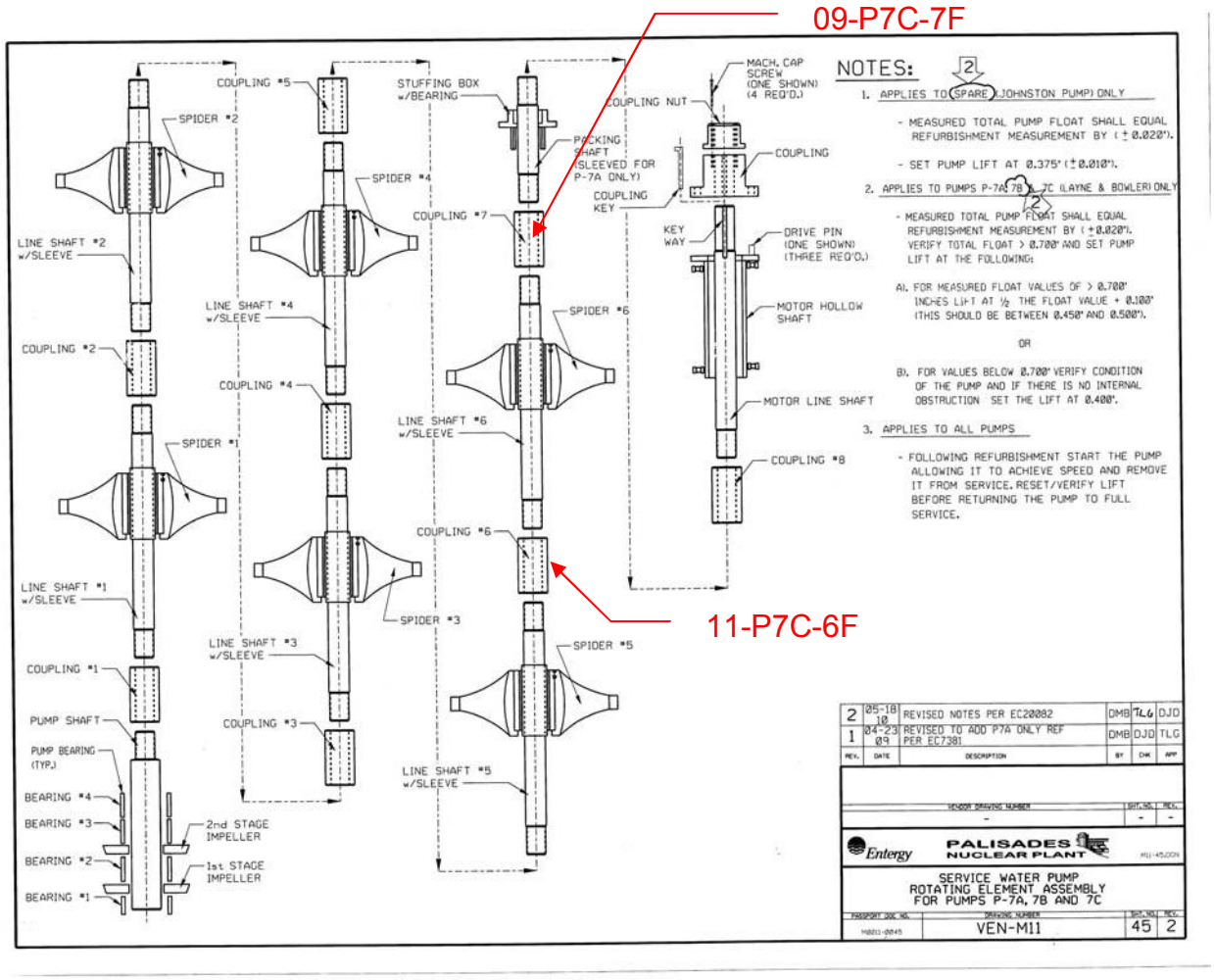

Figure 1-3: SWS Pumps Shaft Assembly [3b]

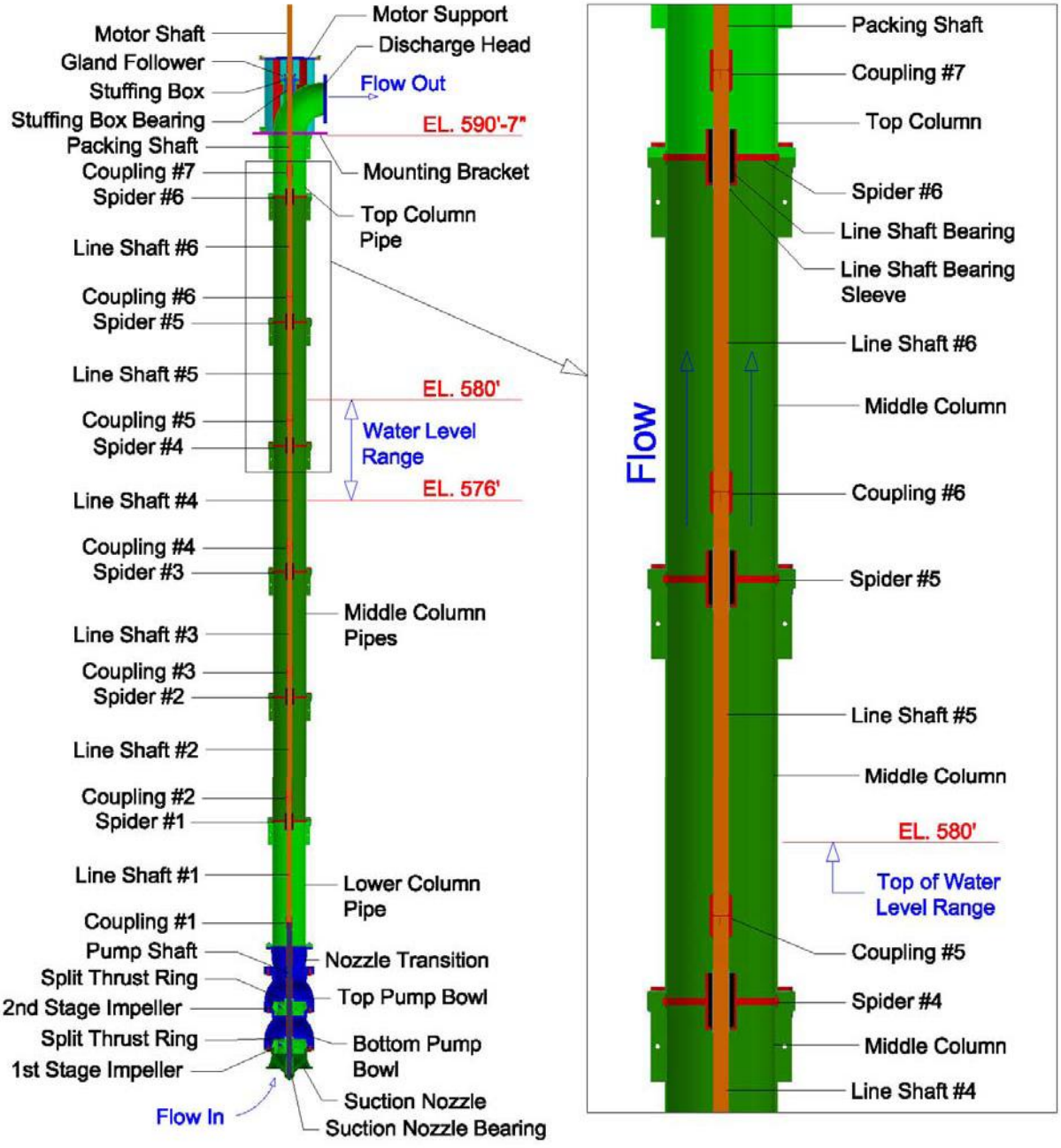

Note: Spider refers to intermediate shaft guidance bushing.

Figure 1-4: PLP SWS Pump Rendering

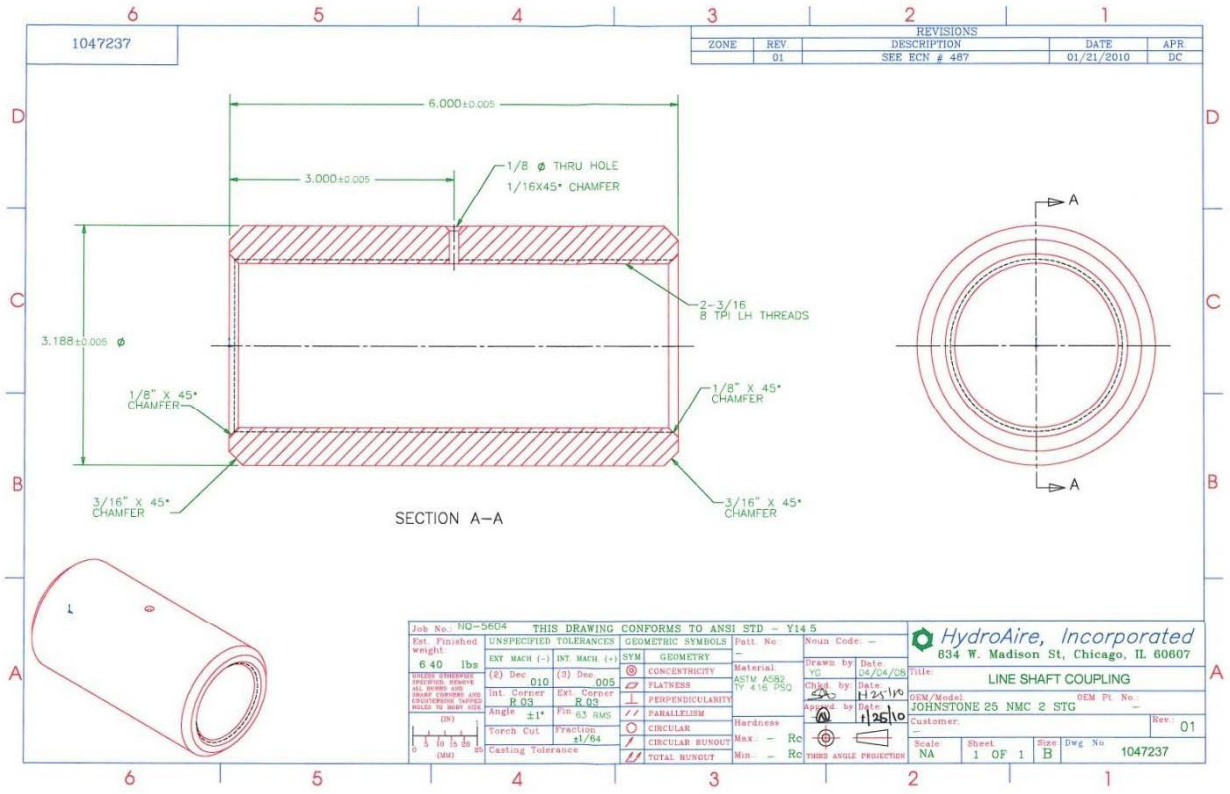

Figure 1-5: Coupling Drawing [20]

2.0 INPUTS/ASSUMPTIONS

The following inputs and assumptions are utilized for this report. Inputs and assumptions requiring verification are identified as such.

2.1 Inputs

1. Specified hardness for the couplings is in the range of 28 to 32 HRC [4].
2. Coupling loads are taken from [15] with hydraulic thrust equal to 8000 lb, torque of 18,694 lb-in and preload of 42,335 lb.
3. Table 2-1 summarizes the SWS pump coupling service history at time of extraction.
4. Based on data provided by PLP and presented in Figure 2-3, the service water basin elevation ranged from 576 ft to 580 ft for the period from January 2009 to August 2011. For the same period, the water temperature ranged from 32°F to 76°F.
5. The SWS pumps are vertical turbine pumps that take suction from the bottom and discharges through the column and out the discharge header pipe. Therefore, line shafts, couplings and components below the stuffing box are exposed to service water when the pumps are on. Based on the service water basin elevation, couplings 1 through 4 are constantly submerged and couplings 5 through 7 are subjected to wet and dry cycles depending on pump state (i.e. on or off). Also depending on water elevation, coupling 5 may be submerged when the pump is off. Refer to Figure 1-4 for a sketch of the service water pump with illustration of water flow and relationship of couplings to basin water elevation variations.
6. The convention used in this report to reference couplings is as follows:

   YY-Pump-CN with Optional F or K

   Where:

   YY= two digit year when coupling was extracted from pump.

   Pump = P7A, P7B or P7C

   CN = Coupling Number

   Optional F = Identifies a coupling that has failed.

   Optional K = Identifies a coupling that exhibits a crack.

   For example: 09-P7C-7F is the failed coupling extracted from Pump 7C in 2009.

2.2 Assumptions

1. There are no assumptions utilized in this report.

Table 2-1:SWS Pump Coupling Life

Pump	Date Installed	Date Extracted	Installed Time (hrs)	Run Time (hrs)	Start/Stops	Notes
P-7A	4/4/09	8/28/11	21,024	16,259	148	1
P-7B	5/12/10	9/1/11	11,391	9,073	70	2
P-7C	6/12/09	9/29/09	2,616	2,414	13	3
P-7C	10/1/09	8/8/11	16,224	14,115	95	4

Notes:

1) Run hours and stops and starts based on total presented in Palisades response to NRC RFI 43 [6] plus average monthly hours from 4/10 to 9/10 times 6 months.
2) Information provided in Figure 2-1.
3) Information provided in Figure 2-2.
4) Run hours and stops and starts based on total presented in Palisades response to NRC RFI 43 [6].

Sontra Yim

From: DeBusscher, Derek [ddebuss@entergy.com]
Sent: Wednesday, September 28, 2011 8:02 AM
To: Sontra Yim
Cc: Forehand, James M
Subject: RE: Palisades comments on LPI report F11358-LR-001
Attachments: RFI 43 Response.doc

Sontra,

P-7B was put into service with the new couplings on 5/12/10 as stated by the WO 20082. From that date I calculated the approximate run time hours to be 9072.5 and the pump start/stops to be 70 since that time. Total installed hours are approximated 11,391 hrs.

I have attached the RFI that was reviewed. Note that the times only include up to 8/9/11. P-7B ran for 703 hrs during August (not 204), and had one additional start.

If there is any other information you need please let me know so we can get this minor issue hashed out as soon as possible.

Thanks.

Derek DeBusscher
BOP Systems Engineering
Palisades Nuclear Power Plant
269-764-2997
ddebuss@entergy.com

Figure 2-1: P-7B Run Time

Data Source: Palisades PI Datalink

Time Start:	6/12/09 0:00	*Update highlighted cells and click "Update Sheet" button.*	Update Sheet (must have PI add-in installed)	
Time Stop:	10/1/09 0:00			
	Service Water Pump P-7C	**None**	**None**	
Total Run Time:	**2414.44**	**hrs**		
	6/12/09 12:22	Started		
1	6/12/09 12:23	Stopped		
	6/12/09 15:03	Started		
2	6/12/09 15:33	Stopped		
	6/12/09 15:34	Started		
3	6/19/09 3:44	Stopped		
	6/19/09 16:17	Started		
4	7/17/09 10:52	Stopped		
	7/17/09 11:42	Started		
5	7/17/09 12:02	Stopped		
	7/17/09 13:22	Started		
6	7/23/09 5:03	Stopped		
	7/23/09 9:04	Started		
7	8/8/09 21:38	Stopped		
	8/8/09 21:39	Started		
8	8/13/09 3:55	Stopped		
	8/13/09 3:56	Started		
9	8/28/09 10:40	Stopped		
	8/28/09 10:41	Started		
10	9/2/09 13:06	Stopped		
	9/9/09 11:15	Started		
11	9/22/09 20:32	Stopped		
	9/22/09 23:38	Started		
12	9/29/09 7:34	Stopped		
	9/29/09 7:35	Started		
13	9/29/09 9:11	Stopped		
14				

Figure 2-2: P-7C Run Time

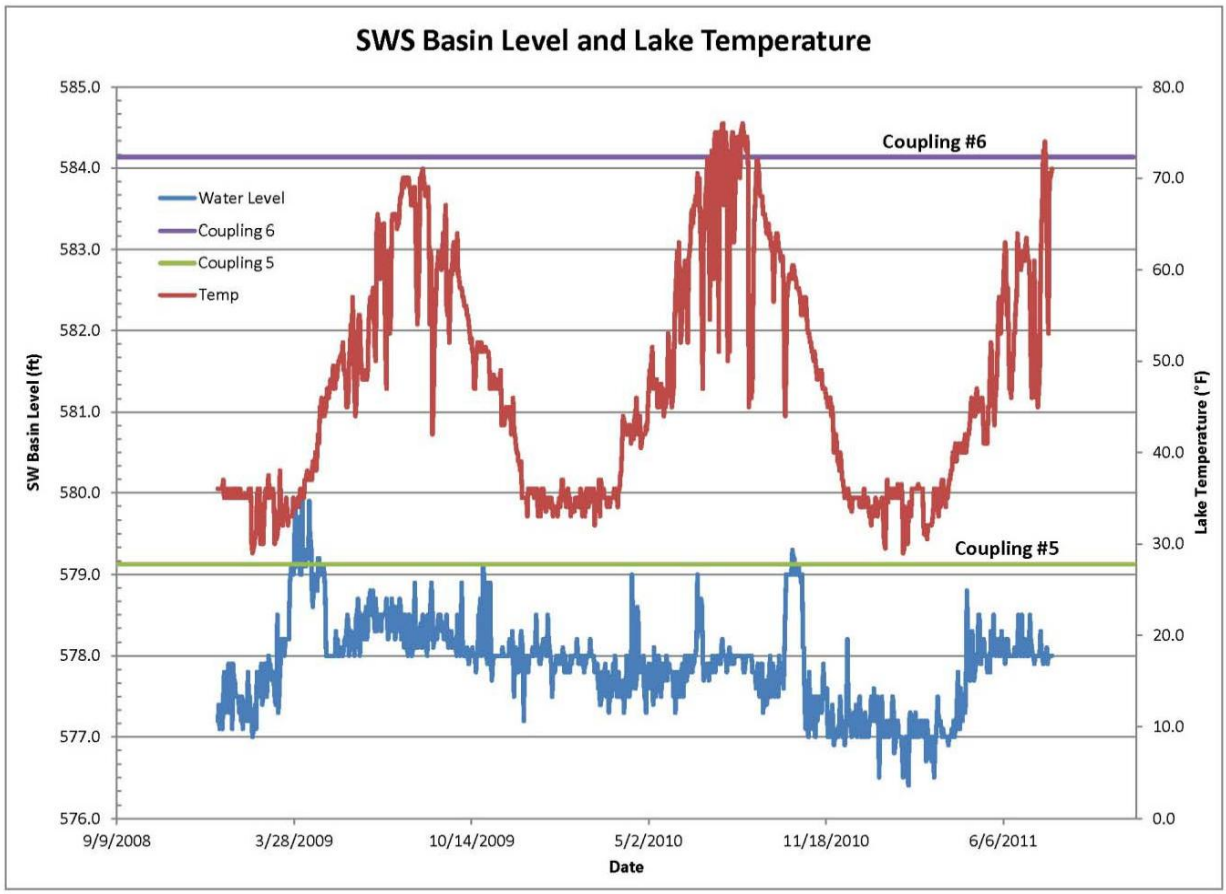

Figure 2-3: SWS Basin Level and Lake Temp Data

3.0 TESTING AND EXAMINATION

The submitted components, including couplings 09-P7C-7F and 11-P7C-6F, were examined and tested in accordance with LPI Procedure F11358-P-001 [5] and the Test Matrix presented in Table 1-1. The result of testing and examination is discussed in the following sections.

3.1 Visual and Stereomicroscopic Examination

3.1.1 P-7C Components

3.1.1.1 2011 Intact Couplings

In all, seven (7) intact couplings (#1 through 5, 7 and 8), disassembled from pump P7C following failure of 11-P7C-6F, were shipped to LPI for examination. Couplings were labeled to indicate the orientation of shafts that connected to the respective coupling. A representative example of an intact coupling is shown in Figure 3-1. The outer diameter of each intact coupling exhibited wrenching marks, which likely occurred during removal of the couplings. Indentations, which are evidence of previously performed hardness tests, were present on both the outer diameter and ends of many couplings with values written adjacent to the indentations of coupling 11-P7C-7 (see Figure 3-2).

Each coupling exhibited a single alignment hole at its center, 0.125 in. in diameter. The coupling ends were chamfered at 45° on both outer (0.187 in.) and inner diameters (0.125 in.). The inner diameter of each coupling is fully threaded.

Visual examination of received intact couplings did not reveal significant signs of corrosion or degradation on the exterior surfaces (unthread surfaces). Some corrosion deposits were noted near the 1/8” diameter alignment hole and at the ends of some intact couplings, however not to the degree exhibited on coupling 11-P7C-6F.

3.1.1.2 Coupling 11-P7C-6F

The fracture surface of 11-P7C-6F is located near the mid-length of the coupling. The fracture surface on the impeller end of coupling 11-P7C-6F was sectioned for analysis, as shown in Figure 3-5. Approximately half of the fracture surface exhibited a smooth “flat” appearance and was aligned perpendicular to the coupling axis. The flat fracture surfaces occur in two regions that both display an elliptical shape emanating from the thread root at the inner diameter and extending to the outer diameter, as shown in Figure 3-5. The elliptical features are typically

associated with cracks that initiate at the thread root (and in this case propagated from the inner to the outer diameter of the coupling). The remaining portion of the fracture surface consisted of slanted fracture, indicating an overload event. The overload event occurred after the flat fractures propagated through the wall thickness.

The thread roots exhibited red/brown corrosion products, as shown in Figure 3-6. Corrosion deposits are visually apparent on the facture surfaces, threads and at the alignment hole of coupling 11-P7C-6F. The corrosion deposit streak at the bottom of the 1/8" diameter shaft alignment hole suggests that the coupling underwent wet and dry cycles (Figure 3-6).

The tips of fracture surfaces on both pieces of fractured coupling 11-P7C-6F exhibited signs of impact from mechanical contact, likely occurring post failure.

3.1.1.3 Coupling 09-P7C-7F

Fractured coupling 09-P7C-7F measured between 2.06" to 3.43" in length. Visual examination of coupling 09-P7C-7F revealed similar fracture surface characteristics to 11-P7C-6F. The fracture surface has a relatively flat region with an elliptical shape emanating from the thread root and extending to the outer diameter (see Figure 3-3). The elliptical feature reveals that the crack initiated at the thread root and propagated to the outer diameter. The remaining portion of the fracture surface was slanted, which indicates a subsequent overload of the remaining ligament. Corrosion deposits are also evident on the facture surface.

3.1.1.4 2011 Shafts

Two shafts (shaft #5 and 6) from pump P-7C were shipped to LPI for visual examination (see 8/17/11 receipt inspection in Attachment B). Visual examination of shaft #5 and #6 showed damage on the ends coupled by coupling 11-P7C-6F (see Figure 3-7). It is postulated that this damage was most likely caused after the initial failure of coupling 11-P7C-6F by repeated impact between the fractured coupling and the shaft ends. This postulate is supported by the blunted fracture surfaces exhibited on the 11-P7C-6F halves.

3.1.2 Couplings from P-7A

Visual inspection of as-received P-7A pump couplings 11-P7A-4 through -7 identified the threads to be well coated with Neolube. A photograph of the as-

received coupling 11-P7A-7 is provided in Figure 3-8. No significant signs of corrosion or degradation on the exterior of couplings were observed. This was in contrast to observations of the P-7C couplings in the as-received condition, where lubricant was not observed to be as well coated on the threads. A comparison of this is shown in Figure 3-9.

Visual inspection of the as-split P-7A couplings revealed them to be well coated with Neolube. The mid section of the couplings contained little to no corrosion products, however some sand-like deposits were present within the middle two-to-three threads of the couplings. The split and cleaned couplings, in preparation for MT, did not reveal any visible indications, as shown in Figure 3-10 for 11-P7A-5.

3.1.3 Couplings from P-7B

A photograph of the as-received couplings 11-P7B-4 through 11-P7B-7 are shown in Figure 3-11. Visual examination of these intact couplings revealed wrench marks on the exterior of all couplings and the presence of Neolube on the interior threads of couplings 11-P7B-5 to -7. No significant signs of corrosion or degradation on the exterior of couplings were observed. The interior of 11-P7B-4 appeared to have been cleaned in the as-received condition.

Couplings 11-P7B-4 though 11-P7B-7 were split longitudinally for fluorescent magnetic particle inspection (MT). The as-split coupling 11-P7B-4 appeared to have been cleaned and exhibited a dye liquid penetrate residue on the threads (see Figure 3-12). The presence of the liquid penetrate on the thread surface is consistent with efforts by Palisades to examine this coupling for possible re-use due to procurement issues with the replacement couplings fabricated from 17-4PH material. As-split couplings 11-P7B-5 through 11-P7B-7 are shown in Figure 3-13 through Figure 3-15. Neolube is present on the threaded surfaces of coupling 11-P7B-5 to 11-P7B-7. However, an apparent band of corrosion product was observed at the center two-to-three threads of couplings 11-P7B-6 and 11-P7B-7. Coupling 11-P7B-5 also exhibited some corrosion at the center threads but not to the extent of couplings 11-P7B-6 and 11-P7B-7. A layer of sand-like material was also present over the corrosion products.

3.2 Dimensional Examination

A dimensional examination of couplings was performed and presented in Table 3-1. Measurements of wall thickness (from the outer diameter to the thread crown) of couplings to evaluate eccentricity are given in Table 3-2.

The dimensioning scheme is shown in Figure 3-4. All intact couplings (i.e. those that did not fail) were found to have outside dimensions within the specified dimensions and tolerances of HydroAire drawing 1047237 [20].

Coupling 11-P7C-6F was received in two halves that each exhibited a circumferential fracture surface. The bottom half (impeller end) of 11-P7C-6F measured between 3.03" and 4.29" in length. The top half (motor end) of the same coupling measured between 1.200" and 3.148" in length.

3.3 Magnetic Particle Examination (MT)

Fluorescent magnetic particle testing (MT) was used to determine if intact couplings contained cracks or other discontinuities. MT was performed on all intact couplings exposed to wet and dry cycles (coupling Nos. 5, 6, and 7) and coupling #4 which is always submerged for all three service water pumps. Couplings were split longitudinally to facilitate access to the inner diameter threaded region for MT inspection. Result of the inspections is provided in Attachment D.

3.3.1 P-7C Couplings

3.3.1.1 Coupling 11-P7C-6F

Visible cracks in coupling 11-P7C-6F were readily observed upon MT examination, as shown in Figure 3-16. The nearly 45 degree MT indication is consistent with torsional loading of the coupling.

3.3.1.2 Intact Couplings 11-P7C-4, -5, and -7

MT did not reveal any indications on couplings 11-P7C-4 and 11-P7C-5. MT revealed an indication, observed as a well-defined bright fluorescent line, at the thread root near the shaft alignment hole of coupling 11-P7C-7K, as shown in Figure 3-17. The MT indication in coupling 11-P7C-7K is approximately 0.86" in length and located along a thread root. At the sectioned location, the indication is a quarter through the thickness.

3.3.2 P-7A Couplings

Following cleaning, couplings 11-P7A-4 through 11-P7A-7 were MT inspected. No indications of linear flaws were observed from the MT inspection of couplings 11-P7A-4 through 11-P7A-7.

3.3.3 P-7B Couplings

Following cleaning, couplings 11-P7B-4 through 11-P7B-7 were MT inspected. MT inspection of couplings 11-P7B-4 through 11-P7B-7, revealed indications at the center (location of corrosion products) of couplings 11-P7B-

5, 11-P7B-6 and 11-P7B-7. Figure 3-18 presents photographs highlighting the crack at the center of 11-P7B-7K revealed by MT. Two relatively small indications were also found at the motor end of coupling 11-P7B-5. No indication was found on coupling 11-P7B-4.

A summary of the as-found crack dimensions on MT inspected couplings is provided in Table 3-3.

3.4 Metallography

Longitudinal specimens were prepared from the coupling material, mounted in plastic, ground, polished, and etched for metallographic examination. General views of the microstructure for one coupling from each pump are shown in Figure 3-19. The microstructure shows prior austenite grain boundaries with colonies of commonly oriented martensite lath inside the grains. This structure is characteristic of a martensitic stainless steel.

Longitudinal specimens were prepared through cracks from fractured and cracked couplings, mounted in plastic, ground, polished, and etched for metallographic examination. Metallographic images are shown in both the as-polished and etched conditions, as shown in Figure 3-20. All cracks displayed a similar appearance of a branching network of cracks along the prior austenite grain boundaries, which is characteristic of intergranular stress corrosion cracking (IGSCC). This cracking mechanism is common for martensitic stainless steels exposed to chloride-containing aqueous and other corrosive environments.

From the metallographic images in Figure 3-20, it appears that IGSCC cracks originate from pits. The thread roots of coupling Nos. 4 to 7 for all pumps were visually examined by stereomicroscopy for pitting. It was observed that pitting occurred at the thread roots of couplings that exhibited cracks, as shown in Figure 3-21. Couplings without cracks exhibited some general corrosion, however contained no readily observable pitting. A representative image of a P-7A coupling showing general corrosion but no pitting at the thread root is presented in Figure 3-22.

3.5 Scanning Electron Microscopy

The fracture surface morphology and composition of the corrosion product were evaluated for the two fractured couplings, 09-P7C-7F and 11-P7C-6F.

The fracture surfaces of 11-P7C-6F and 09-P7C-7F were examined in a scanning electron microscope (SEM) to evaluate the crack initiation and propagation mechanism. Deposits on the fracture surfaces of couplings 11-P7C-6F and 09-P7C-7F were analyzed by energy dispersive x-ray spectroscopy (EDS) in the SEM. As shown in Figure 3-23, the spectrum contained large peaks for iron, chromium, manganese, and silicon from corrosion products of the base material. The high chromium level in the spectrum, shown in Figure 3-23, is likely attributed to a local concentration of chromium carbides in the X-ray sampling volume. An additional EDS spectrum, taken over a larger area of the fracture surface, is provided in Figure 3-24. Also exhibited was a large peak for oxygen and smaller peaks of chlorine and sulfur, indicating the presence of oxides, chlorides and sulfur species. Chlorides and sulfides from the environment are known to cause corrosion and SCC in martensitic stainless steels.

The fracture surface was cleaned in an ultrasonic bath containing an acetone/methanol mixture prior to examination in a SEM at 20 kV accelerating potential. SEM examination revealed the fracture surface morphology to exhibit a rock-candy appearance, characteristic of intergranular stress corrosion cracking (IGSCC), as shown in Figure 3-25. This cracking mechanism is common for martensitic stainless steels exposed to chloride-containing aqueous and other corrosive environments.

3.6 Physical and Mechanical Properties

3.6.1 Tensile Test

Tensile specimens were prepared from couplings as indicated in the Test Matrix (Table 1-1). The results of the tensile test on the specimens are included in Attachment F and summarized in Table 3-4. The tensile test results were in the approximate range for Type 416 stainless steel with an intermediate temper based on specified hardness values in ASTM A582 [7]. Yield strength values ranged from 108 to 142 ksi and the elongation ranged from 12.8 to 17.9 %.

3.6.2 Composition of Base Metal

The base metal compositions of all couplings within the Test Matrix (Table 1-1) were evaluated by chemical analysis and the results are provided in Table 3-5. The results indicate that the chemical composition of all tested couplings conform to the chemical requirements of ASTM A582 Type 416 stainless steel [7].

3.6.3 Hardness Surveys

Surface hardness surveys were performed in accordance with the requirements of ASTM E18-07 [8] with the results presented in Attachment E and summarized in Table 3-6. Unless otherwise noted, surface hardness was measured on the ends (motor and impeller ends) of each coupling.

Through thickness hardness of couplings extracted in 2011 were measured near the center of each coupling from the outer diameter (OD) to the inner diameter (ID) of tested couplings at two diametrically opposite locations. Hardness measurements on coupling 09-P7C-7F were taken at the mid-wall along the length of the coupling from the center to the end of the coupling. Results of the through thickness Rockwell C hardness measurements are presented in Table 3-7.

3.6.4 Charpy V-Notch (CVN) Impact Testing

Charpy V-Notch (CVN) impact test specimens with radial notches facing the inner diameter were machined and tested in accordance with ASTM Standard E23 [10] over a temperature range of 32°F to 152°F. Results of impact testing are given in Table 3-8.

Table 3-1: Measurement of Coupling Outside Dimensions

Coupling	Length (in.)	OD (in.)
11-P7C-1	6.000	3.186
11-P7C-2	6.002	3.190
11-P7C-3	5.998	3.187
11-P7C-4	5.995	3.189
11-P7C-5	6.000	3.187
11-P7C-6F	(a)	3.186
11-P7C-7	5.997	3.187
11-P7C-8	5.998	3.187
09-P7C-7F	(b)	3.187
11-P7A-4	6.000	3.187
11-P7A-5	5.999	3.189
11-P7A-6	6.000	3.188
11-P7A-7	6.000	3.188
11-P7B-4	5.995	3.189
11-P7B-5	5.996	3.189
11-P7B-6	6.001	3.188
11-P7B-7	6.000	3.188

Notes: (a) coupling 11-P7C-6F was fractured near the center of the length and measurements of fractured pieces are described in the text, (b) only one half of the fractured coupling 09-P7C-7F was sent to LPI and the measurements of this piece of coupling are described in the text.

Table 3-2: Measurement of Coupling Wall Thickness

Coupling	Wall thickness (Motor End)				Wall Thickness (Impeller End)			
	t_1	t_2	t_3	t_4	t_1	t_2	t_3	t_4
11-P7C-1	0.566	0.566	0.565	0.567	0.568	0.566	0.565	0.566
11-P7C-2	0.567	0.568	0.567	0.569	0.566	0.565	0.567	0.567
11-P7C-3	0.567	0.567	0.568	0.567	0.571	0.566	0.570	0.569
11-P7C-4	0.574	0.567	0.569	0.569	0.568	0.569	0.571	0.569
11-P7C-5	0.571	0.570	0.570	N/A	0.568	0.570	0.572	N/A
11-P7C-6F (a)	N/A	N/A	N/A	N/A	N/A	0.568	0.569	N/A
11-P7C-7	0.572	0.571	0.569	0.568	0.568	0.570	0.569	0.570
11-P7C-8	0.563	0.566	0.567	0.567	0.567	0.566	0.564	0.566
09-P7C-7F (b)	N/A	N/A	N/A	N/A	0.569	0.569	0.568	0.567
11-P7A-4	0.565	0.567	0.567	0.567	0.568	0.567	0.567	0.568
11-P7A-5	0.566	0.566	0.566	0.567	0.568	0.568	0.566	0.567
11-P7A-6	0.566	0.567	0.566	0.566	0.568	0.567	0.567	0.567
11-P7A-7	0.568	0.568	0.567	0.566	0.567	0.568	0.568	0.568
11-P7B-4	0.568	0.569	0.571	0.569	0.568	0.568	0.568	0.568
11-P7B-5	0.566	0.567	0.567	0.567	0.568	0.566	0.566	0.568
11-P7B-6	0.569	0.568	0.568	0.567	0.568	0.569	0.568	0.567
11-P7B-7	0.565	0.566	0.566	0.566	0.566	0.566	0.567	0.567

Notes: (a) the top portion of fractured coupling No. 6 was not removed from shaft, (b) only the bottom half of fractured coupling 09-P7C-7F was available.

Table 3-3: MT Detected Crack Dimensions

Coupling	Crack Location	Crack Length Along Thread Root (in.)	Crack Depth (in)
11-P7C-7K	Center	0.86	0.125
11-P7B-5K	Center	1.25	0.065
	Motor End	0.25 and 0.19 (a)	0.02
11-P7B-6K	Center	0.50	0.132
11-P7B-7K	Center	0.50	0.043

Note (a): These two indications were located close to each other and toward the motor end of the coupling. All other indications were found at the center of couplings.

Table 3-4: Tensile Test Results

Coupling	Specimen Identification	Yield Strength (ksi)	Tensile Strength (ksi)	Elongation (%)
11-P7C-5	5-1	134	148	17.9
	5-2	131	147	16.2
11-P7C-6F	6-1	139	155	16.7
	6-2	142	155	15.7
11-P7C-7K	7-1	138	151	13.3
	7-2	137	152	15.5
11-P7A-5	A5-1	132	146	14.1
	A5-2	136	153	14.6
11-P7A-6	A6-1	112	126	16.2
	A6-2	108	123	16.1
11-P7A-7	A7-1	136	151	12.8
	A7-2	136	150	15.4
11-P7B-5K	5-1	118	136	17.9
	5-2	118	136	14.6
11-P7B-6K	6-1	131	144	14.2
	6-2	126	140	15.2
11-P7B-7K	7-1	114	129	17.3
	7-2	115	129	16.5

Table 3-5: Metal Composition of Couplings (Wt. %)

	Element								
Standard	**C**	**Cr**	**Cu**	**Mn**	**Mo**	**Ni**	**P**	**S**	**Si**
ASTM A582 TP 416 [7]	0.15 max	12.00 – 14.00	ns	1.25 max	0.60 max	ns	0.060 max	0.15 min	1.00 max
Couplings									
11-P7C-5	0.1	12.93	0.16	1.09	0.03	0.14	0.007	0.51	0.23
11-P7C-6F	0.12	12.9	0.16	0.85	0.03	0.14	0.015	0.36	0.23
11-P7C-7K	0.11	12.92	0.16	0.68	0.03	0.14	0.02	0.34	0.25
09-P7C-7F	0.12	12.38	0.12	1.13	0.05	0.19	0.041	0.32	0.46
11-P7A-5	0.14	13.06	0.071	0.74	0.07	0.22	0.018	0.35	0.42
11-P7A-6	0.10	12.16	0.077	0.83	0.12	0.43	0.021	0.22	0.34
11-P7A-7	0.13	12.97	0.073	0.65	0.06	0.22	0.017	0.35	0.42
11-P7B-5K	0.13	12.1	0.082	0.72	0.08	0.28	0.02	0.37	0.37
11-P7B-6K	0.12	12.0	0.079	0.7	0.078	0.27	0.02	0.29	0.37
11-P7B-7K	0.12	12.0	0.078	0.72	0.078	0.27	0.02	0.34	0.37

ns – not specified

Table 3-6: Surface Hardness Survey of Couplings

Coupling	End	Average (HRC)	Measurements (R_C)
11-P7C-1	top	30.5	30.1, 30.6, 30.2, 30.4, 30.7, 31.1
	bottom	27.3	29.1, 29.8, 25.0, 26.0, 26.1, 27.7
11-P7C-2	top	27.6	29.7, 25.5, 27.0, 30.2, 25.9, 27.1
	bottom	27.0	25.8, 26.0, 27.6, 27.5, 29.0, 26.0
11-P7C-3	top	27.9	26.5, 28.0, 26.0, 28.6, 29.8, 28.2
	bottom	31.3	32.1, 31.5, 32.0, 29.9, 31.0, 31.0
11-P7C-4	top	31.5	30.0, 33.6, 29.4, 31.5, 30.6, 33.8
	bottom	30.8	29.7, 28.1, 30.8, 31.8, 32.1, 32.1
11-P7C-5	top	29.7	31.1, 29.6, 29.6, 30.0, 29.0, 29.0, 29.1, 30.0
	bottom	29.6	28.9, 29.5, 29.4, 29.0, 29.9, 30.9, 30.5, 27.9, 30.2
11-P7C-6F	top	–	(a)
	bottom	33.3	33.1, 33.0, 33.1, 33.0, 33.1, 33.5, 33.6, 33.6
11-P7C-7K	top	32.2	31.5, 31.9, 32.0, 32.2, 32.6, 32.2, 32.2, 32.6
	bottom	30.6	30.6, 31.1, 31.3, 28.7, 30.0, 31.4, 31.0, 31.0
11-P7C-8	top	32.2	32.0, 31.8, 31.4, 32.0, 33.0, 32.7
	bottom	–	(b)
09-P7C-7F	top	–	(c)
	bottom	32.1	33.7, 33.1, 32.8, 32.0, 30.2, 31.8, 31.2
11-P7A-5	top	32.5	32.5, 32.0, 32.5, 32.0, 33.0, 33.0
	bottom	29.9	28.0, 31.5, 31.5, 30.0, 30.5, 28.0
11-P7A-6	top	25.3	25.5, 25.5, 25.0, 25.5, 25.0, 25.5
	bottom	23.8	24.5, 23.5, 23.5, 25.0, 22.0, 24.0
11-P7A-7	top	31.5	31.0, 31.5, 32.0, 32.0, 32.5, 31.0
	bottom	28.7	28.0, 28.0, 27.0, 30.0, 29.0, 30.0
11-P7B-5K	top	27.6	28.0, 28.0, 27.5, 28.5, 26.5, 27.0
	bottom	26.1	25.0, 27.0, 26.5, 25.0, 27.0, 26.0
11-P7B-6K	top	29.9	30.0, 30.0, 30.5, 30.0, 30.0, 29.0
	bottom	28.5	27.5, 29.0, 28.0, 28.5, 28.5, 29.5
11-P7B-7K	top	28.3	28.0, 28.0, 28.5, 29.0, 28.5, 28.0
	bottom	26.1	25.5, 27.0, 26.0, 27.0, 24.5, 26.5

Notes: (a) top side of coupling No. 6 was kept in its as-received position on shaft No. 6, (b) deposits on the bottom of coupling No. 8 were kept intact and prevented hardness testing of the underlying base metal, (c) only bottom section of coupling 09-P7C-7F was received.

Table 3-7: Through Thickness Hardness of Couplings

Coupling	Location	Measurements from OD to ID (R_C)
11-P7C-5	1	27.2, 28.0, 28.0, 27.7, 28.0, 27.1
	2	31.5, 30.9, 30.4, 30.2, 30.2, 30.7
11-P7C-6F	1	31.5, 32.7, 32.0, 32.1, 32.2, 32.0
	2	31.5, 32.2, 31.9, 32.1, 31.5
11-P7C-7K	1	31.2, 32.0, 31.7, 31.9, 31.3, 31.8
	2	32.0, 32.0, 32.0, 31.9, 32.6, 32.0
11-P7A-5	1	33.0, 29.9, 33.2, 33.0, 33.6, 32.2
	2	32.9, 32.9, 33.0, 32.6, 32.8, 33.1
11-P7A-6	1	24.0, 24.0, 24.0, 24.0, 24.0, 24.0
	2	24.5, 24.0, 24.0, 24.0, 24.5, 24.0
11-P7A-7	1	31.0, 31.5, 31.0, 31.5, 31.0, 31.0
	2	32.0, 31.5, 32.0, 31.0, 31.0, 31.0
11-P7B-5K	1	27.0, 27.5, 27.5, 28.0, 27.9, 27.5
	2	28.5, 28.0, 28.6, 28.0, 27.7, 28.1
11-P7B-6K	1	28.8, 29.0, 29.1, 29.4, 29.8, 29.8
	2	29.2, 29.9, 30.0, 30.0, 30.1, 30.2
11-P7B-7K	1	28.2, 28.0, 27.9, 27.9, 28.0, 28.5
	2	28.1, 28.8, 28.7, 28.5, 28.4, 28.6
09-P7C-6F	(a)	34.8, 35.9, 35.2, 36.0, 36.3, 36.8, 37.1

Notes: (a) Hardness measurements on 09-P7C-6F were taken at the mid-wall along the length of the coupling from the center to the end of the coupling.

Sample through thickness hardness test specimen.

Table 3-8: CVN Impact Test Results

Coupling	Specimen Identification	Test Temperature (°F)	Absorbed Energy (ft-lb)	Lateral Expansion (in.)	Percent Shear (%)
11-P7C-5	5-C2	32	9	0.005	<10
	5-C4	32	9	0.006	<10
	5-C1	70	10	0.007	10
	5-C6	70	10	0.007	10
	5-C8	70	10	0.007	10
	5-C3	100	11	0.007	20
	5-C5	100	10	0.006	20
	5-C7	150	15	0.011	50
11-P7C-6F	6-C2	32	6	0.003	<10
	6-C4	32	8	0.006	<10
	6-C1	70	9	0.005	10
	6-C5	70	10	0.006	10
	6-C3	100	11	0.007	10
	6-C6	153	14	0.008	50
11-P7C-7K	7-C2	32	7.5	0.003	<10
	7-C1	75	10	0.008	10
	7-C3	100	11	0.008	10
09-P7C-7F	709-C3	32	4	0.004	<10
	709-C4	32	3	0.004	<10
	709-C1	75	5	0.005	<10
	709-C2	75	6	0.002	<10
	709-C5	100	6	0.003	<10
	709-C6	152	6	0.006	<10
11-P7A-5	5-A3	32	7	0.003	<10
	5-A4	32	7	0.002	<10
	5-A1	75	8	0.006	10
	5-A2	75	9	0.005	10
	5-A5	100	13	0.009	30
11-P7A-6	6-A3	32	3	0.002	<10
	6-A4	32	3	0.002	<10
	6-A1	75	6	0.006	10
	6-A2	75	6	0.008	10
	6-A5	100	9	0.012	10
11-P7A-7	7-A3	32	11	0.005	<10
	7-A4	32	9	0.004	<10
	7-A1	75	12	0.009	20

Coupling	Specimen Identification	Test Temperature (°F)	Absorbed Energy (ft-lb)	Lateral Expansion (in.)	Percent Shear (%)
	7-A2	75	12	0.010	20
	7-A5	100	18	0.015	50
11-P7B-5K	B5-9	0	9	0.006	10
	B5-10	0	10	0.007	10
	B5-1	32	14	0.013	20
	B5-2	32	16	0.014	40
	B5-7	32	12.5	0.011	20
	B5-8	32	13	0.011	20
	B5-3	76	22	0.018	>90
	B5-4	76	29	0.018	>90
	B5-5	100	28	0.016	>90
	B5-6	150	26	0.017	>90
11-P7B-6K	B6-9	0	5	0.004	<10
	B6-10	0	5	0.004	<10
	B6-1	32	8	0.004	<10
	B6-2	32	5	0.005	<10
	B6-7	32	6	0.005	<10
	B6-8	32	5.5	0.003	<10
	B6-3	76	11	0.008	10
	B6-4	76	10	0.009	10
	B6-5	100	21	0.015	80
	B6-6	150	21	0.015	>90
11-P7B-7K	B7-9	0	8	0.007	10
	B7-10	0	9	0.007	10
	B7-1	32	12	0.008	20
	B7-2	32	11	0.009	20
	B7-7	32	11	0.009	10
	B7-8	32	13.5	0.013	20
	B7-3	76	11	0.015	50
	B7-5	100	22	0.016	>90
	B7-6	150	32	0.022	>90

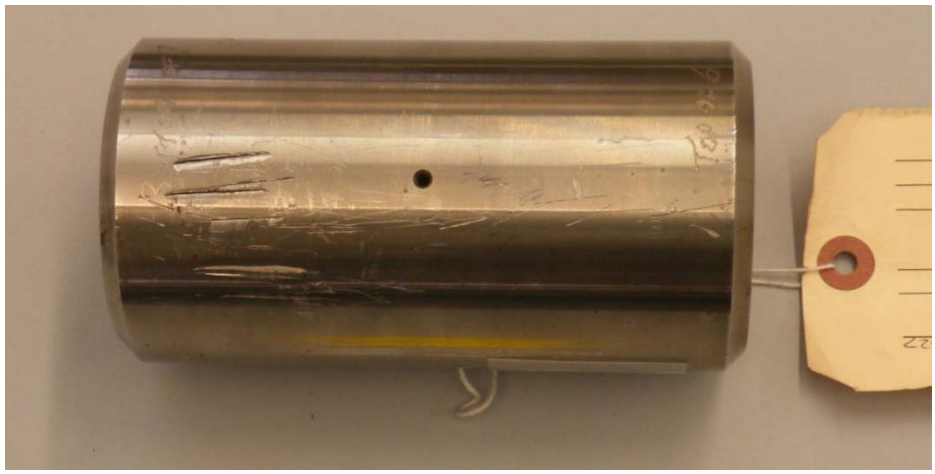

Coupling 11-PC-7 in as-received form. Shaft numbers engraved on the ends. Coupling exhibited wrenching marks on outer diameter.

Figure 3-1: As-Received 11-P7C-7

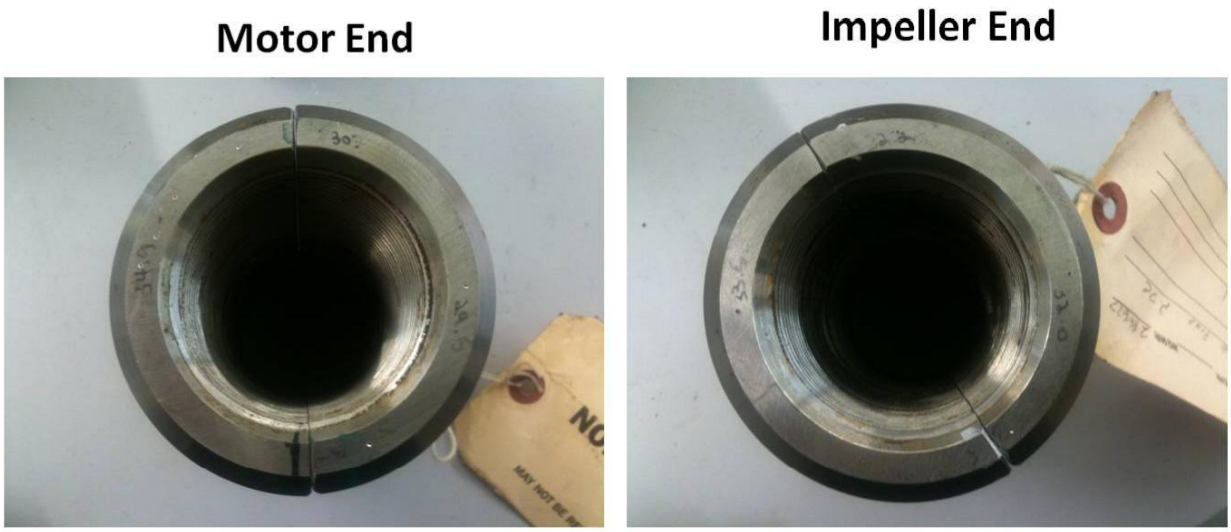

Hardness measurement indentations are present on both ends. Measurement values were 34.9, 30.7, 29.5 and 29.4 on motor end and 33.5, 32.2, 32.0 and 32.5 on impeller end.

Figure 3-2: Hardness Indentation and Values Written on 11-P7C-7

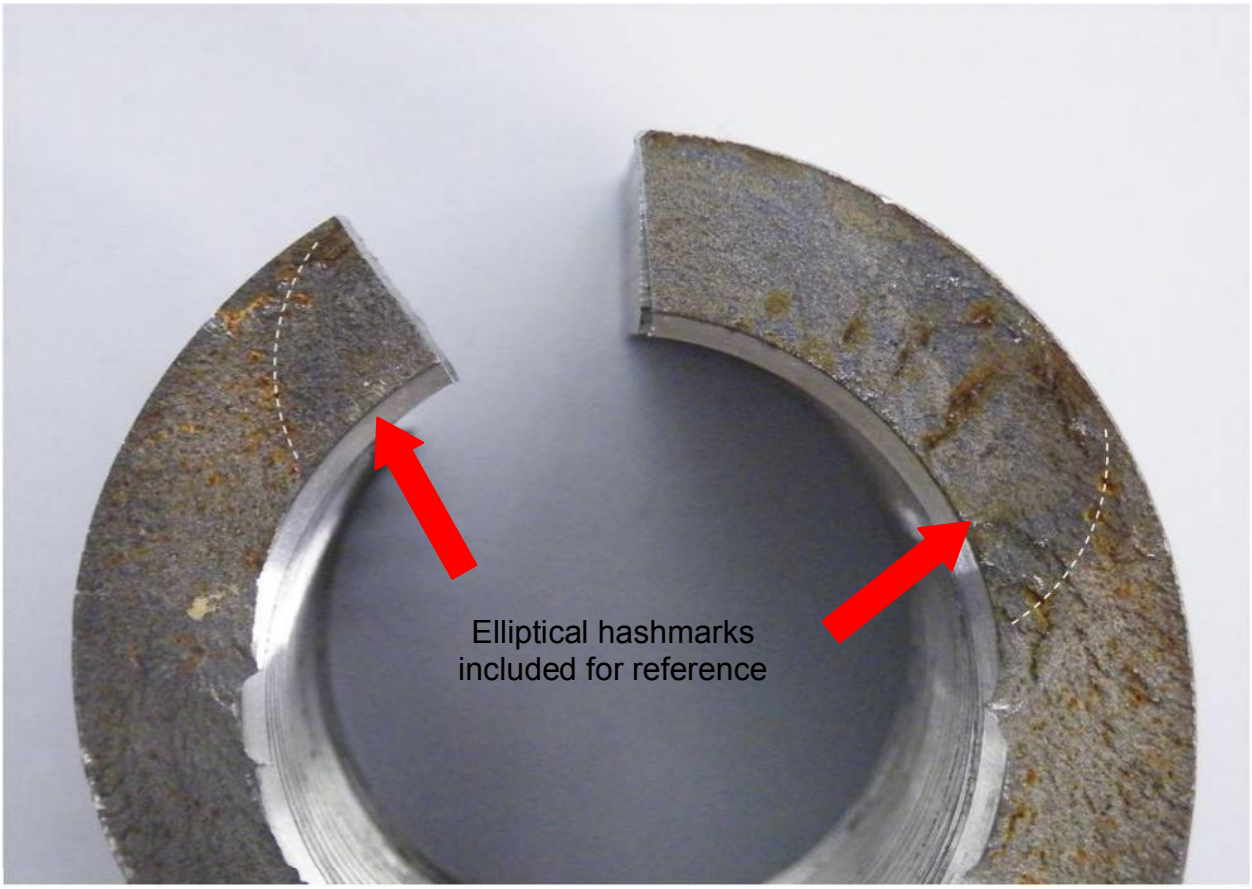

Figure 3-3: 09-P7C-7F Fracture Surface Showing Elliptical Feature

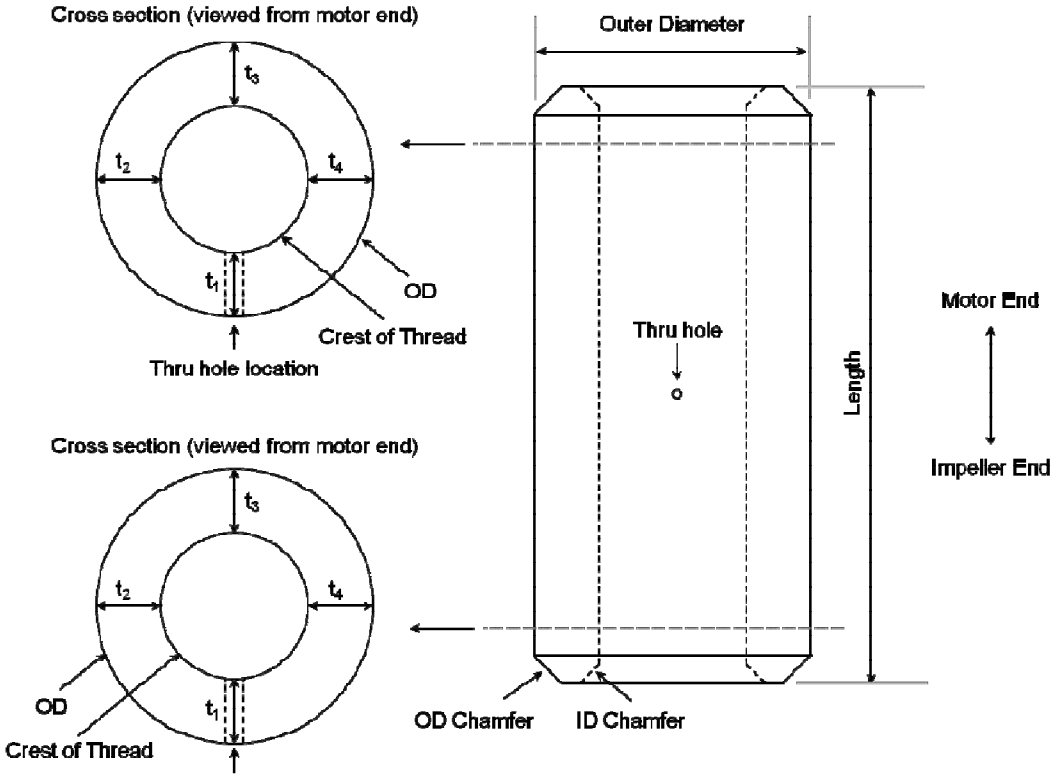

Figure 3-4: Coupling Dimensioning Scheme

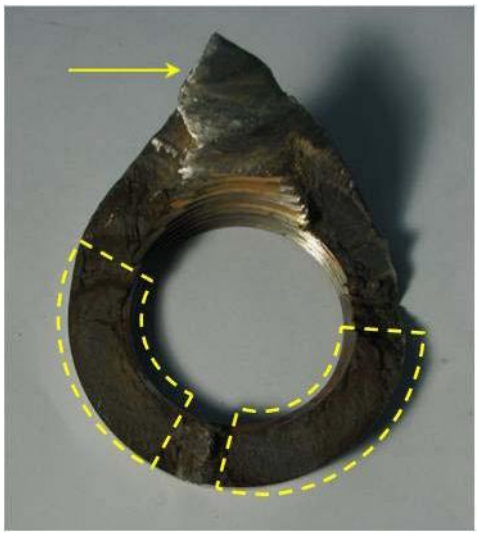

(a) Fracture surface was sectioned from the coupling for analysis. Tip exhibited blunting from mechanical damage (arrow).

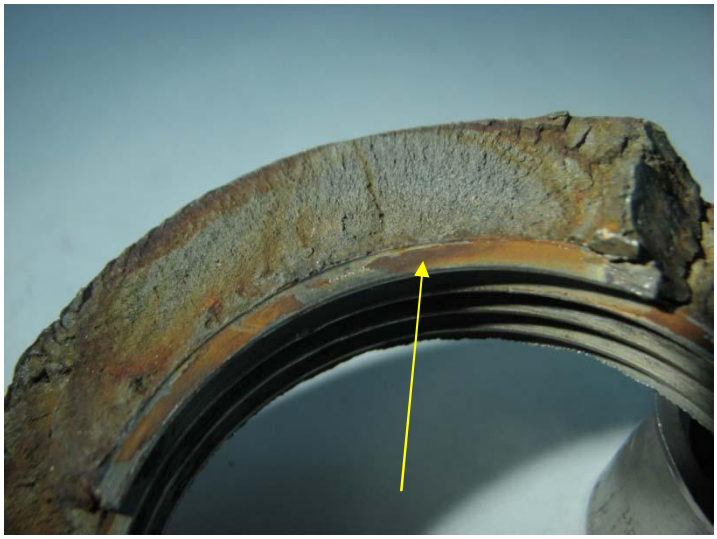

(b) Elliptical pattern of crack on flat fracture surface, relative to coupling axis. Also, red/brown corrosion product found on the insides of coupling threads (arrow)

Figure 3-5: Visual of Fracture Surface on Coupling 11-P7C-6F

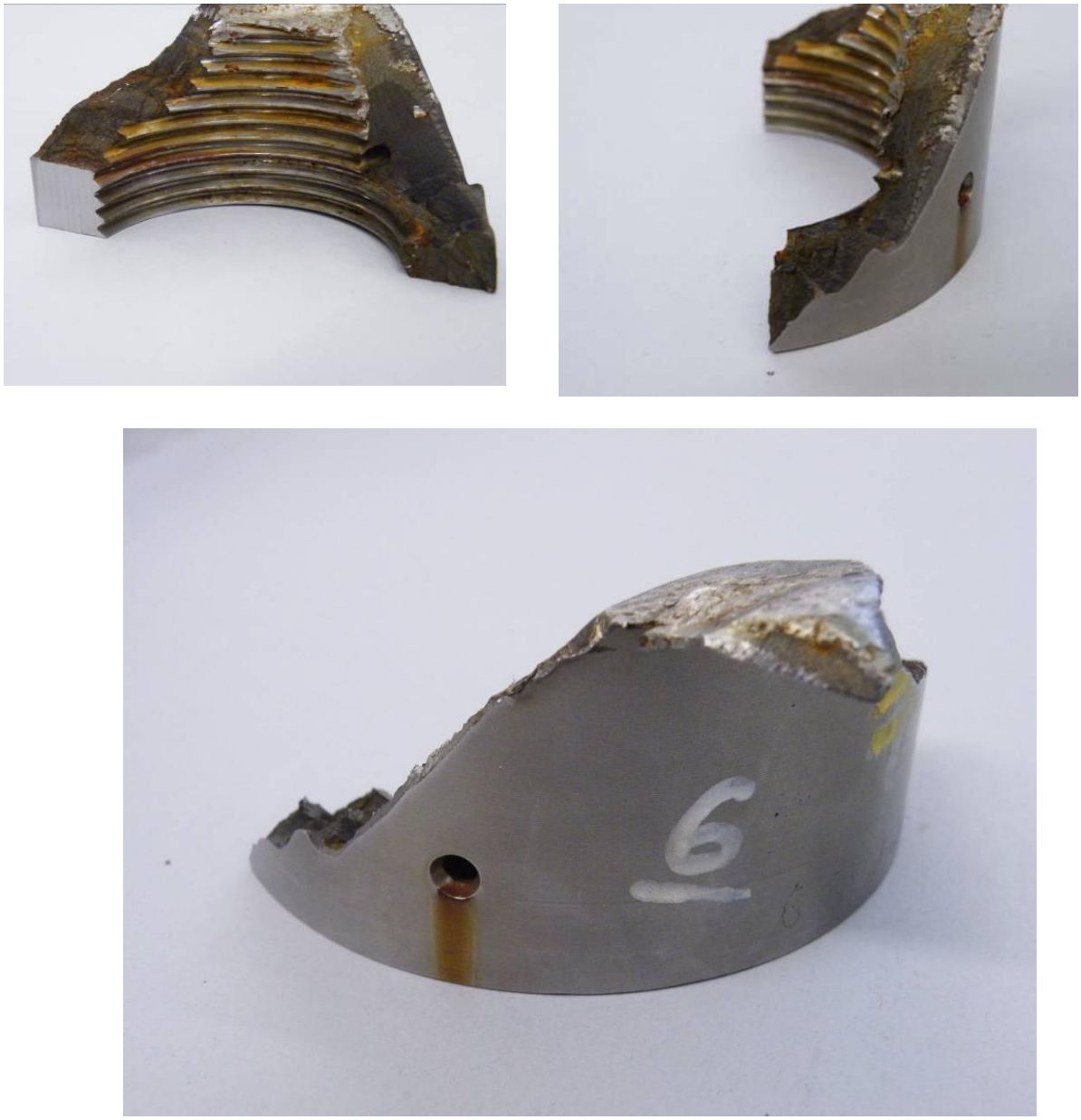

Figure 3-6: 11-P7C-6F showing Corrosion Deposit

Half of coupling 11-P7C-6F remaining on shaft No. 6 exhibited damage on its fracture surface from contact with the mating coupling half and shaft 5, which likely occurred after fracture event.

End of shaft No. 5 exhibited gouging damage likely from post 11-P7C-6F final failure.

Figure 3-7: Ends of Shaft 5 and 6 Coupled by 11-P7C-6F

Pump P-7A Coupling No. 1 through 8 were submitted to LPI.

Coupling Nos. 4, 5, 6 and 7 (11-P7A-4 through -7) were selected for analysis

Coupling No. 7 (11-P7A-7) shown in its as-received condition.

Notice the neolube on the threads.

Figure 3-8: As-Received Coupling No. 11-P7A-7

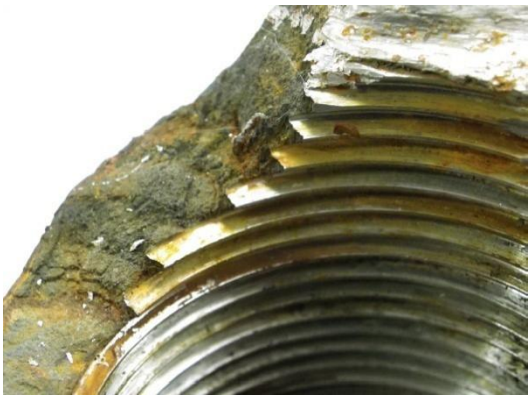

Coupling No. 11-P7C-6F

11-P7C-7K in the as-received condition does not exhibit the same level of neolube on threaded surface as 11-P7A-7

11-P7A-7 in the as-received condition exhibits significant amounts of neolube on thread surface

Figure 3-9: Contrast Thread Coating (As-Received) on P-7C Failed and Cracked Couplings to P-7A Coupling

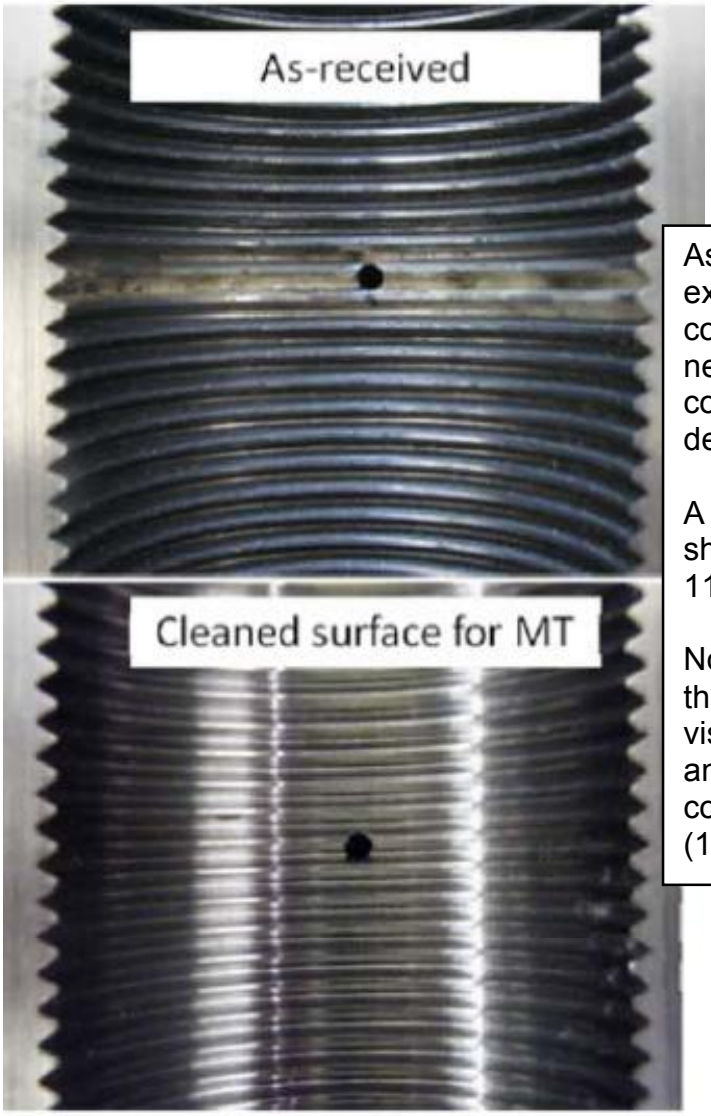

As-received couplings exhibited a greasy grey coating on threads, and near the center of the coupling some surface deposits.

A cleaned surface is shown for coupling No. 11-P7A-5

No cracks along the thread root were visually observed for any of the cleaned couplings (11-P7A-4, 5, 6, 7)

Figure 3-10: Visual Observation of Coupling No. 11-P7A-5

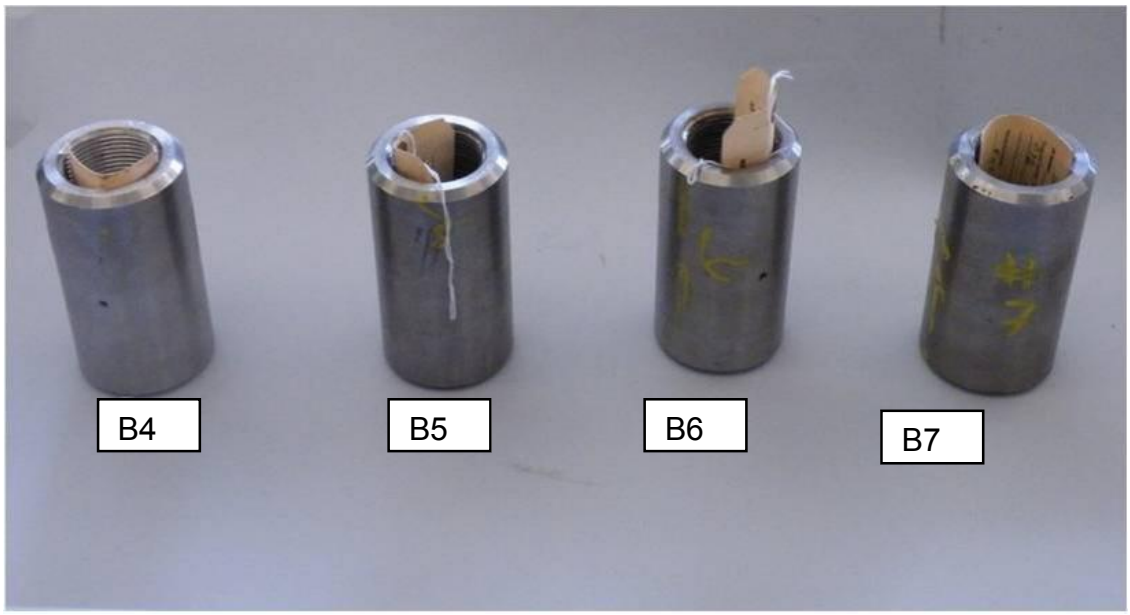

Figure 3-11: As-Received Couplings 11-P7B-4 through 11-P7B-7

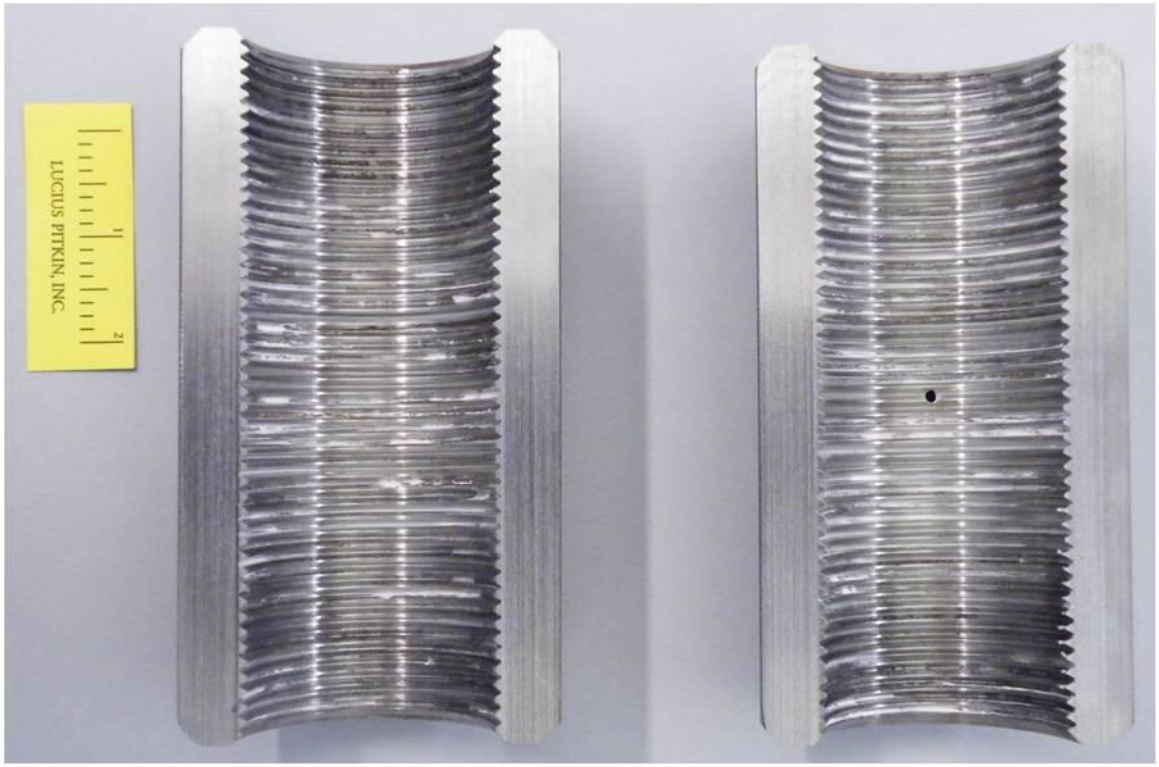

Figure 3-12: As-Split Coupling 11-P7B-4

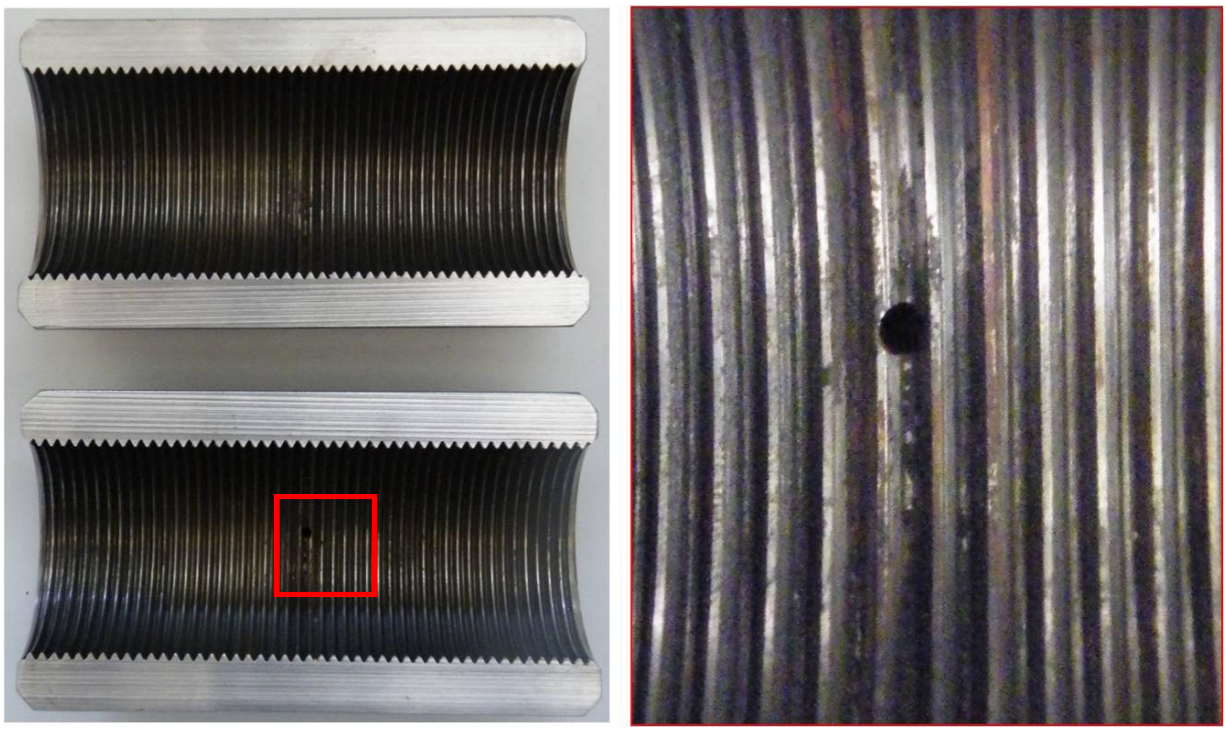

Figure 3-13: As-Split Coupling 11-P7B-5

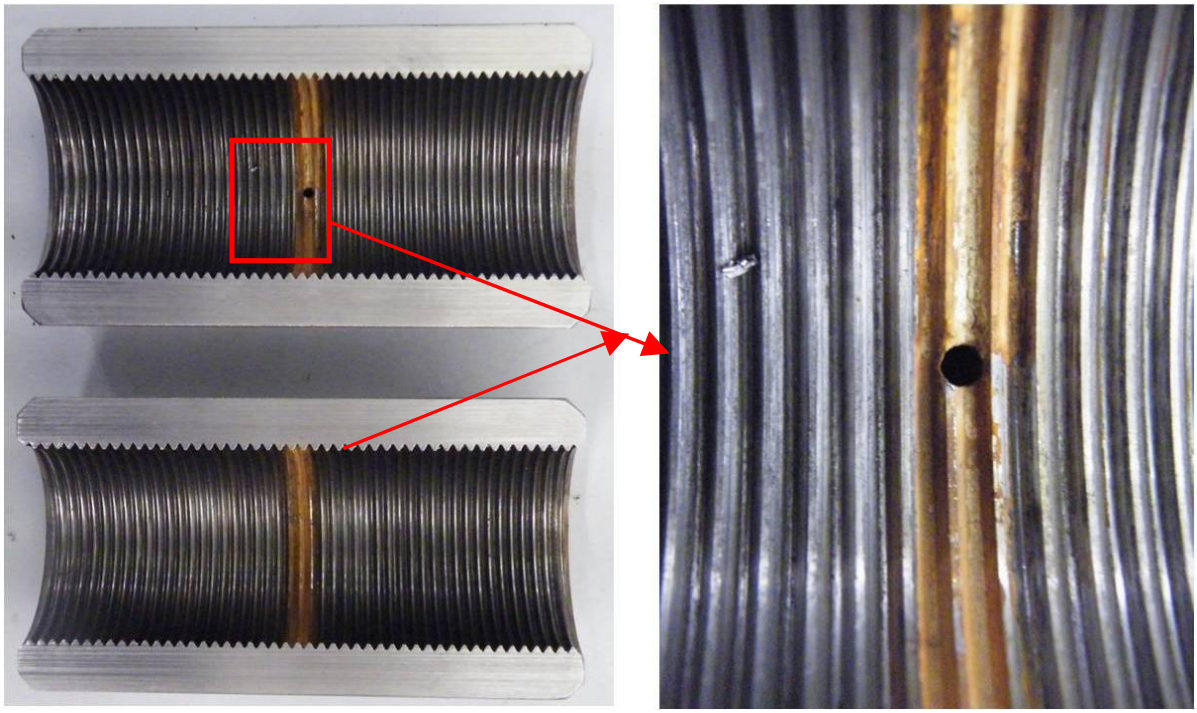

Figure 3-14: As-Split Coupling 11-P7B-6

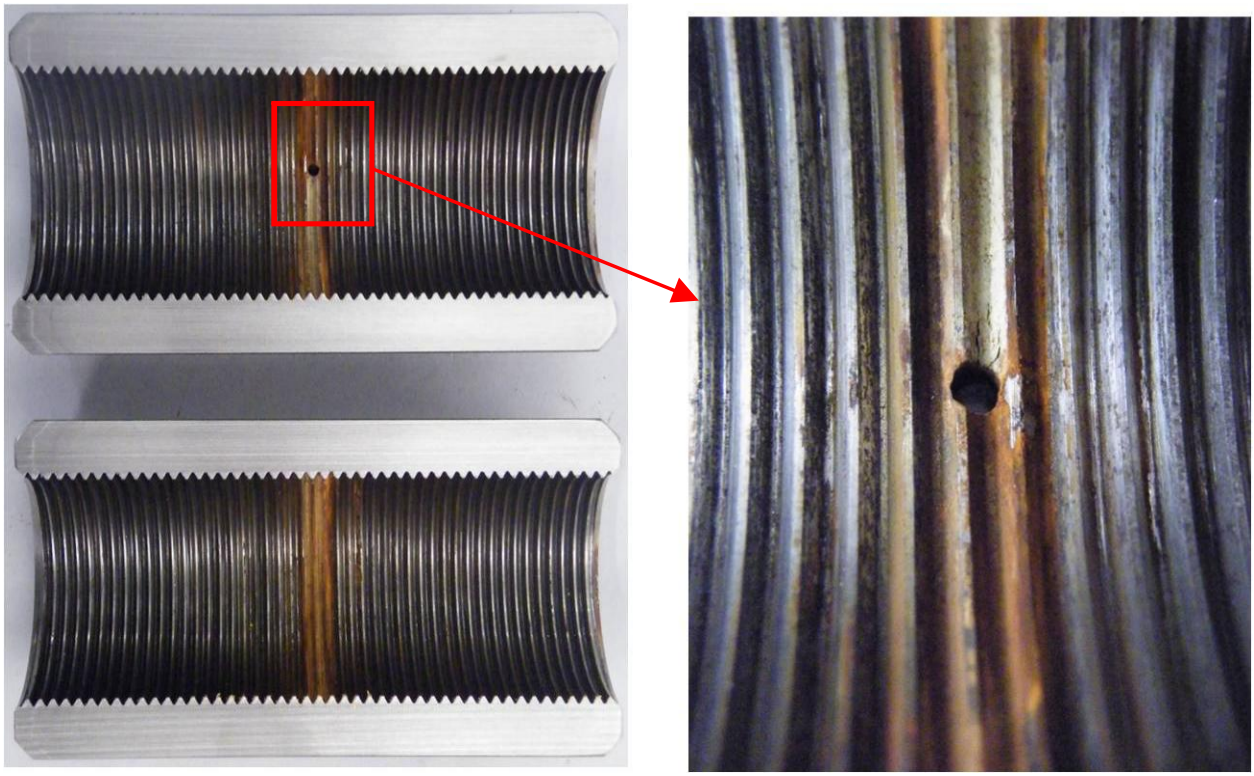

Figure 3-15: As-Split Coupling 11-P7B-7

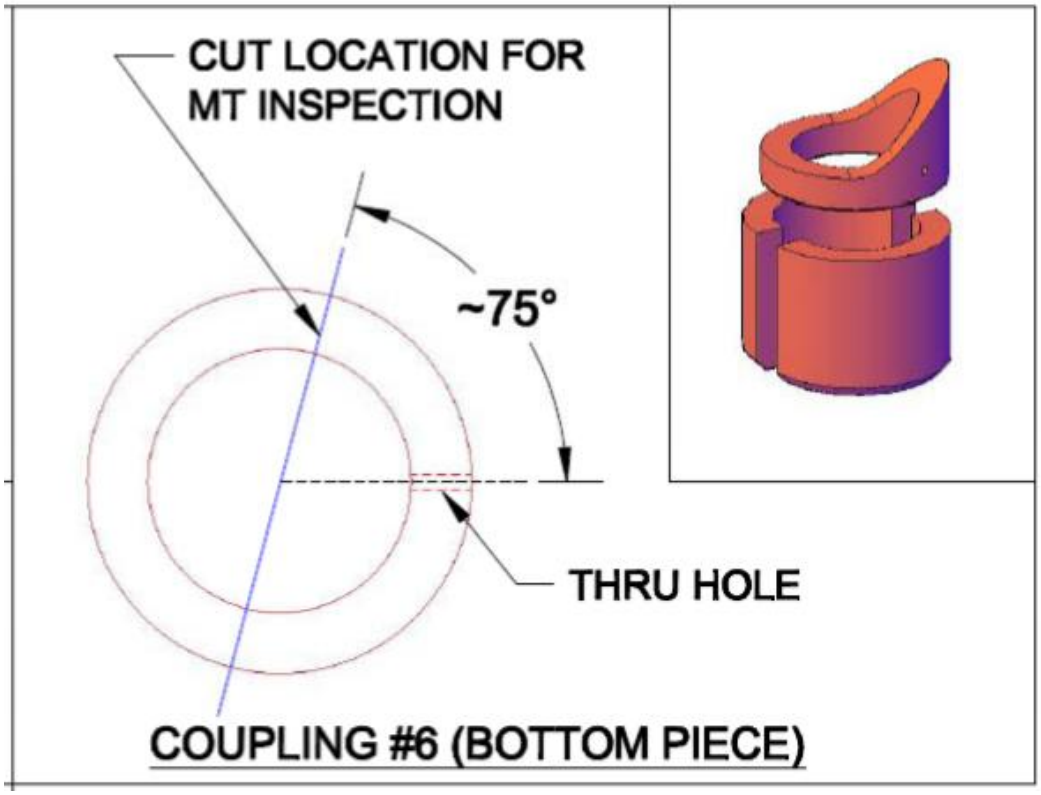

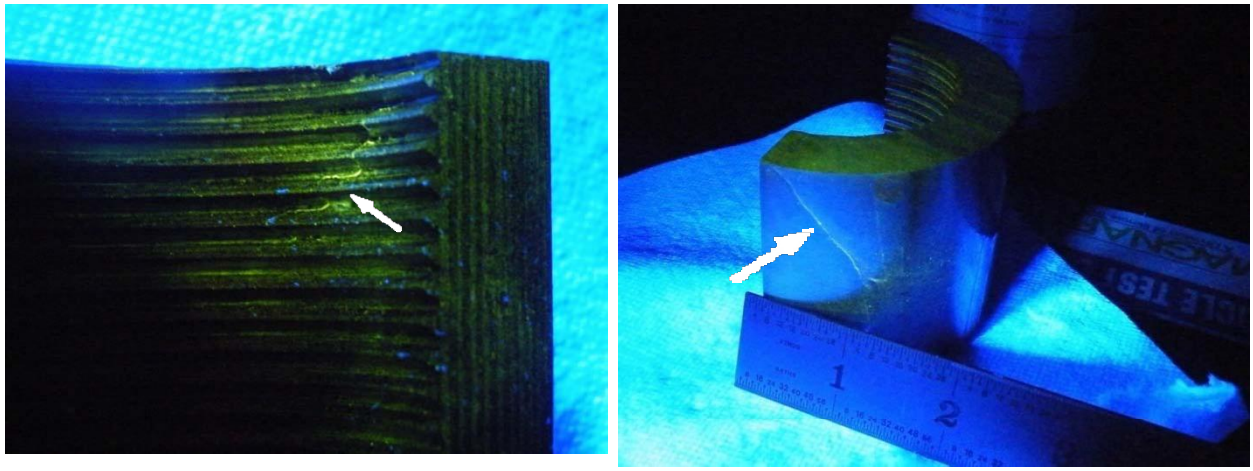

After fracture surface was sectioned, a remaining portion of coupling 11-P7C-6F was MT inspected. Arrows show location of indications.

Figure 3-16: MT Highlighting Un-Opened Fracture on Coupling 11-P7C-6F

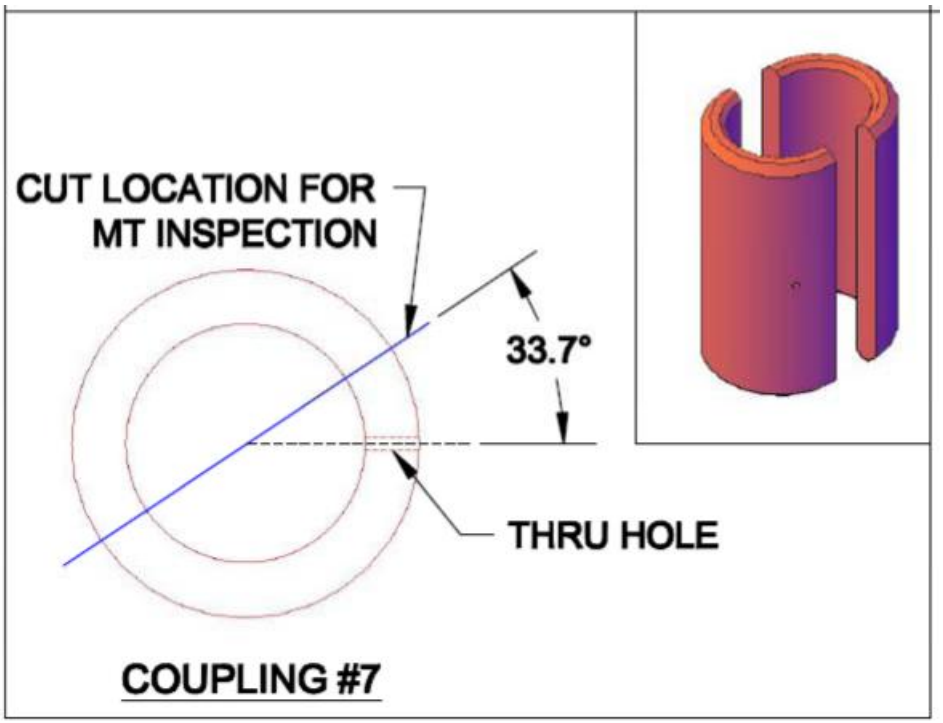

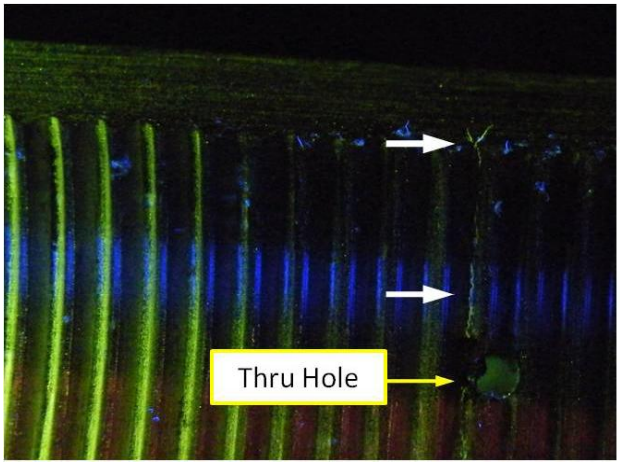

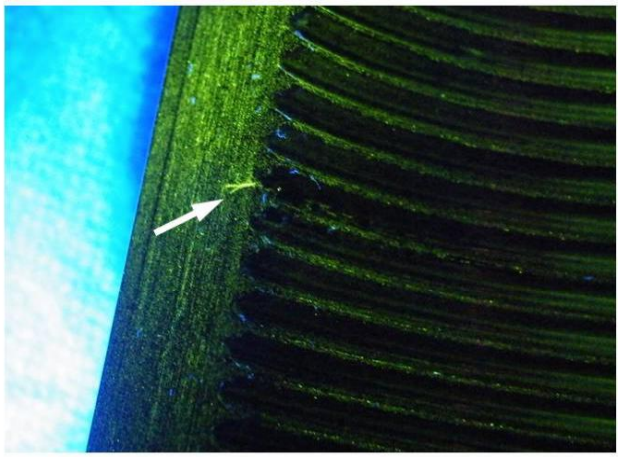

Top sketch show the cut line for coupling 11-P7C-7. Fluorescent MT examination of this coupling reveals an indication, shown by a well-defined fluorescent line, initiating from a thread root and propagating in the radial direction. The left and right images show the same indication on the two sections of this coupling after cutting in half longitudinally. Arrows show location of the indication.

Figure 3-17: MT Highlighting Crack on Coupling 11-P7C-7K

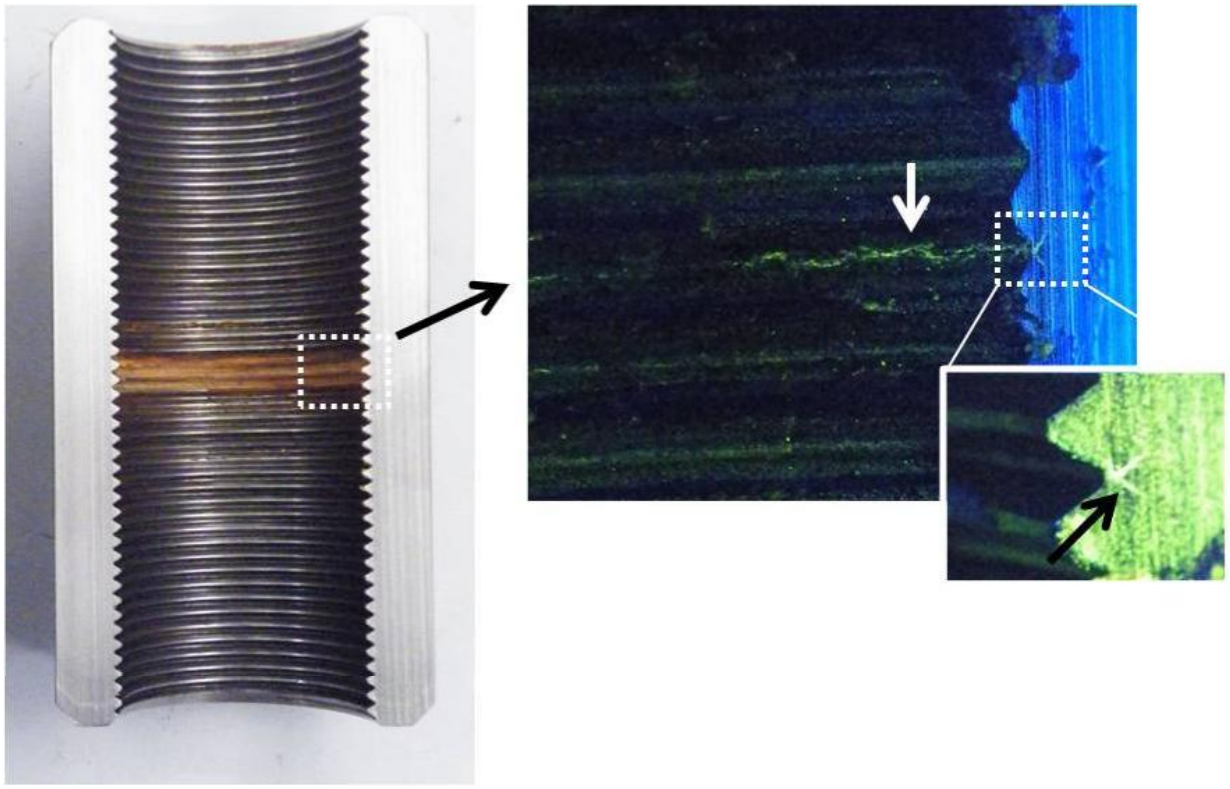

Figure 3-18: MT Highlighting Crack on Coupling 11-P7B-7K

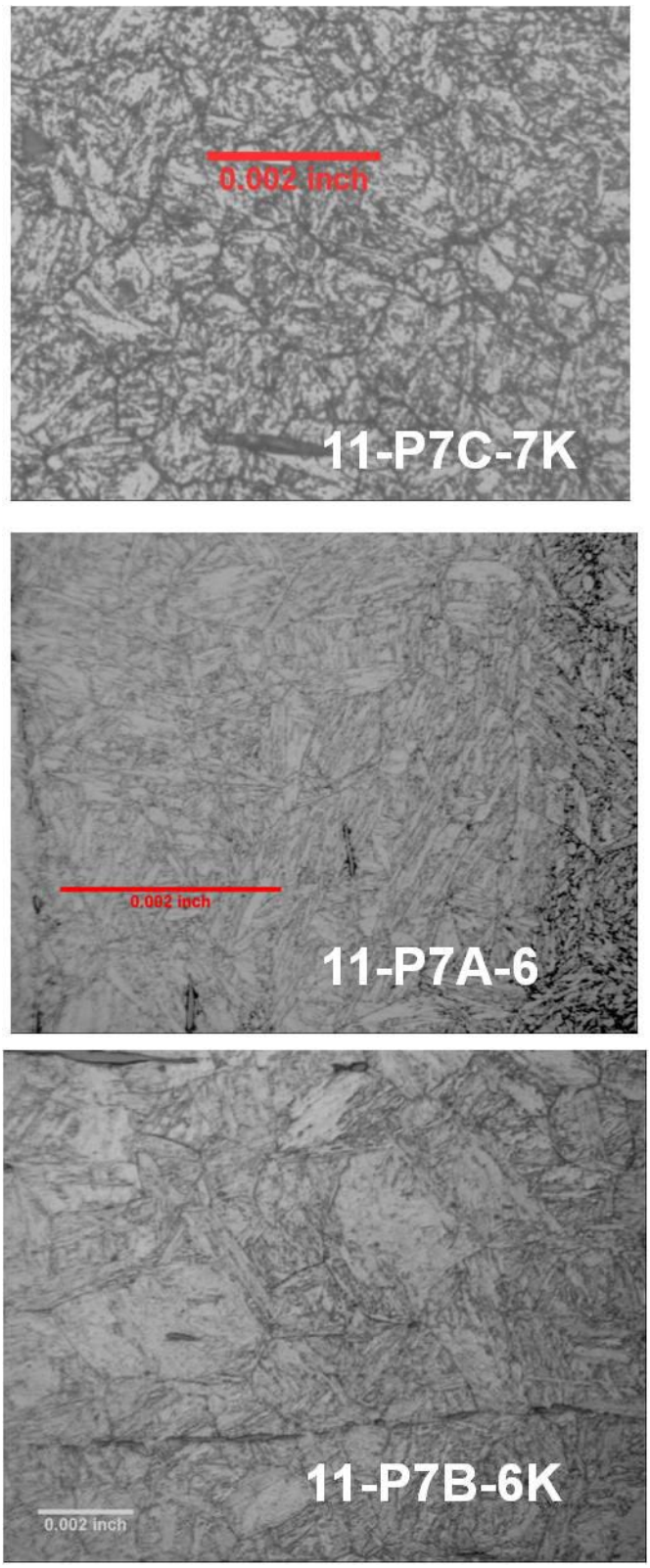

Figure 3-19: General microstructure of coupling material

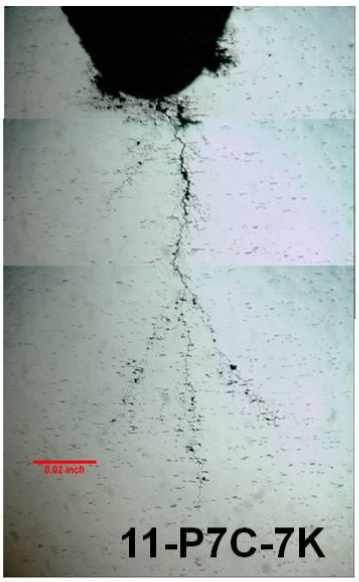

As-polished condition and viewed at 50x.

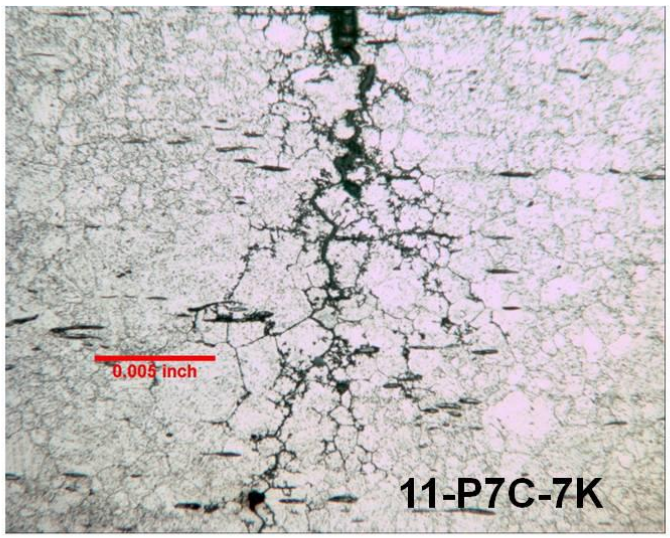

Etched condition viewed at 200x.

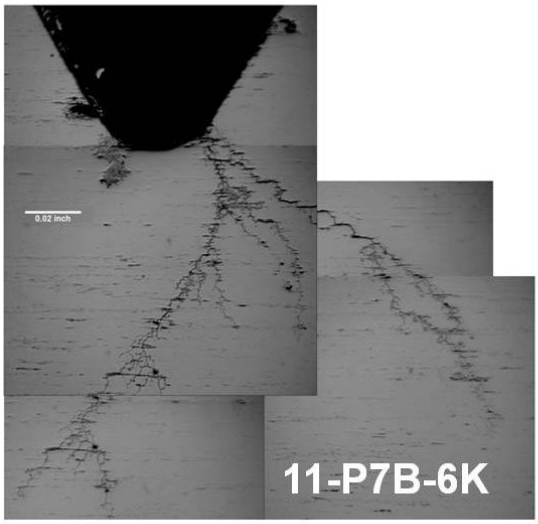

As-polished condition
50X, scale bar 0.02 in.

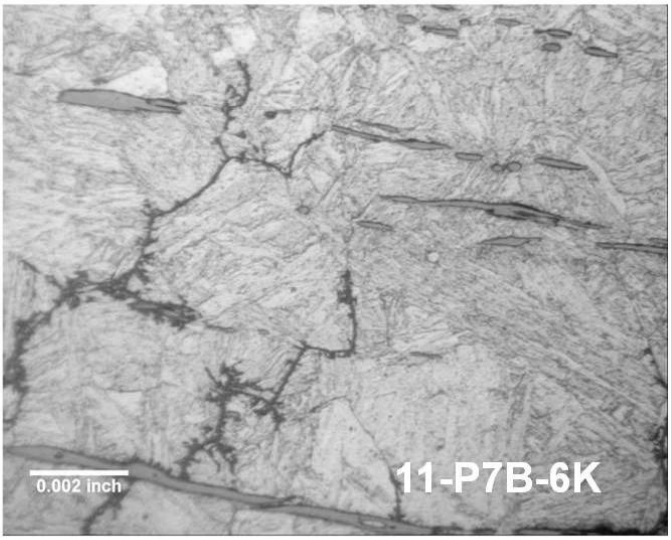

Etched condition, 400X, scale bar 0.002 in.)

Images of SCC cracks in coupling 11-P7C-7K (top) and 11-P7B-6K (bottom) showing the network of cracks that follow the prior austenite grain boundaries.

Figure 3-20: As-polished (left) and Etched (right) Microscopy

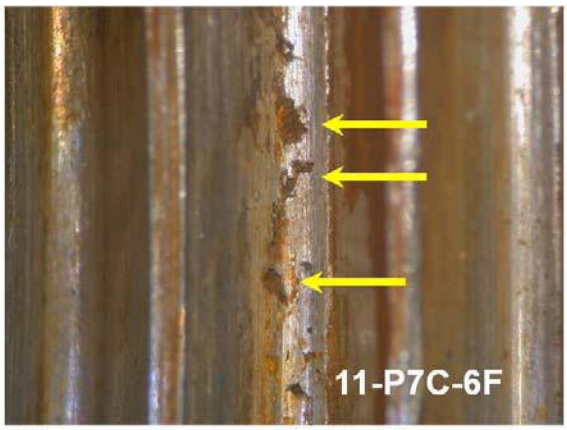

Pitting at root near middle of fractured Coupling No. 6 (Stereomicroscopy 15X)

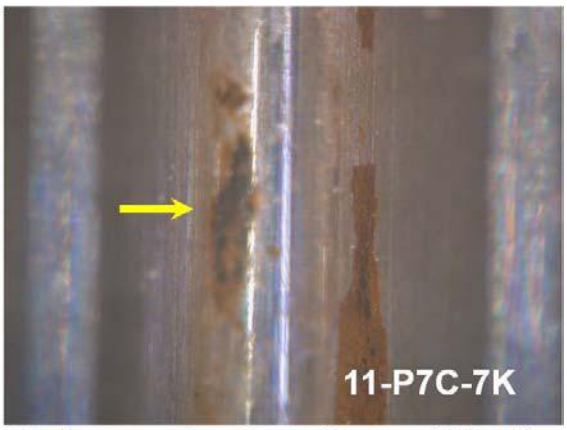

Pitting near the root and near middle of Coupling No. 7 (Stereomicroscopy 40X)

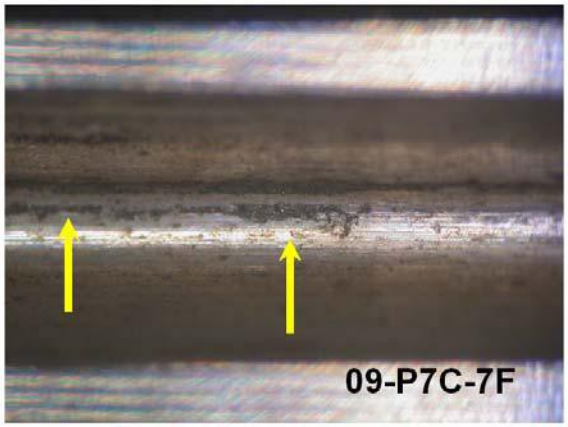

Pitting near root at middle of fractured Coupling No. 7 from 2009 event (Stereomicroscopy 30X)

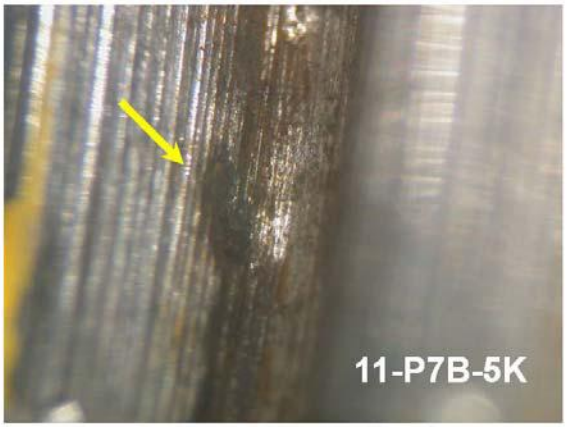

Pitting near root at middle of Coupling No. 5 (Stereomicroscopy 40X)

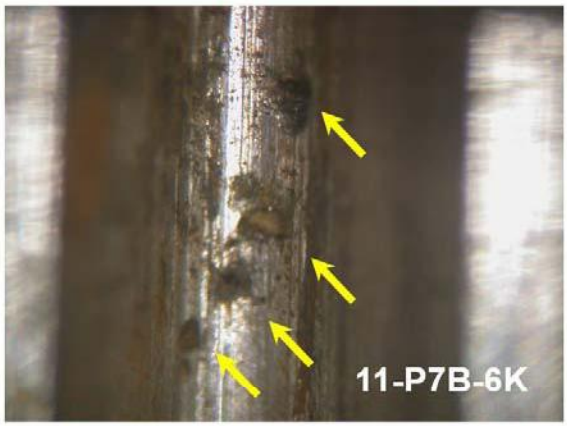

Pitting at root near middle of Coupling No. 6 (Stereomicroscopy 50X)

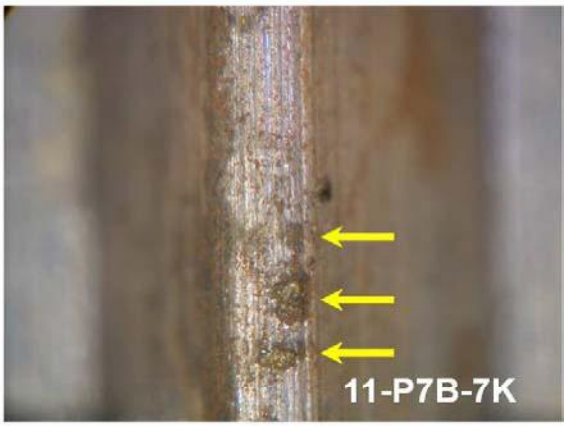

Pitting at root near middle of Coupling No. 7 (Stereomicroscopy 50X)

Figure 3-21: Pitting observed in couplings with cracks or fractures

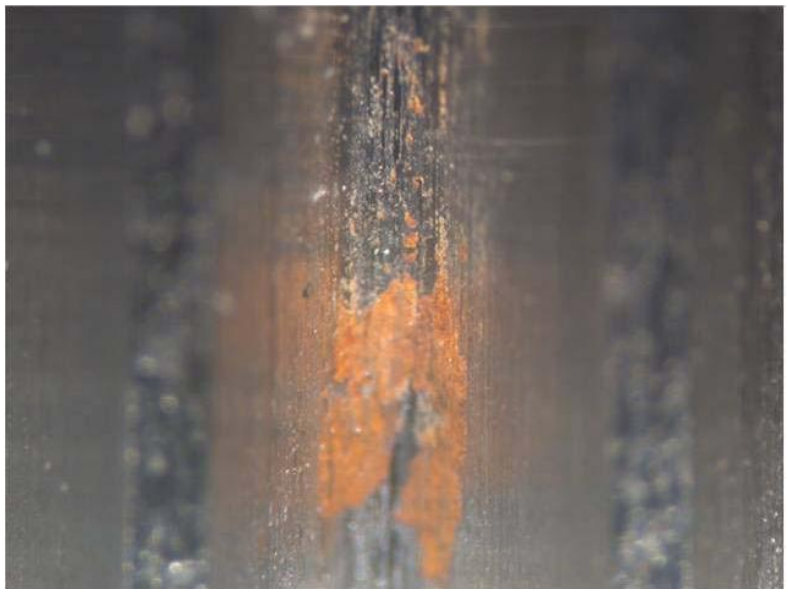

Figure 3-22: Representative Image of P-7A Coupling Showing No Pitting

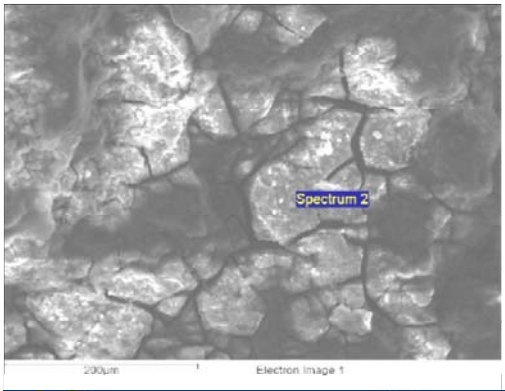

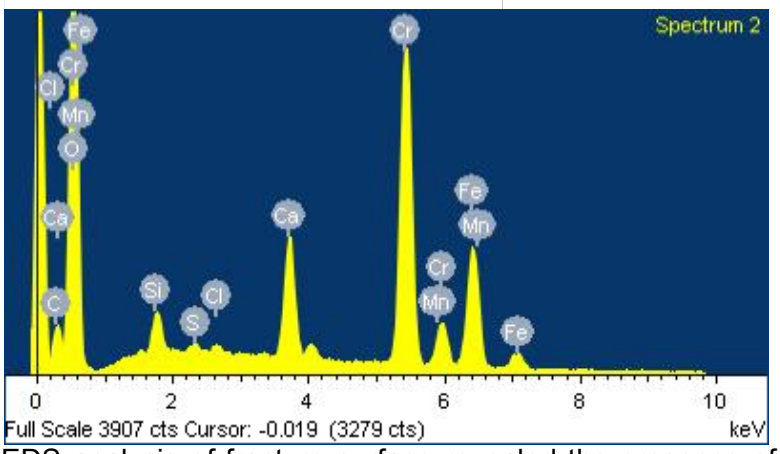

Element	Weight%
O	40.1
Si	1.7
S	0.3
Cl	0.3
Ca	5.9
Cr	29.5
Mn	0.4
Fe	Bal.

EDS analysis of fracture surface revealed the presence of corrosive agents (chlorides, oxides and sulfides), consistent with stress corrosion cracking. The high chromium level in the spectrum is likely attributed to local chromium carbides in the EDS sampling volume.

Figure 3-23: EDS of Coupling 11-P7C-6F Surface Deposit – Spectrum 2

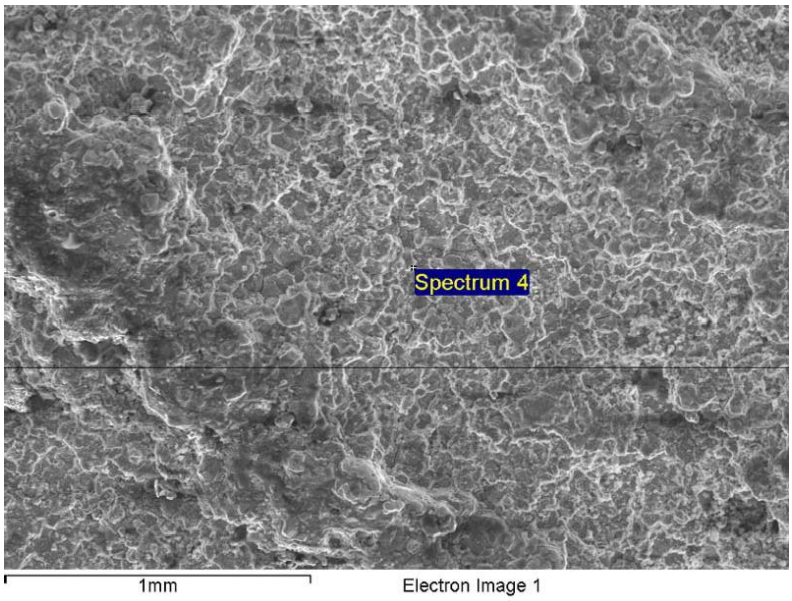

Element	Weight %
O	7.5
Si	0.9
S	0.3
Cl	0.3
K	0.2
Ca	0.4
Cr	14.6
Mn	1.6
Fe	Bal.

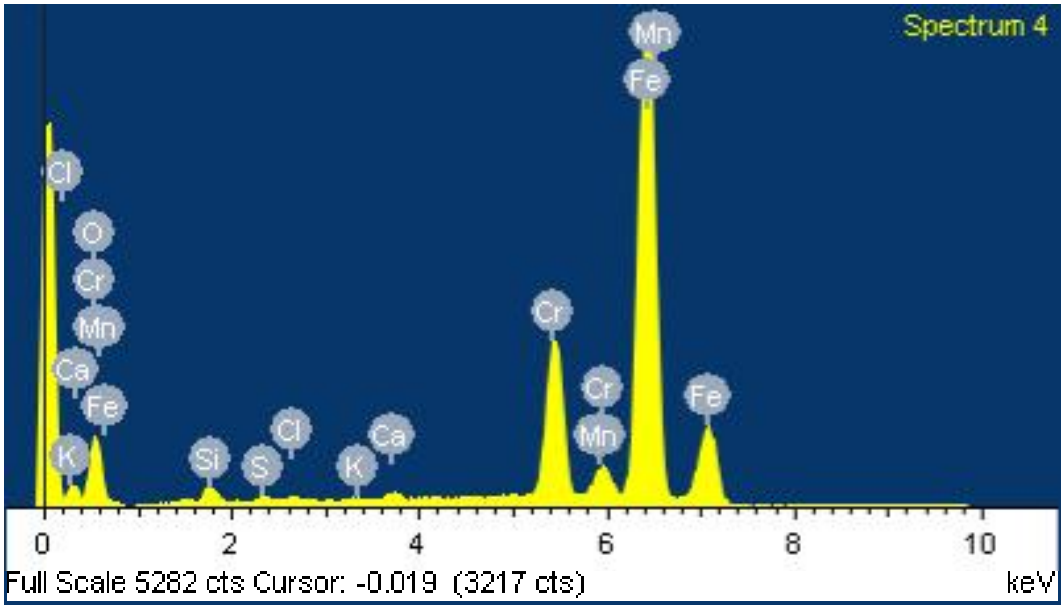

Figure 3-24: EDS of Coupling 11-P7C-6F Surface Deposit – Spectrum 4

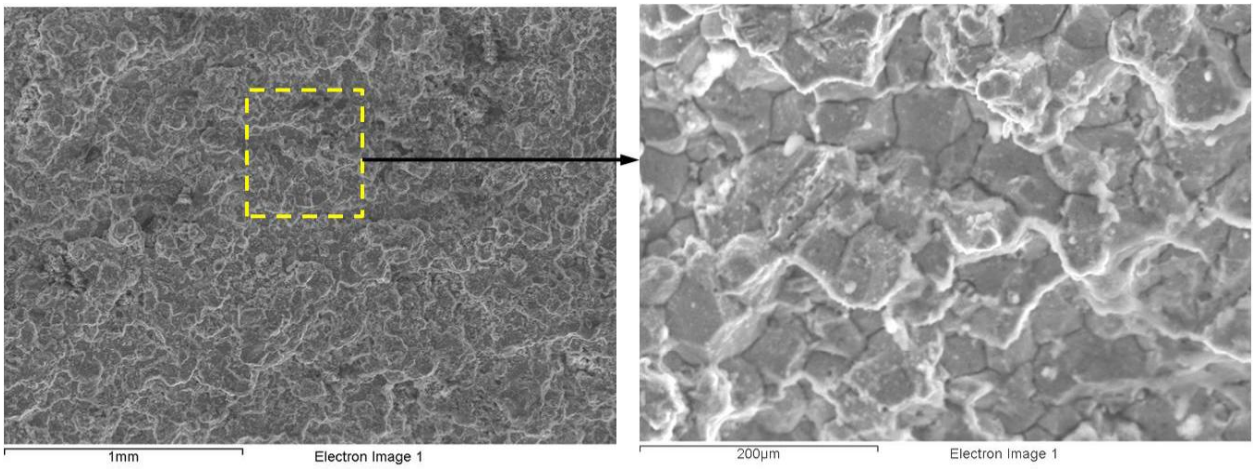

Fracture surface morphology exhibited a rock-candy appearance, characteristic of intergranular stress corrosion cracking. This is typical of a quench and tempered steel, such as a 400 series martensitic steel.

Figure 3-25: SEM of Coupling 11-P7C-6F Surface

4.0 DISCUSSION OF RESULTS/EVALUATION

Metallurgical examination and testing of failed couplings 11-P7C-6F and 09-P7C-7F, documented in Section 3.0, identified the failure mechanism to be stress corrosion cracking (SCC) and more specifically intergranular SCC (IGSCC). Stress corrosion cracking is a failure process of a material subjected to sufficient tensile stress in a corrosive environment for which the material is susceptible. IGSCC is SCC along grain boundaries. SCC "…is a subcritical crack growth phenomenon involving crack initiation at selected sites, crack propagation, and overload final fracture of the remaining section. Failure by SCC is frequently encountered in seemingly mild chemical environments at tensile stresses well below the yield strength of the metal. The failures often take the form of fine cracks that penetrate deeply in to the metal, with little or no evidence of corrosion on the nearby surface or distortion of the surrounding structure. Therefore during casual inspection no macroscopic evidence of impending failure is seen [24]."

Each of the three criteria 1) susceptible material, 2) corrosive environment and 3) tensile stress, considered to be necessary for SCC to occur, as it relates to the service water pump couplings, is discussed in the following subsections.

4.1 Susceptible Material

The coupling material was specified to be ASTM A582 Type 416 SS, tempered to a hardness in the Rockwell C range of 28 to 32 (HRC) [3c]. ASTM A582 Type 416 SS is a free-machining martensitic stainless steel with relatively high sulfur content that gives it excellent machining characteristics, while providing generally low corrosion resistance for a 12% chromium stainless steel.

ASTM standard A582 [7] provides chemical and hardness requirements for the coupling material. No requirements for toughness or tensile strength are provided in ASTM standard A582 [7]. Per ASTM A582 [7], the hardness range for 416 stainless in the tempered condition is 248-302 Brinell which equates to 24.2-32.1 HRC. The couplings were specified in the narrower 28 to 32 HRC range to mitigate the effects of galling during pump assembly and operation [4].

Heat treatment of the couplings to achieve the specified properties can be garnered from the heat traces provided in Attachment A. The heat traces provided in Attachment A are re-plotted for the hardening and tempering heat treatments and presented in Figure 4-1 and Figure 4-2. The re-plotted heat traces are in relative time with zero being the time at which the heat treatment started for each batch.

According to the heat treatment process described in Attachment VI of the root cause evaluation report for CR-PLP-2009-04519 [1] and the heat trace in Figure 4-1, the couplings were hardened by quenching (rapid cooling) using nitrogen in a vacuum furnace from approximately 1870°F that quickly cooled the parts to ambient. The microstructure transforms from austenite to martensite when the couplings are quenched. The ASM metals handbook [26] and heat treater's guide [25] recommends an austenitizing temperature in the range of 1695°F to 1850°F for 416 SS. The austenitizing temperature of 1870°F, exceeds the recommended maximum of 1850°F. The effect of austenitizing temperature on the as-quenched hardness of three martensitic grades is shown in the figure to the right (extracted from [26]). It shows that "the hardness increases with increasing austenitizing temperature to about 1800°F, then decreases because of austenite retention and (occasionally) the formation of delta ferrite. Certain subtle anomalies in these steels that should be considered before specifying a heat treating procedure are exemplified in the opposing injurious effects of the high and low extremes of austenitizing temperature, depending on the subsequent tempering temperature [26]." The ASM heat treater's guide [25], recommends using the low side of the austenitizing range when tempering is to exceed 565°C (1050°F), which would be applicable to the subject couplings given their tempering treatment.

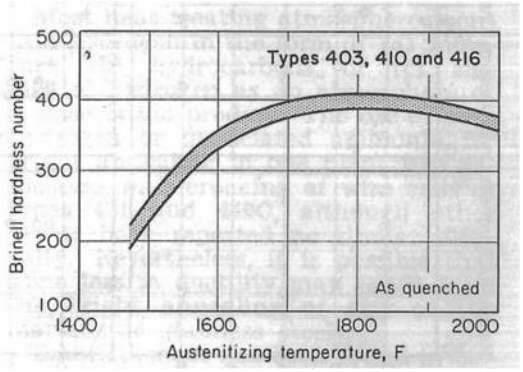

The ASM heat treating handbook [26] and guide [25], recommends a tempering temperature range of 1050°F to 1125°F for hardness in the range of 25 to 31 HRC. Also, "Tempering at 370°C to 565°C (700°F to 1050°F) [is] not recommended for parts requiring high toughness and optimum corrosion resistance. Causes a marked dip in impact resistance and lowered stress corrosion cracking resistance. Double tempering [is] beneficial. Cool to room temperature between tempers [25]." The effect of tempering temperature on the stress-corrosion characteristics of two martensitic stainless steels at a stress level of 80ksi in a salt fog cabinet is

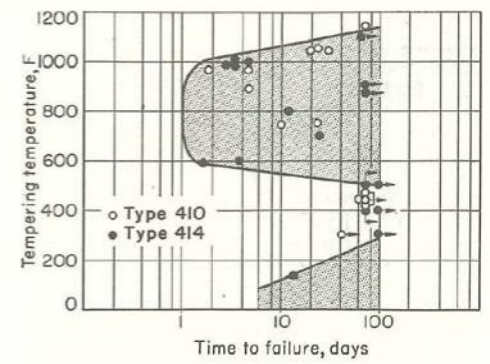

provided in the figure to the right [26].

Referring to the heat traces in Figure 4-2, the couplings were tempered in the range of 1025°F to 1090°F. This range encompasses a double temper. The double temper was performed to attain the specified hardness of 28 to 32 HRC. The first temper is in the range of 1050°F to 1080°F. Based on the first tempers, the austenitizing temperature of 1870°F (see Figure 4-1), not only exceeds the recommended maximum of 1850°F (as discussed above) but is on the wrong side of the recommended range.

Referring again to Figure 4-2, notice that the couplings extracted from P-7A were single tempered whereas the couplings installed and extracted from P-7B and P-7C were double tempered. Although double tempering could be beneficial, the second temper of the P-7C couplings under Hydro-Aire work order (WO) 202017 (yellow line) and 202067 (red line) were at approximately 1025°F, which is in the range that should be avoided.

Testing showed that surface hardness ranged from 24.5 to 33.6 HRC and through-thickness hardness measurements of 2011 extracted couplings ranged from 24.0 to 33.6 HRC. Through-thickness hardness measurements of coupling 09-P7C-6F ranged from 34.8 to 37.1HRC with an average of 36HRC. These through hardness values for coupling 09-P7C-6F are comparable to the results reported in Consumer Energy Lab Report 0900609 attached in [1]. Based on the surface and through thickness hardness testing results there is no correlation with couplings that were within the specified hardness range and couplings that were cracked or failed. That is, some couplings with out-of-specification hardness (e.g. 11-P7A-5) did not exhibit cracks whereas some couplings within specification (11-P7B-5K through -7K) exhibited cracks. Thus, out-of-specification hardness is not the root cause of observed cracks and failures.

No requirements for CVN impact test absorbed energy are specified in ASTM Standard A582. Nevertheless, the impact tests reveal low absorbed energy that indicates low fracture toughness of the coupling material. Low fracture toughness correlates to stress corrosion cracking (SCC) susceptibility.

Based on the material properties from metallurgical testing and heat treatment provided in Figure 4-1 and Figure 4-2 , it is concluded that the material is susceptible to SCC.

4.2 Corrosive Environment

The Service Water System (SWS) takes cooling water from Lake Michigan via pumps P-7A, P-7B and P-7C for the removal of waste and decay heat. For the period between January 2009 to August of 2011, service water basin level ranged from elevation 576' to 580'. For the same period, the water temperature ranged from 32°F to 76°F (see Section 2.1).

Chlorination occurs on a daily basis and consists of the addition of sodium hypochlorite (i.e. bleach) upstream of the traveling screens to control microbial species in the SWS. A water sample was taken by the Palisades chemistry department on 8/19/11 downstream of YS-0134 in the chemistry cold lab prior and post chlorination of the Service Water System. The chemistry water sample data is presented below.

	Pre Chlorination	**Post Chlorination**
Date/Time	8/19/2011 14:10	8/19/2011 18:48
Chlorination in Progress	No	Yes
Temperature	22.8 C	22.5 C
PH	8.30	8.21
Dissolved Oxygen	9 ppm	10 ppm
Chloride Concentration	9.72 ppm	10.2 ppm

This data indicates that chloride levels are relatively low and not significantly increased by chlorination of the service water. At these service water chloride concentrations, potential for pitting and SCC in the couplings is expected to take much longer for couplings that are continuously submerged than those in the wet/dry region. This is due to the intermittent nature of the service water pumps and the alignment hole, whereby couplings above the normal water basin will experience wet/dry cycles that can concentrate chlorides and other corrosive anion species on the middle thread surfaces (where the shafts touch). Visual examination of failed coupling 11-P7C-6F supports this hypothesis with corrosion product staining on the area below the alignment hole and on the center internal threads found to have cracks.

4.2.1 Effect of Neolube

The couplings threaded surfaces were observed to be coated, to varying degrees, with lubricant during the visual inspection (see Section 3.1). Per PLP work instructions WI-SWS-M-03 [30] and WI-SWS-M-04 [31], Neolube

No. 1 is applied to the threaded surfaces of the pump shaft during the assembly of the shaft.

Neolube No. 1 is a dry, conductive lubricant film, used extensively at nuclear facilities to prevent seizing, fretting, galling and resists abrasion of rubbing surfaces.

According to work instructions WI-SWS-M-03 [30] and WI-SWS-M-04 [31], Neolube No. 1 is to be applied to the shaft threads during assembly of the pump shaft. The work instruction for P-7A, WI-SWS-M-03 [30], excludes application of Neolube No. 1 on the three threads nearest the end of line shafts. The work instruction for P-7B and P-7C, WI-SWS-M-04 [31], does not provide such exclusion on application of Neolube No. 1. A review of WI-SWS-M-03 Revision 0, which was applicable for the extracted P-7A couplings, indicates the same exclusion of Neolube, without specific mention of “No. 1”, on the three threads nearest the ends.

Visual inspection of the as-split P-7A couplings (see Section 3.1.2) revealed Neolube application inconsistent with the work instruction [30]. As-split P-7A couplings exhibited generous amounts of Neolube on the threads, including the center of the coupling. Neolube at the center of the couplings would not be expected if the last three shaft threads were not coated. Visual inspection of the as-split P-7B and P-7C couplings indicated less Neolube compared to P-7A. No cracks were observed by MT on tested P-7A couplings.

The potential for corrosion as a result of application of this lubricant to the shaft and coupling arises from the composition of Neolube. Neolube No. 1 is composed of 99% pure furnace graphite particles in isopropanol with a thermoplastic resin binder (see technical datasheet in Attachment A). Graphite, due to its position on the galvanic series is known to attack stainless steel and other less noble metals [35]. The article presented in [34], also suggests that lubricants containing graphite should not be in contact with stainless steels in seawater. However the percentage of graphite by weight in Neolube is relatively small, approximately 2.5% (3.3% total solids content x 75% graphite content = 2.5%). For galvanic corrosion there typically needs to be more noble material than less noble.

It is postulated that the thermoplastic binder in Neolube inhibits corrosive species in the service water environment from attacking the coupling material. The percentage of graphite in Neolube (~2.5% overall) is not sufficient to attack the couplings unless the thermoplastic binder is washed

away while the graphite remains. In this case, a local galvanic cell could be established when water drains from the coupling and only a small amount of electrolyte is present on the coupling.

Although the effect of Neolube on pit formation and SCC in the couplings is not clear, no cracks or pits were found in P-7A couplings that received a generous coating of Neolube. This evidence suggests that the small amount of graphite present in Neolube did not corrode the coupling material and, in fact, the Neolube composition might actually serve as an inhibiter to corrosive species in the service water. To better understand the effects of Neolube on couplings, further testing would be required.

4.3 Tensile Stress

The fracture surface revealed that coupling 11-P7C-6F failed due to stress corrosion cracking initiating from two initiation sites (pits) in the thread root and propagating in a semi-elliptical manner perpendicular to the coupling axis through the thickness until overload of the remaining ligament. To support this failure mechanism, an evaluation of the coupling stresses was performed to determine if tensile stresses are sufficient to initiate SCC.

The function of the couplings is to couple the various segments of shafts (i.e. line shafts, packing shaft and motor shaft) together in order to transmit the motor torque to the impeller approximately 40 feet below. The design of the couplings is such that the shaft ends can bear against each other, which can lead to tensile and shear stresses across the coupling.

The couplings and shafts are assembled to ensure equal threading of the two shafts within a coupling by the use of an alignment aid inserted in the 1/8” hole on the side of the coupling. Once the shafts touch the alignment aid, it is removed and, then, motor torque is relied upon to tighten up the shaft-coupling assembly. With application of motor torque, it is postulated that the two shafts will tighten and bear against each other within the coupling (see Figure 4-4) which will induce compression on the shaft. The shaft compression is reacted as tension across the coupling. Also when the shafts butt up against each other within the coupling, a circumferential gap between the shaft and coupling is created due to the end geometry of the two shafts. The gap in conjunction with the alignment hole would enable deposits to collect at the exposed thread roots of the shaft intersecting plane.

To estimate the tensile stresses across the couplings, a finite element analysis (FEA) model of the coupling was created in ANSYS [13]. ANSYS is

a multipurpose finite element analysis software program and is verified and validated in accordance with LPI Procedure 4.1 [16], as documented within [17].

4.3.1 FEA Model Description

A half FEA model of an intact coupling was developed using ANSYS and consists of the steel body, alignment hole and threads. The model was constructed of the eight-node brick element, SOLID45 (see Figure 4-5). The symmetric boundary condition, U_z=0 and U_θ=0, is applied on the inner surface as shown in Figure 4-6.

ASTM A582 Type 416 stainless steel material properties for the coupling FEA model are as follows:

Young's modulus: 29.2 x 10^6 psi
Poisson's ratio: 0.3

Coupling threads are 2-3/16, 8 TPI (see Figure 1-5), which is not a common thread form. Specific thread properties are not available in the Machinery's Handbook [14]. Therefore, internal thread properties of the coupling are taken to be the average internal diameter of 2-1/4, 8 TPI and 2-1/16, 8 TPI per the Machinery's Handbook [14].

4.3.2 Loading Condition

Loading on the coupling model consists of the weight of components below the coupling, hydraulic thrust and motor torque. The loads are extracted from HydroAire calculation NQ5940 [15].

Two motor torque loading scenarios (MTS) are considered for transmittal of the motor torque across the coupling: 1) motor torque is transmitted across the coupling from shaft to coupling purely by thread friction (MTS1; see Figure 4-3) and 2) motor torque is transmitted across the coupling by bearing of the shaft ends against each other within the coupling (MTS2; Figure 4-4). To simulate uneven shaft alignment within the coupling, a bending moment is also considered as a load. These loads are combined as follows for evaluation of the couplings.

Load Combination 1 (LC1) = Weight + Thrust + MTS1

For this load combination, component weight and hydraulic thrust is combined with the motor torque loading scenario 1 (MTS1) in which motor torque is transmitted across the coupling purely by friction. Axial

thrust, F = 8,780 lb, is evenly distributed on the nodes at the inner surfaces of each thread (see Figure 4-7). Torque, T=18694 in-lb [15], is first converted into circumferential force, F by T=F*R where R is the coupling friction radius and then evenly applied on the same nodes that the axial thrust load is applied.

Load Combination 2 (LC2) = Weight + Thrust + MTS2

For this load combination, the weight and axial thrust is applied in the same manner as in LC1. Bearing of the shafts within the coupling will induce tensile stress across the coupling. The tensile force of 42 kips is evenly distributed to the first three threads from the contact plane of the two shafts (see Figure 4-8). Typically with threaded connections, the first few threads near the plane of induced load carry the majority of this load [18]. For this assessment, the first three threads were considered to carry the load.

Load Combination 3 (LC3) = Weight + Thrust + MTS2 + Moment

For this load combination, loads are applied in the same manner as LC2 with the addition of a moment on the coupling to account for misalignment or other postulated scenarios that can induce bending across the coupling. A bending moment equivalent to 20% of the stress induced by MTS2 of approximately 4,962 in-lb (see below) was also applied to the coupling. This moment was converted into axial force, Fz, and applied on the nodes on the end cross-section based on the nodes' y direction distance from center (see Figure 4-9).

$OD := 3.187 \cdot in$ Out diameter of coupling

$ID := \frac{(2.125 + 2.25) \cdot in}{2}$ Internal diameter of coupling

$Sp := \frac{\pi \cdot (OD^2 - ID^2)}{4}$ Area of cross-section of coupling

$Fp := 42335 \cdot lb$ Clamping force

$\sigma := \frac{Fp}{Sp}$

$Ip := \left(\frac{\pi}{64}\right) \cdot (OD^4 - ID^4)$ Area moment of inertia of coupling

$Mom := 0.2\sigma \cdot \frac{Ip}{\frac{OD}{2}}$

$Mom = 413.5\,lb\,ft$ Moment can result in 20% stress result from clamping force

4.3.3 FEA Results

1) LC1: In this case, the circumferential stress, axial stress and first principal stress are relatively low due to the even distribution of loads on the coupling (see Figure 4-10). Axial tensile stresses at the thread root are on the order of 3.5 to 5 ksi. This result indicates that if the motor torque is transmitted across the coupling purely by thread frictional resistance, then the coupling tensile stresses are relatively low.

2) LC2: This load combination results in high stress concentrations at the thread root of the coupling at the contact plane of the two shafts. Axial tensile stresses at the thread root are over 10 times greater than LC1 with stresses on the order of 60 to 70 ksi. The stress distribution at the middle thread root across the coupling wall for this load combination root is presented in Figure 4-12.

3) LC3: This load combination does not significantly increase stresses at the thread root of the coupling from LC2. The additional bending moment on the coupling produces additional stresses on the outside diameter of the coupling. However it does not appreciably increase stresses at the thread root where SCC initiation is observed.

Average tensile stresses at the first thread root for each load combination is summarized in the matrix below.

Load Combination	Average Tensile Stress (psi)
LC1: No Bearing	3,790
LC2: Shaft Bearing	60,506
LC3: Bearing Shaft and Bending	60,476

The limiting load combination is LC2. The resulting tensile stress indicates that the failure was not a single overload event since the average yield and tensile strength are approximately 136 ksi and 151 ksi (see Section 3.6), respectively.

The Figure 4-12 stress distribution is based on reacting the applied shaft end compression load from the applied motor torque across three threads[3] per shaft end. Considering the two shafts meeting approximately in the center of the coupling, the three threads below the centerline react the lower shaft compression loading, the three threads above the centerline react the compression loading in the upper shaft. However, tolerances in machining of the threads could translate into different load and stress distribution across the threads. If the load is distributed to fewer or greater number of threads than the three assumed, then the tensile stress at the thread root could range according to the load distribution to the threads.

For example, if the shaft bearing loads were distributed across six threads instead of three, the maximum tensile stress would be on the order of 30 ksi. Based on the FEA and depending on the number of threads sharing the load, it is not un-reasonable for tensile stresses to range from approximately 20 ksi to 80 ksi at the thread root.

4.4 SCC Process

The time to failure of a susceptible material in a given environment is dependent on the applied tensile stress, as shown in the Figure 4-14 schematic. The plot compares applied stress or load to the logarithm of exposure time in an environment and illustrates the time to failure increases significantly with decreasing applied stress. The crack propagation time, t_{cp} is taken to be the difference between the time of failure, t_f, minus the time of initiation, t_{in}. The time at failure is typically known. However, the time of

[3] Based on extensive testing, as presented in various literature sources [32], the threads nearest the plane of load application carry the majority of the applied loading.

initiation is highly alloy-environment and applied stress dependant and thus is an unknown without specific test data. The initiation time is also highly dependent upon pre-existing flaws that may have been introduced during heat treatment or thread fabrication. Therefore, predicting initiation time is difficult. Unless there are preexisting flaws, a distribution of 80% initiation and 20% propagation is considered reasonable for the life of a component subject to SCC process as suggested by Figure 4-15.

The SCC process usually occurs in three stages:

1) crack initiation and stage 1 propagation,
2) stage 2 or steady-state propagation (independent of stress intensity), and
3) stage 3 crack propagation or final fracture.

A typical plot of crack growth rate (da/dt) versus stress intensity illustrating the three stages of SCC propagation is presented in Figure 4-16. The figure illustrates a threshold stress-intensity, K_{1SCC}, for SCC initiation and stage 1 propagation. The threshold stress-intensity is dependent upon interaction of the alloy and environment (alloy-environment). Stage 1 propagation is followed by Stage 2 crack propagation where the crack growth velocity is independent of stress intensity. Stage 2 crack growth velocity is limited to the alloy-environment interaction such as the mass transfer of corrosive environmental elements up the crack to the crack tip.

Stage 3 propagation is dependent upon stress intensity, until the critical level, K_{1c} to produce mechanical overload of the remaining ligament. The crack propagation time is the sum of the time at each stage, $t_{cp}=t_1+ t_2+ t_3$.

A plot of crack growth rate (da/dt) versus stress intensity for 12% chromium and 0.2% carbon alloy at various tempering temperature per [22] is provided in Figure 4-17. The generic categorization of 12% Cr and 0.2% C would cover the 416 SS coupling material. Based on tempering heat traces for the extracted service water couplings presented in Figure 4-2, the 550°C (1022°F) curve is appropriate. Figure 4-17 shows that the threshold stress-intensity, K_{1SCC} for the 550°C curve is approximately $20Mpa\sqrt{m}$ $(\sim 18ksi\sqrt{in})$ and the stage 2, stress intensity independent crack growth rate is approximately 2.3E-4 in/hr per [22].

For a stress distribution of 20 to 80 ksi, the stress intensity at the thread root (without pits) of the coupling can range from $6ksi\sqrt{in}$ to $26ksi\sqrt{in}$ as demonstrated below.

$j := 0..3$

$d_{thread} = 0.068\,in$ Thread height

$a := \frac{d_{thread}}{2}$ $a = 0.034\,in$ Load assumed to act at center of threads.

$\sigma_j :=$

20ksi
55ksi
70ksi
80ksi

$K_j := \sigma_j \cdot \sqrt{\pi \cdot a}$ [33] $K_j =$

6.5	$ksi\cdot\sqrt{in}$
17.9	
22.8	
26.1	

Therefore, based on three threads taking the load and resulting tensile stress of 70 ksi (see Figure 4-12), the stress intensity of $23ksi\sqrt{in}$ would be sufficient to initiate a crack. If the tensile stress at the thread root is 55 ksi or less, then the stress intensity would fall below the threshold stress intensity, K_{1SCC} of $18ksi\sqrt{in}$ and SCC initiation would not be expected. However, if a pit were to form at the thread root, the stress intensity would be higher for a given tensile stress. For example, a pit 0.01" deep and tensile stress of 55 ksi would result in a stress intensity of approximately $24ksi\sqrt{in}$ (see below), which is greater than the threshold stress intensity for SCC initiation.

$Q := 0.9$ $M := 1$

$d_{pit} := 0.01in$ Assumed pit depth

$a := d_{pit} + a$ $a = 0.044\,in$

$\sigma_j :=$

20ksi
55ksi
70ksi
80ksi

$K_j := 1.12\sigma_j \cdot \sqrt{\frac{\pi \cdot a}{Q}} \cdot M$ [33] $K_j =$

8.8	$ksi\cdot\sqrt{in}$
24.1	
30.7	
35	

Once a crack initiates, the stress intensity would increase with increasing crack length, however the crack rate is limited to the stage 2 propagation rate until the critical fracture stress intensity, K_{1c} resulting in overload failure.

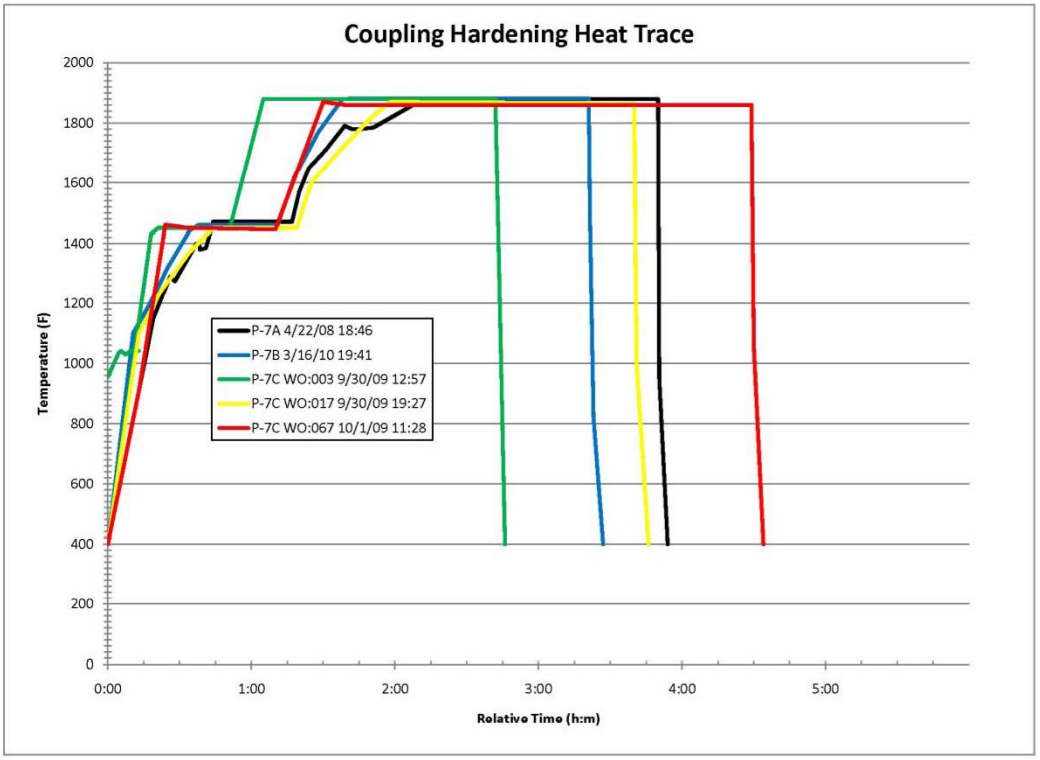

Figure 4-1: Hardening Heat Traces

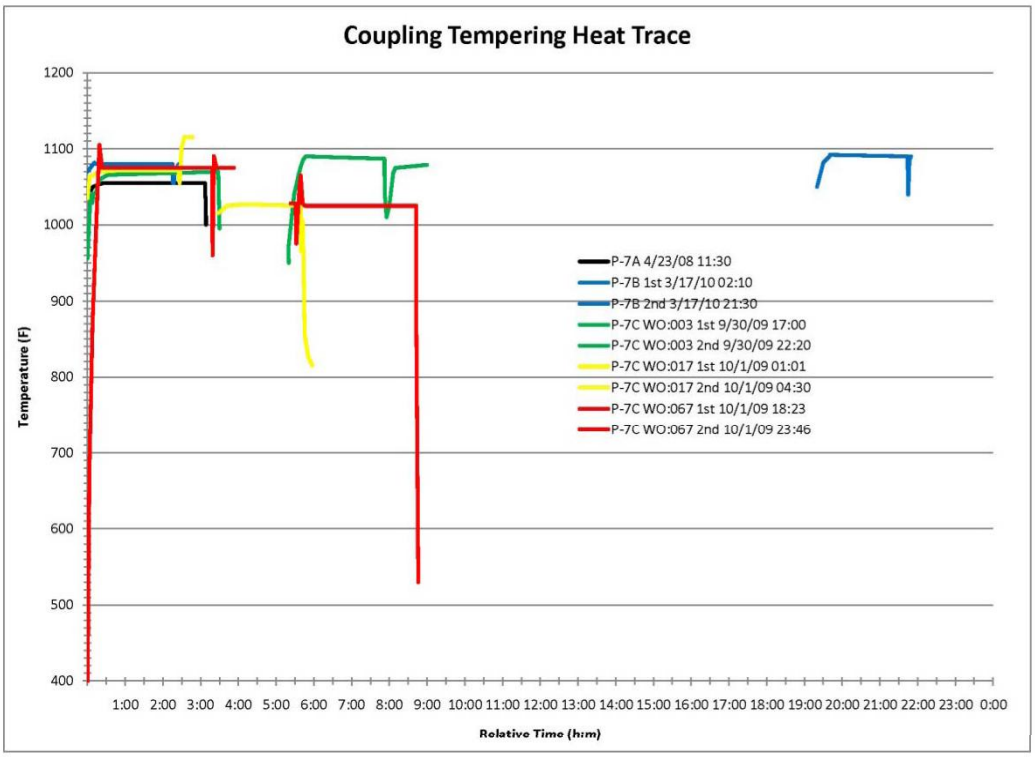

Figure 4-2: Tempering Heat Traces

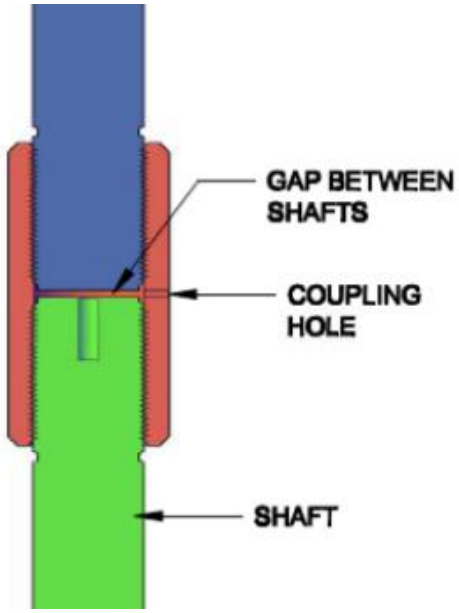

Figure 4-3: MTS1: Shaft Not Bearing

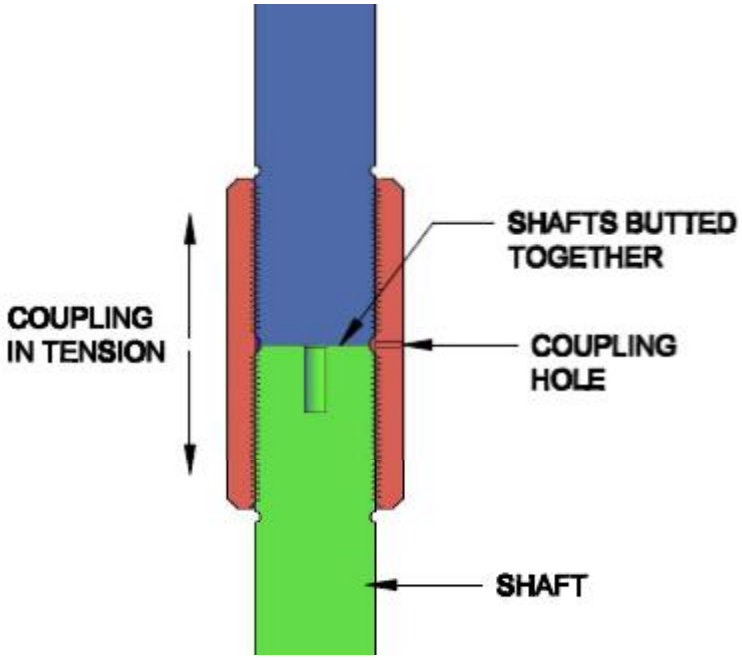

Figure 4-4: MTS2: Shaft Bearing

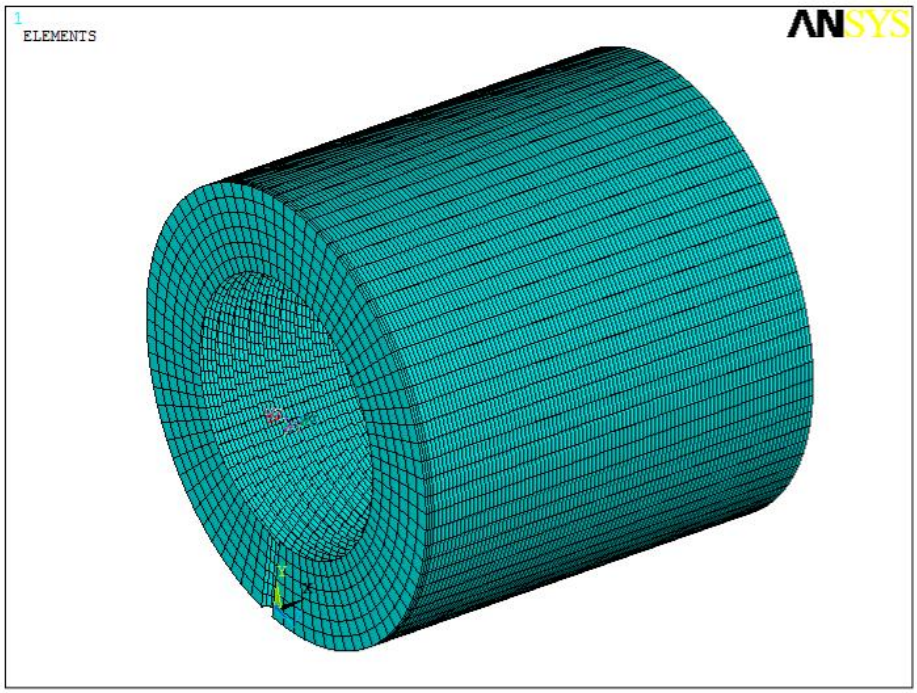

Figure 4-5: Half FEA model of coupling

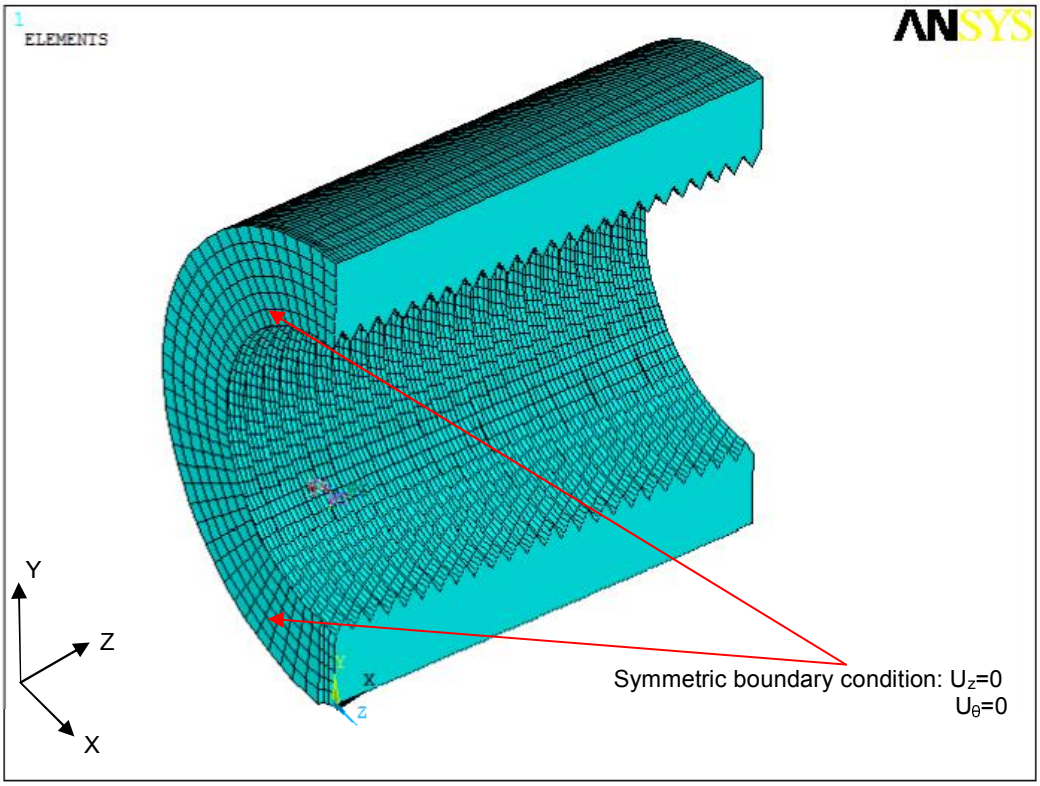

Local coordinate system numbered 11 is cylindrical coordinate system

Figure 4-6: Cross-section of half FEA coupling model

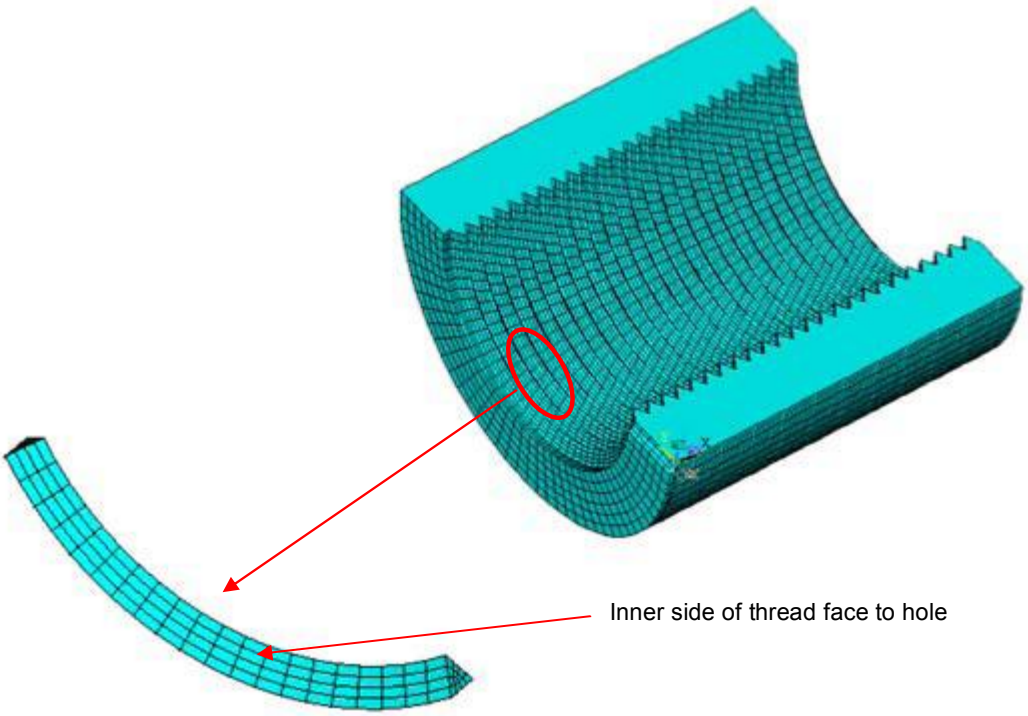

Figure 4-7: Load application Sketch of loading condition in no bearing case

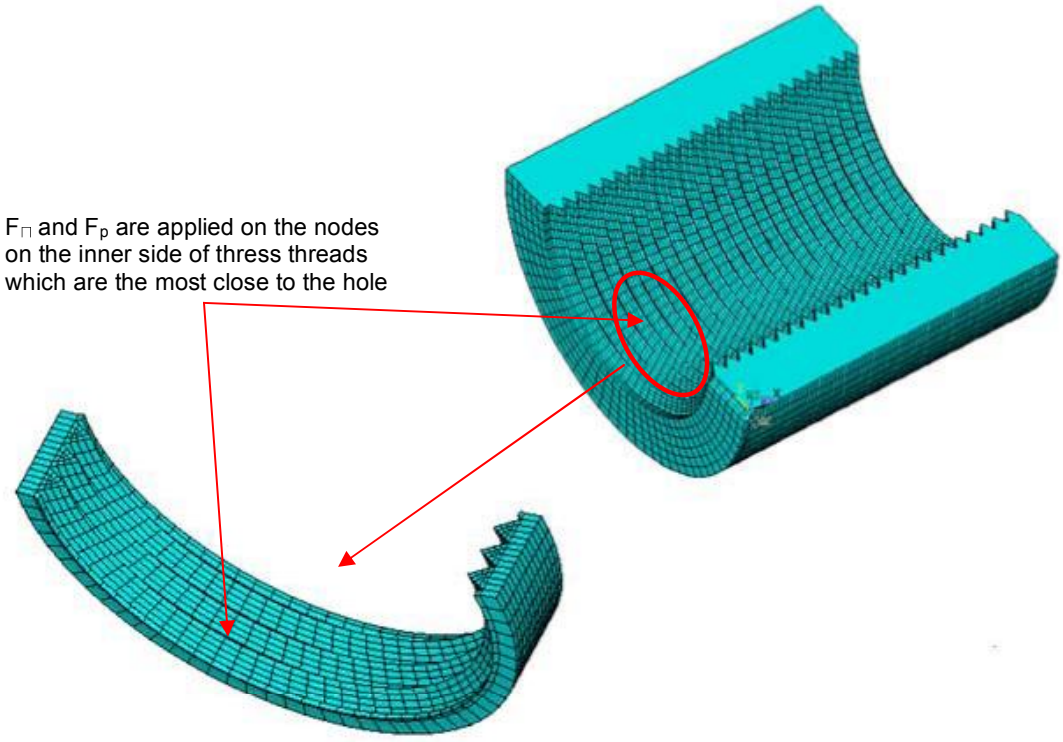

Figure 4-8: Sketch of loading condition in shafts bearing case

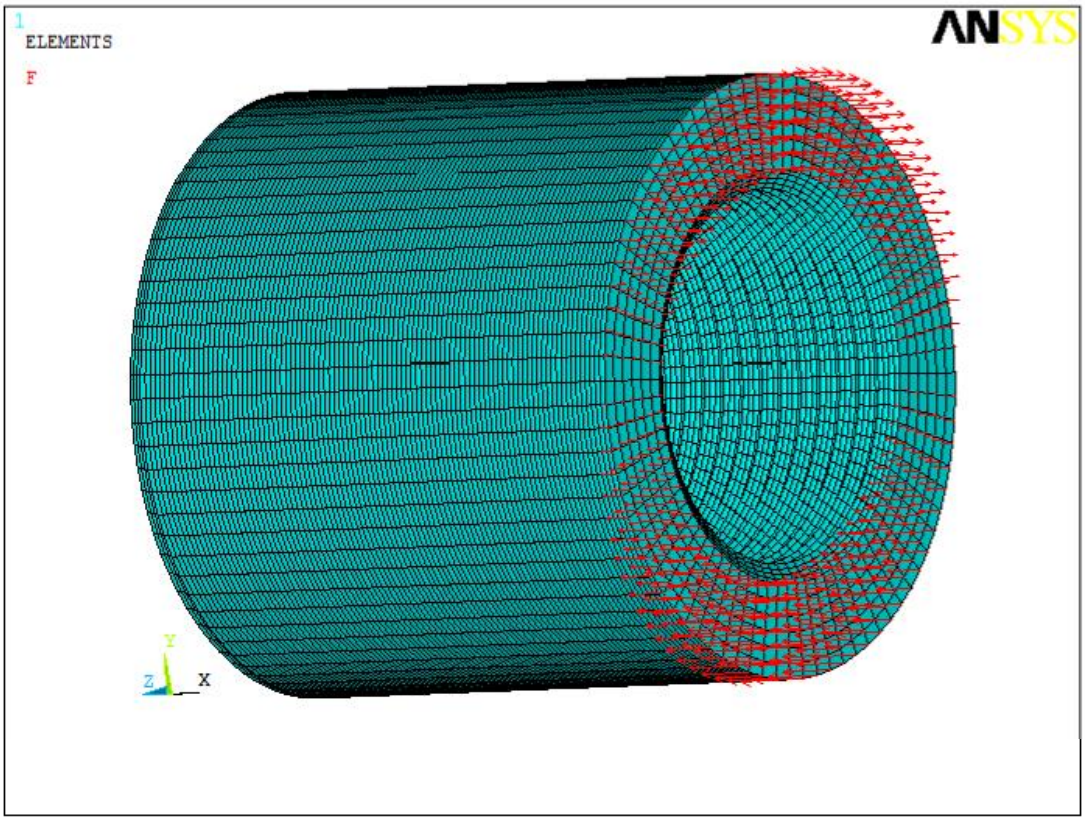

Figure 4-9: Sketch of axial force result from bending moment

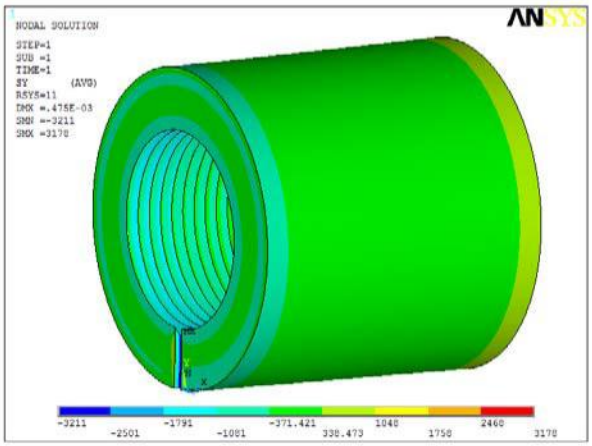

Circumferential Stress

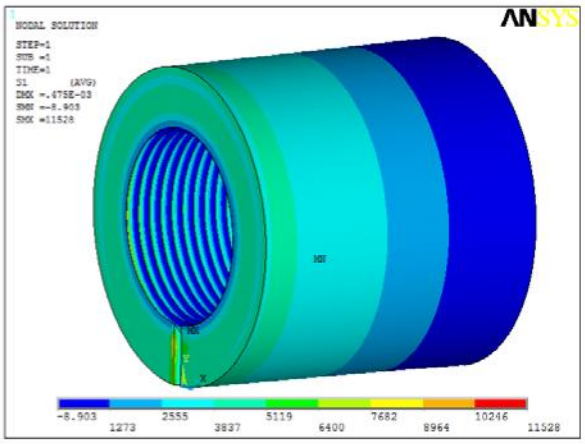

1st Principal Stress

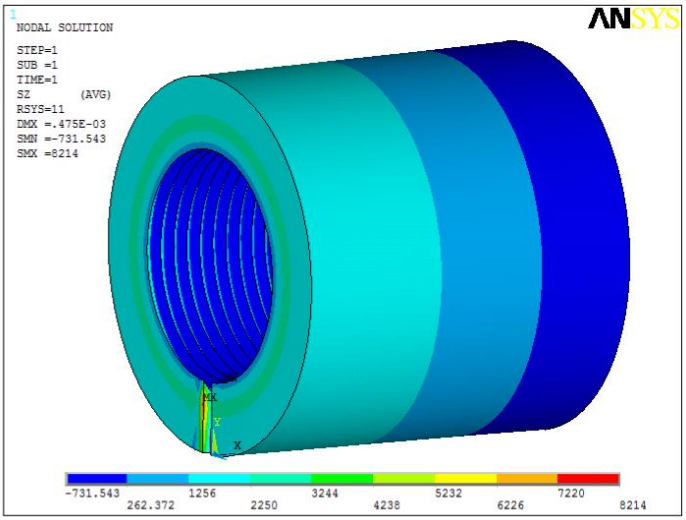

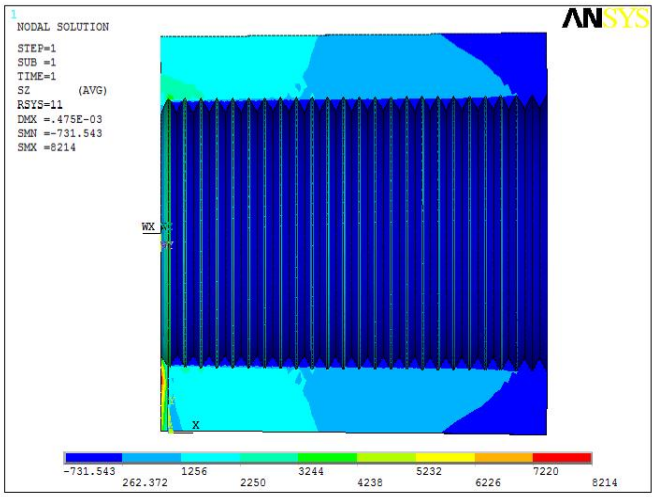

Axial Stress

Figure 4-10: Resultant stresses for LC1

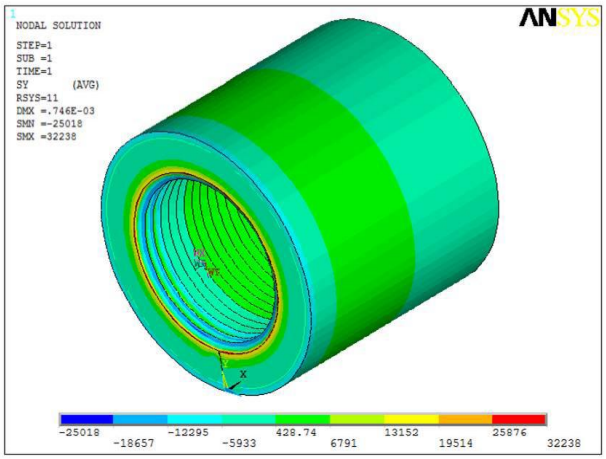

Circumferential Stress

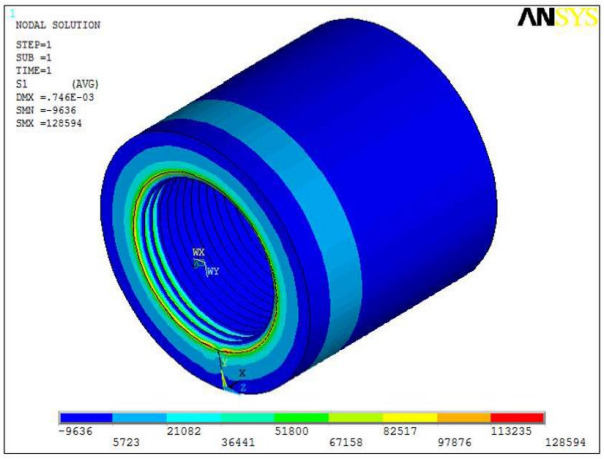

1st Principal Stress

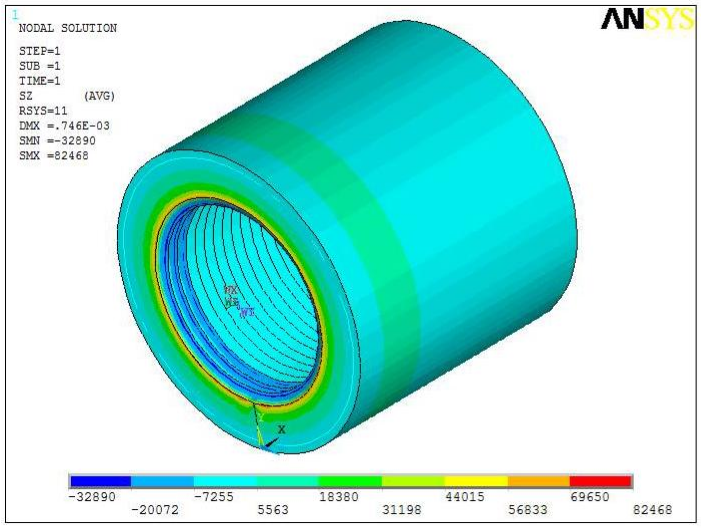

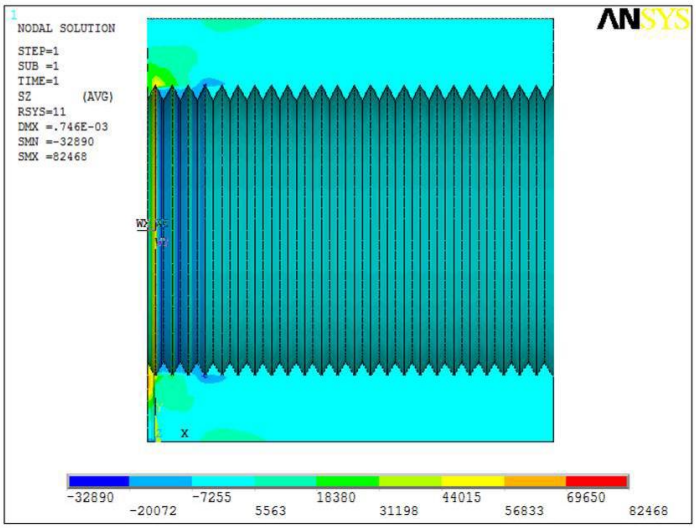

Axial Stress

Figure 4-11: Resultant stresses for LC2

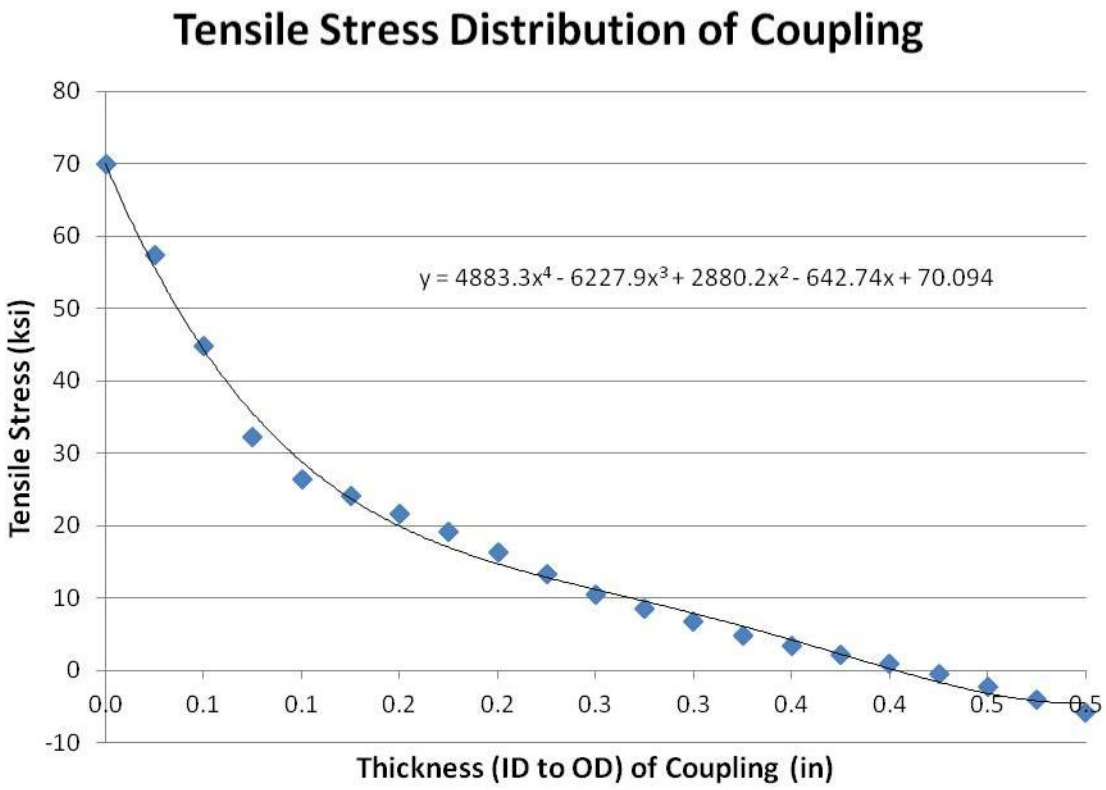

Figure 4-12: Tensile Stress Distribution Across Wall Thickness of Coupling – LC2
(Based on three threads reacting out applied load)

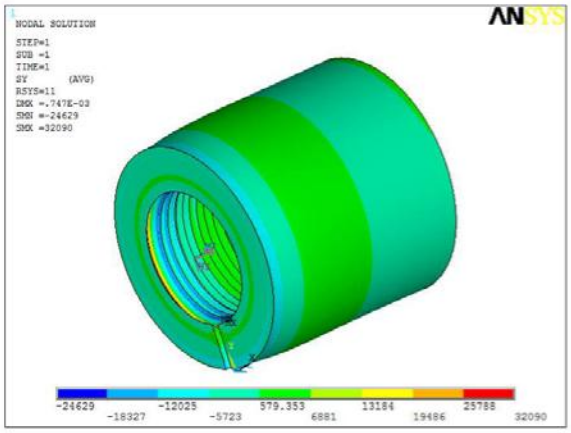

Circumferential Stress

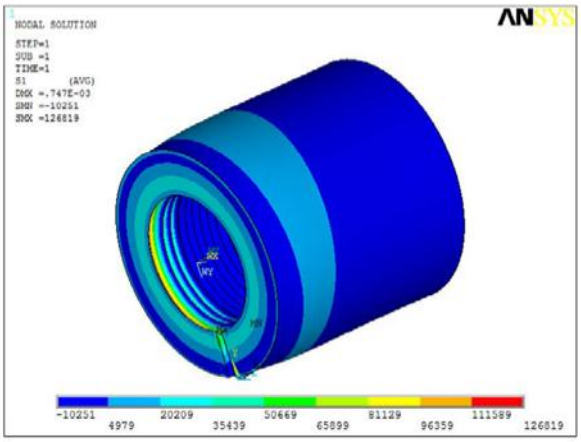

1st Principal Stress

Axial Stress

Figure 4-13: Resultant stresses for LC3

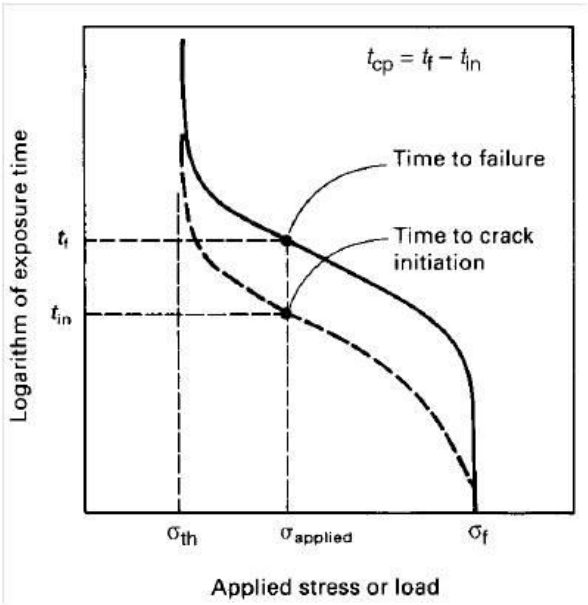

Figure 4-14: Time to Failure vs Applied Stress [23]

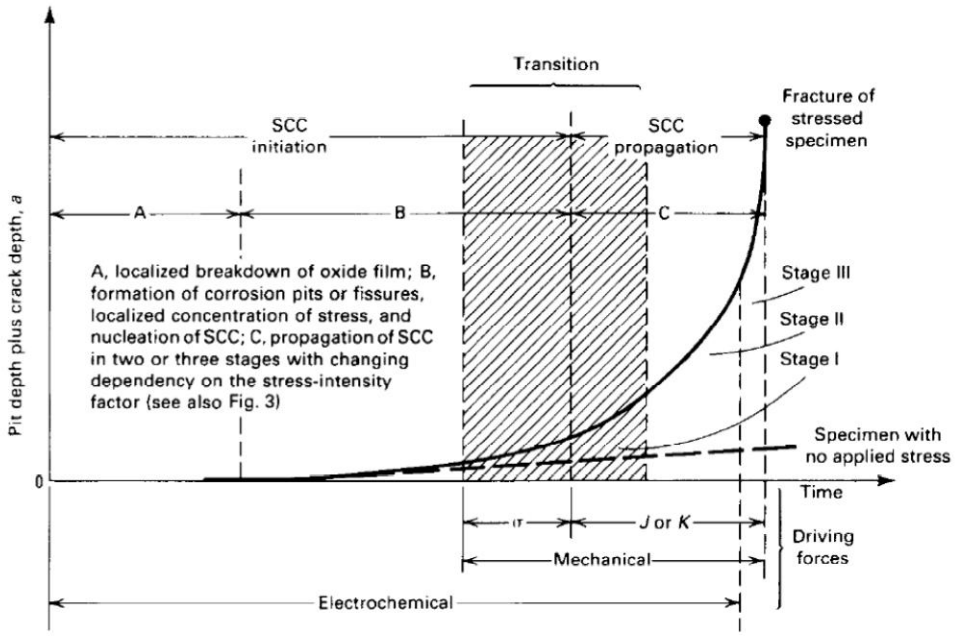

Fig. 2 The relative influences of electrochemical and mechanical factors in the corrosion and SCC damage of a susceptible material. The shaded area represents the transition of driving force from dominance by electrochemical factors to chiefly mechanical factors. Precise separation of initiation and propagation stages is experimentally difficult. Stimulation of cracking by atomic hydrogen may also become involved in this transition region.

Figure 4-15: SCC Process [28]

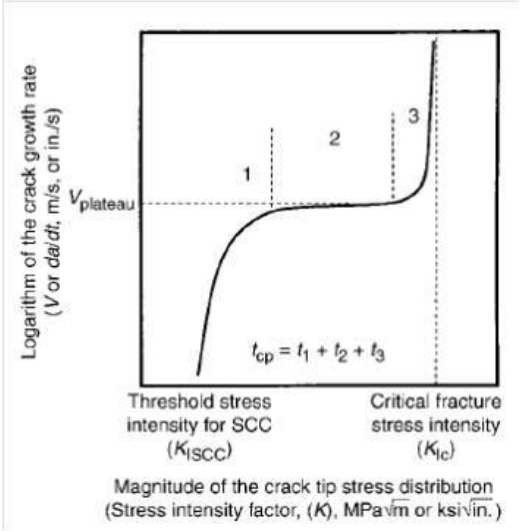

Figure 4-16: Crack Growth Rate (da/dt) versus stress intensity w/Three Stages of Crack Growth [23]

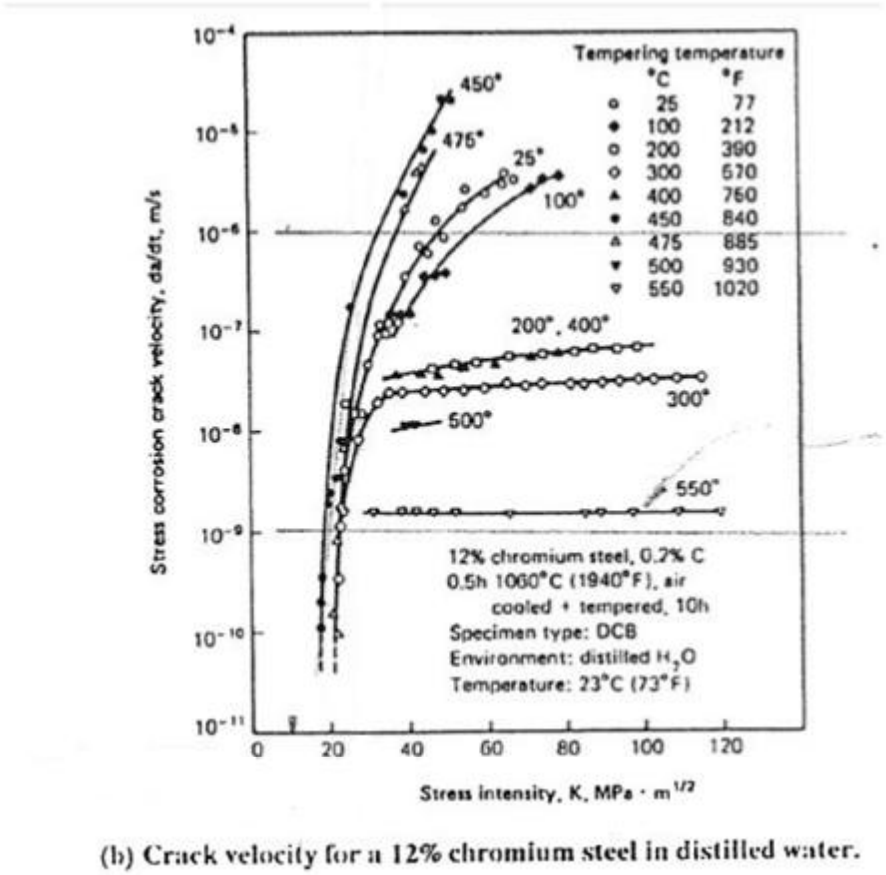

(b) Crack velocity for a 12% chromium steel in distilled water.

Figure 4-17: Effects of Tempering Temperature and Applied Stress-Intensity factor on Velocity of Stress-Corrosion Cracking [22]

5.0 SUMMARY/RECOMMENDATION

In August 2011, a Type 416 stainless steel (SS) coupling fractured in Service Water System (SWS) pump P-7C at Palisades Nuclear Plant (PLP). A previous coupling fracture occurred in the same pump in 2009. As a result of the recent failure, some couplings extracted from all three pumps at the PLP site were examined by magnetic particle testing that revealed four additional cracked couplings from pumps P-7C and P-7B, but not P-7A.

Metallurgical analysis of fractured and cracked couplings revealed that the failure mechanism involved intergranular stress corrosion cracking (IGSCC) along the prior austenite grain boundaries. This cracking mechanism is common for martensitic stainless steels exposed to chloride-containing environments.

Susceptibility of martensitic stainless steels to SCC is known to be dependent on tempering temperature. A review of heat treatment records for the couplings showed a first temper around 1075°F to 1100°F and, for the P-7B and P-7C couplings, a second temper at 1025°F. The second temper was performed because the resulting hardness following the first temper was not within the specified value of 28 to 32 HRC. Literature findings show that martensitic stainless steel alloys tempered around 1050°F are particularly susceptible to corrosion and SCC [25, 26]. The specified heat treatment required to achieve the designed hardness (28-32 HRC) and strength makes this martensitic stainless steel particularly susceptible to corrosion and SCC. Furthermore, the heat treatment did not conform to recommendations in the ASM guides for heat treating Type 416 SS as prescribed in [25, 26]. The austenitizing temperature of 1870°F exceeded the maximum recommended range of 1695°F to 1850°F and were on the wrong side of the range when considering the tempering temperatures in the range of 1050°F to 1080°F. That is, per ASM guides [25, 26] austenitizing temperatures should be on the low side, when tempering above 1050°F. A second temper was performed on couplings installed in P-7B and P-7C at 1025°F, which is in the range not recommended by ASM of 700°F to 1050°F [25, 26] that typically results in temper embrittlement and SCC. The heat treatment experienced by the couplings, which did not strictly conform to ASM guidelines [25, 26], increased the materials susceptibility to corrosion and SCC.

Cracks emanated from thread root regions and were predominantly found at the center of couplings that was exposed to a service water environment containing chlorides. Chlorides are known to cause pitting and SCC in martensitic stainless steels [29]. Couplings exhibiting cracks were also subjected to wet and dry cycles that could significantly increase concentrations of chloride species on the threaded surfaces due to the alignment hole enabling ingress and egress of water with

pump on/off cycles. General corrosion was observed in the threaded region for nearly all couplings, including those with no evidence of cracking. The couplings containing cracks exhibited pitting at the thread roots, and it appeared that SCC cracks emanated from the pits. Chemical analysis via EDS of IGSCC fracture surfaces exhibited detectable amounts of chlorine, which is indicative of chlorides, thereby providing evidence that this species contributed to the SCC. Other corrosive species that could contribute to SCC in the couplings may be present in the service water basin. To assess the aqueous environment experienced by the couplings, it is recommended that hydrogen sulfide and chloride concentration samples be taken at the packing leak-off drain line to determine if there any local differences in corrosive species concentration.

Finite element analysis (FEA) was used to model tensile stresses in couplings, which must be present for SCC to occur, along with a susceptible material and corrosive environment. The calculated peak tensile stresses at the thread root were estimated to be around 70 ksi, which is judged to be sufficient to enable SCC. However, the presence of pits may have increased the stress intensity such that SCC could occur at lower stress.

It was noted that Neolube was generously applied to couplings in pump P-7A, which did not exhibit cracks. Cracked couplings in pump P-7B had some Neolube, while failed and cracked couplings in pump P-7C had no noticeable amount of Neolube in the as-received condition. It is not clear if Neolube played a significant role in limiting pit formation and SCC in couplings. However, well-coated couplings in pump P-7A did not exhibit pits or cracks at the thread root even though it had been in service the longest and had the greatest run time upon extraction.

Metallurgical analysis of fractured and cracked couplings revealed SCC to be an issue for Type 416 SS couplings in the service environment. The wet and dry cycles experienced by couplings Nos. 5, 6, and 7 likely created elevated chloride levels that lead to pitting corrosion and SCC. As evidence, five out of nine couplings in the wet and dry region were found to contain SCC cracks. No cracks were found on tested couplings that were continuously submerged. Because Type 416 SS martensitic stainless steel is particularly susceptible to corrosion and SCC in halide environments and heat treatment to achieve the desired balance between hardness and toughness is difficult, this class of alloy is not an optimal choice for the service water pump couplings. It is recommended that a different material with superior corrosion resistance to SCC while maintaining designed strength requirements is selected.

6.0 REFERENCES

1. Entergy Palisades Root Cause Evaluation for CR-PLP-2009-04519, “Service Water Pump P-7C Failure to Provide Discharge Pressure” 3/4/2010, Rev. 1
2. Entergy Palisades Root Cause Evaluation Report for CR-PLP-2011-03902, “Service Water Pump 7-C Line Shaft Coupling Failure”
3. Entergy Palisades Drawing
   a. Entergy Drawing No.M-213, Rev. 93 “Piping and Instrumentation Diagram Service Water, Screen Structure and Chlorinator”
   b. Entergy Drawing No. VEN-M-11-Sht 45, Rev. 2 “Service Water Pumps Modified Line Shaft Components For Pumps P-7A, P-7B and P-7C”
   c. Entergy Drawing No. VEN-M-11-Sht 0055,
4. Entergy Engineering Change (EC)-50000121762
5. LPI Procedure F11358-P-001, “Procedure for Metallurgical Examination of SW Pump P-7C Coupling Components”, Rev. 1
6. PLP Response to NRC Special Investigation Team RFI # 43 “Operating Service History Since Last Coupling Failure”
7. ASTM A582/A582M, “Standard Specification for Free-Machining Stainless Steel Bars”, 2005.
8. ASTM E 18-07, “Standard Test Method for Rockwell Hardness of Metallic Materials”
9. ASTM E8/E8M-09, “Standard Test Methods for Tension Testing of Metallic Materials”
10. ASTM E23-07ae1 “Standard Test Methods for Notched Bar Impact Testing of Metallic Materials”
11. ASTM E3-11, “Standard Guide for Preparation of Metallographic Specimens”
12. ASTM E407-99, “Standard Practice for Microetching Metals and Alloys”
13. ANSYS Mechanical Software, ANSYS Inc., Southpoint, Canonsburg, PA 15317
14. OBERG E, et al. “Machinery’s Handbook” 25th Ed. Industrial Press
15. HydroAire Calculation NQ5940, “Maximum combined shear stress calculation for threaded coupling”, Rev. 3
16. LPI Procedure 4.1, “Software Control”, Rev. 2
17. ANSYS Inc., LPI Report No. V&V-ANSYS-11, ”Verification and Validation of ANSYS”, Rev. 3
18. Shigley’s, “Mechanical Engineering Design” McGraw Hill
19. Structural Integrity Report 1100112.401, “Additional Review of Palisades Service Water Pump Couplings”, Rev. 0 March 2011.
20. HydroAire Inc. Drawing No. 1047237 “Line Shaft Coupling Johnstone 25 NMC 2 STG” Sht. 1/1, Rev. 1
21. Flowserve Materials Newsletter Volume 3, Number 4 “Embrittlement of Martensitic Stainless Steels”, September 2004.

22. M.O. Speidel "Corrosion Fatigue in Fe-Ni-Cr Alloys", NACE-5 Stress Corrosion Cracking and Hydrogen Embrittlement of Iron Base Alloys, National Association of Corrosion Engineers, Houston, 1977, p. 1071 to 1094.
23. ASM Handbook, Volume 13A: Corrosion: Fundamentals, Testing, and Protection, "Stress-Corrosion Cracking", R.H. Jones, Battelle Pacific Northwest National Laborator, 2003 ASM International
24. ASM Handbook, Volume 11: Failure Analysis and Prevention, "Stress-Corrosion Cracking", Revised by W.R. Warke, 2002 ASM International
25. ASM Heat Treater's Guide: Practices and Procedures for Irons and Steels, Datasheet for 416, 416Se, 2nd Edition, ASM International 1995
26. ASM Metals handbook, Heat Treating, Cleaning and Finishing, 8th Edition Vol. 2
27. NRC Information Notice 2007-05: "Vertical Deep Draft Pump Shaft and Coupling Failures", February 9, 2007.
28. ASM Handbook, Volume 13A "Evaluating Stress-Corrosion Cracking", S.D. Cramer, B.S. Covino, Jr, Revised by Bopinder Phull
29. ASM Metals Handbook, "Corrosion" 9th Edition, Vol. 13, 1987, pp. 1129-1133
30. Palisades Nuclear Plant Work Instruction WI-SWS-M-03, "Service Water Pump P-7A Removal, Inspection, and Reinstallation", Rev. 4
31. Palisades Nuclear Plant Work Instruction WI-SWS-M-04, "Service Water Pumps P-7B and P-7C Removal, Inspection, and Reinstallation", Rev. 4
32. Pilkey, Walter "Peterson's Stress Concentration Factors", 2nd Edition,. © 1997 John Wiley & Sons
33. R.W. Hertzberg, "Deformation and Fracture Mechanics of Engineering Materials", 2nd Edition John Wiley & Sons.
34. Atlas Specialty Metals Tech Note No. 7, "Galvanic Corrosion", May 2006
35. Journal of Composite Materials Vol. 24, "Corrosion Between a Graphite/Polymer Composite and Metals" January 1990.
36. R.E. Avery, et al., "Stainless Steel for Potable Water Treatment Plants (PWTP) – Guidelines"